LOAN DOCUMENT

PHOTOGRAPH THIS SHEET

DTIC ACCESSION NUMBER

LEVEL

INVENTORY

EPA-600/R-98-033

DOCUMENT IDENTIFICATION

APR 98

DISTRIBUTION STATEMENT A
Approved for Public Release
Distribution Unlimited

DISTRIBUTION STATEMENT

ACCESSION FOR
NTIS GRA&I
DTIC TRAC
UNANNOUNCED
JUSTIFICATION

BY

DISTRIBUTION/

AVAILABILITY CODES

DISTRIBUTION	AVAILABILITY AND/OR SPECIAL	
A-1		

DISTRIBUTION STAMP

DATE ACCESSIONED

DATE RETURNED

19990609 034

DATE RECEIVED IN DTIC

REGISTERED OR CERTIFIED NUMBER

PHOTOGRAPH THIS SHEET AND RETURN TO DTIC-FDAC

HANDLE WITH CARE

DTIC FORM 70A JUN 90

DOCUMENT PROCESSING SHEET

PREVIOUS EDITIONS MAY BE USED UNTIL STOCK IS EXHAUSTED.

LOAN DOCUMENT

United States
Environmental Protection
Agency

EPA-600/R-98-033 PP309

April 1998

EPA

Research and Development

HEAT TRANSFER EVALUATION
OF HFC-236ea WITH HIGH
PERFORMANCE ENHANCED TUBES IN
CONDENSATION AND EVAPORATION

Prepared for

Strategic Environmental Research and
Development Program

Prepared by

National Risk Management
Research Laboratory
Research Triangle Park, NC 27711

FOREWORD

The U.S. Environmental Protection Agency is charged by Congress with protecting the Nation's land, air, and water resources. Under a mandate of national environmental laws, the Agency strives to formulate and implement actions leading to a compatible balance between human activities and the ability of natural systems to support and nurture life. To meet this mandate, EPA's research program is providing data and technical support for solving environmental problems today and building a science knowledge base necessary to manage our ecological resources wisely, understand how pollutants affect our health, and prevent or reduce environmental risks in the future.

The National Risk Management Research Laboratory is the Agency's center for investigation of technological and management approaches for reducing risks from threats to human health and the environment. The focus of the Laboratory's research program is on methods for the prevention and control of pollution to air, land, water, and subsurface resources; protection of water quality in public water systems; remediation of contaminated sites and groundwater; and prevention and control of indoor air pollution. The goal of this research effort is to catalyze development and implementation of innovative, cost-effective environmental technologies; develop scientific and engineering information needed by EPA to support regulatory and policy decisions; and provide technical support and information transfer to ensure effective implementation of environmental regulations and strategies.

This publication has been produced as part of the Laboratory's strategic long-term research plan. It is published and made available by EPA's Office of Research and Development to assist the user community and to link researchers with their clients.

E. Timothy Oppelt, Director
National Risk Management Research Laboratory

EPA REVIEW NOTICE

EPA-600/R-98-033
April 1998

HEAT TRANSFER EVALUATION OF HFC-236ea WITH HIGH PERFORMANCE ENHANCED TUBES IN CONDENSATION AND EVAPORATION

by

S.-M. Tzuoo
M.B. Pate
Iowa State University
Ames, IA 50011

EPA Cooperative Agreement No. CR820755-01-4

Project Officer:

Theodore G. Brna
U.S. Environmental Protection Agency
National Risk Management Research Laboratory
Air Pollution Prevention and Control Division
Research Triangle Park, NC 27711

Prepared for:

U.S. ENVIRONMENTAL PROTECTION AGENCY
OFFICE OF RESEARCH AND DEVELOPMENT
WASHINGTON, DC 20460

ABSTRACT

This research evaluates the heat transfer performance of HFC-236ea for high performance enhanced tubes which have not been previously used in Navy shipboard chillers. Shell-side heat transfer coefficient data are presented for condensation on a Turbo-CII tube, pool boiling on Turbo-B and Turbo-BII tubes, and spray evaporation on Turbo-B and Turbo-CII tubes as well as a 1575-fpm (1575-fins-per-meter) tube. These tubes with a typically nominal outside diameter of 19.1 mm (3/4 inch) were evaluated at a saturation temperature of 2°C (35.6°F) in evaporation and 40°C (104°F) in condensation.

The condensation and pool boiling results for the high performance enhanced tubes in this study were compared with the results for a plain tube and two integral finned tubes (1024-fpm and 1575-fpm tubes), which were evaluated in an earlier study. The comparison shows that the high performance enhanced tubes are able to promote heat transfer processes better than the plain tube, and especially, better than the integral finned tubes that are currently being used with CFC-114 the Navy shipboard chillers. It was found that the Turbo-CII tube, Turbo-BII tube, and Turbo-B tube performed best in condensation, pool boiling, and spray evaporation, respectively.

The comparative heat transfer performance of spray evaporation with pool boiling was made by using a Turbo-B tube and a 1575-fpm tube. Under the range of liquid refrigerant feed rates evaluated, the superiority in heat transfer for spray evaporation over pool boiling was found to exist only at low heat loads (below 30 kW/m^2).

This report was submitted in fulfillment of CR820755-01-4 by Iowa State University under the sponsorship of the U.S. Environmental Protection Agency through the EPA/DoD/DOE Strategic Environmental Research and Development Program (SERDP). This report covers a period from October 1992 to March 1995.

CONTENTS

Contents (continued)

LIST OF FIGURES

List of Figures (continued)

LIST OF TABLES

List of Tables (continued)

List of Tables (continued)

LIST OF ABBREVIATIONS AND SYMBOLS

ABBREVIATIONS

a	constant in the Webb and Murawski correlation
A	surface area (m^2)
A1	the surrounding portion of a tube bundle in the spray zone (m^2)
A2	the overlapped area between two neighboring spray cones (m^2)
bw	the width of a tube bundle (m)
Cp	specific heat at constant pressure (J/kg·K)
d	the optimal height of nozzles from the tubes in a spray evaporator system (m)
D	tube diameter (m)
fpi	fins per inch
fpm	fins per meter
h	shell-side heat transfer coefficient ($W/m^2 \cdot K$)
h_i	in-tube heat transfer coefficient ($W/m^2 \cdot K$)
i	enthalpy (J/kg)
k	thermal conductivity (W/m·K)
L	tube length (m)
LMTD	logarithmic mean temperature difference (°C)
$\dot{m}$	mass flow rate (kg/s)
N/A	not available
OL	the optimal distance between two neighboring nozzles in a spray evaporator system (m)
Pr	Prandtl number
q	heat transfer rate (W)
R	thermal resistance (K/W)
Re	Reynolds number
RR	recirculation rate (dimensionless)
STC	Sieder-Tate coefficient (a constant)
T	temperature (°C)
ΔT	temperature difference between the tube wall and the saturated refrigerant (°C)

U_o	overall heat transfer coefficient based on the outer surface area of a tube ($W/m^2 \cdot K$)
UN	uncertainty in heat transfer coefficient (± %)
y	the fraction of the total refrigerant flow exiting the test section as vapor in spray evaporation

SYMBOLS

β	the angle of a spray cone (degree)
Γ	condensate mass flow rate per unit tube length (kg/m·s)
π	a constant (= 3.14159)
μ	dynamic viscosity ($N \cdot s/m^2$)

Superscripts

"	unit area basis ($1/m^2$)
n	exponent in the Webb and Murawski correlation

Subscripts

i	tube-side (in-tube); inside
in	inlet
liq	liquid
N	total number of tube rows measured from the top row of a bundle
NR	row number counted from the top row of a bundle
o	shell-side; outside
out	outlet
r	root
sat	saturated refrigerant
spr	spray evaporation
vap	vapor
w	tube wall

ACKNOWLEDGMENTS

This research was supported by the Environmental Protection Agency (EPA) in cooperation with the United States Navy under EPA Cooperative Agreement Number CR820755-01-4. Funding for this work was provided by the Strategic Environmental Research and Development Program (SERDP) through the EPA (a joint program of the Department of Defense, the Department of Energy, and the Environmental Protection Agency), and this support is gratefully acknowledged.

The authors would like to express their gratitude to the project officer, Theodore G. Brna, for his help and suggestions throughout the work.

Special thanks are extended to the Wolverine Tube, Inc. for providing the test tubes (1024-fpm, 1575-fpm, Turbo-CII, Turbo-B, and Turbo-BII tubes), and the Trane Co. for supplying the spring-type turbulators.

The support of Department of Mechanical Engineering at Iowa State University where this work was done is also greatly appreciated.

CHAPTER 1

INTRODUCTION

BACKGROUND

Because of their high heat transfer performance, tubes with enhanced geometries are widely used in heat exchangers in refrigeration and air-conditioning systems. This research (Phase II) evaluates the shell-side heat transfer performance of HFC-236ea with the use of the high performance enhanced tubes that have not yet been used in Navy shipboard chillers.

Based on simulation results for a simple vapor compression cycle, HFC-236ea was found by Bare [1] to operate similarly to CFC-114 in capacity, performance, and system pressures. The refrigerant of interest in this study, known as either HFC-236ea or R-236ea, has no depleting potential of stratospheric ozone and is considered to be a prospective replacement for CFC-114 (also known as R-114) in Navy shipboard chillers. HFC-236ea has a molecular formula of $CF_3CHFCHF_2$, a molecular weight of 152.01, and normal boiling point of 6.5°C. In addition, it is non-flammable as is CFC-114. The basic properties of HFC-236ea at the operating temperatures of 2°C and 40°C are presented in Appendix A.

The feasibility of the HFC-236ea system's replacing the existing CFC-114 system was assessed in Phase I [2], a study of the comparative heat transfer performance of CFC-114 and HFC-236ea for a plain tube and two types of conventional finned tubes (1024-fpm and 1575-fpm tubes) that are presently used with CFC-114 in shipboard chillers. The project summary of the Phase I report is presented in Appendix B for reference. The investigation of the heat transfer performance of HFC-236ea was extended from the Phase I study of conventional finned tubes during shell-side condensation and pool boiling to the current study (Phase II) of high performance enhanced tubes (Turbo-CII, Turbo-B, and Turbo-BII tubes) during shell-side condensation, pool boiling, and spray evaporation.

Since new enhancement geometries have been introduced [3] and since no practical correlations exist to predict heat transfer coefficients as a function of refrigerant types and tube surface geometries, experiments are the most reliable means to determine the heat transfer coefficients provided by the high performance enhanced tubes proposed for alternative refrigerants. The focus of this study is to evaluate the shell-side heat transfer performance of HFC-236ea using selected high performance enhanced tubes. Note also that, as stated above, none of these tubes have been previously installed in shipboard heat exchangers.

RESEARCH PROGRAM

Objectives

This study (Phase II) evaluated the heat transfer performance of HFC-236ea during shell-side condensation and pool boiling on the high performance enhanced tubes that have never been installed in shipboard chillers. In addition, spray evaporation, which might provide higher heat transfer rates and require lower refrigerant inventory than pool boiling, was evaluated. In view of the shipboard space limitation and the need for energy conservation in the world, a compact heat exchanger providing high heat transfer performance with a small amount of refrigerant is desirable.

This research obtained HFC-236ea data tested with high performance tubes for the redesign of existing and optimization of new chillers employing HFC-236ea. The comparative heat transfer performance of the integral finned tubes for HFC-236ea with that for CFC-114 was previously evaluated in the Phase I study [2] for retrofitting the existing CFC-114 system.

Scope

Since a detailed literature review on the subject of shell-side refrigerant heat transfer was prepared previously in Phase I [2], this report does not attempt to review all the available literature, but rather focuses on comparing the test results obtained in the earlier study with those in this study (Phase II) to assess the applicability of the high performance enhanced tubes relative to conventional finned tubes in shell-side heat exchangers.

Heat transfer research was performed on three types of high performance enhanced tubes (Turbo-B, Turbo-BII, and Turbo-CII), which have not yet been used in commercial shipboard chillers. Using mainly the same test facility which allows analysis of three different heat transfer forms (condensation, pool boiling, and spray evaporation), data were taken for condensation on a Turbo-CII tube that is designed to enhance shell-side condensation, pool boiling on Turbo-B and Turbo-BII tubes which are recommended for use in nucleate boiling and spray evaporation on Turbo-CII and Turbo-B tubes, as well as on a 1575-fpm integral finned tube. The three tubes (i.e., an enhanced condensation tube, an enhanced boiling tube, and an integral finned tube) tested in spray evaporation were chosen from each of the three tube groups with distinctively different surface geometries.

The refrigerant saturation temperatures were set at 2°C for both pool boiling and spray evaporation and at 40°C for condensation, which are typical operating temperatures in evaporators and condensers of Navy shipboard water chillers, respectively. The heat flux ranged from 15 kW/m^2 to 40 kW/m^2 for condensation and pool boiling, and 10 kW/m^2 to 30 kW/m^2 for spray evaporation.

The shell-side heat transfer performance of HFC-236ea for the high performance enhanced tubes evaluated in this study was compared with that for the plain tube and integral finned tubes, which were tested in an earlier study. The focus of this investigation was to determine the optimum tube types for shell-side heat transfer

(condensation, pool boiling, and spray evaporation) of HFC-236ea and also the better heat transfer form between pool boiling and spray evaporation for evaporation of HFC-236ea. The comparative heat transfer performance of HFC-236ea for spray evaporation with pool boiling was also made by using a Turbo-B tube and a 1575-fpm tube. Since a smaller refrigerant volume is required for performing spray evaporation relative to pool boiling, a spray evaporator rather than a flooded evaporator might potentially reduce the initial cost for building a vapor-compression system.

The condensation and pool-boiling data taken for the plain tube and integral finned tubes in Phase I [2] were compared with the results obtained in this study using the same test section previously used. In this study, data were taken by increasing the heat loads for condensation and by decreasing the heat loads for pool boiling. Each tube type for spray evaporation was tested with increasing and decreasing heat flux. Repeat runs were performed on different days for all the tubes tested in these three heat transfer forms.

Data are mainly presented in the form of heat transfer coefficients versus heat flux, since the heat transfer coefficients for the three heat transfer forms evaluated depend on the heat load.

CHAPTER 2

CONCLUSIONS

The heat transfer performance of HFC-236ea was evaluated during shell-side condensation and pool boiling in Phase I [2] for a plain tube and two conventional low-fin tubes (1024-fpm and 1575-fpm tubes). The integral low-fin tube types have been used for many years in shell-and-tube heat exchangers of CFC-114 chillers installed in Navy ships. As the next step, the heat transfer performance of HFC-236ea was evaluated when the high performance enhanced tubes were used during condensation, pool boiling, and spray evaporation. Since these tube types have not been employed in the Navy shipboard chillers, the results reported herein can be applied to the design of new chillers.

For condensation of HFC-236ea at 40°C, the high performance Turbo-CII tube performed better than the plain tube and the integral finned tubes, which were tested in an earlier study. The heat transfer coefficients for the Turbo-CII tube were approximately double those for the integral finned tubes and 5 to 10 times those for the plain tube.

For pool boiling of HFC-236ea at 2°C, the Turbo-BII and Turbo-B tubes provided higher heat transfer performance compared with the plain tube and integral finned tubes, which were tested in a previous study. The Turbo-BII tube outperformed the other tube types tested and provided heat transfer coefficients 1.2 to 1.7 times those of the Turbo-B tube. In turn, the Turbo-B tube yielded 1.1 to 1.3 times the heat transfer coefficients of the 1024-fpm tube, 1.4 to 1.5 times the values of the 1575-fpm tube, and 1.8 to 2.2 times the values of the plain tube. The heat transfer coefficient in pool boiling increased with increasing heat flux.

For spray evaporation of HFC-236ea at 2°C, the Turbo-B tube performed better than the 1575-fpm tube and Turbo-CII tube. The Turbo-B tube provided 1.1 to 1.2 times the heat transfer coefficients of the Turbo-CII tube, and 1.6 to 1.8 times the values of the 1575-fpm tube. With increasing heat flux, the heat transfer coefficient in spray evaporation increased until the heat flux reached around 15 kW/m^2 and then decreased afterward.

Pool boiling and spray evaporation of HFC-236ea were compared for a 1575-fpm tube and a Turbo-B tube. In general, spray evaporation provided better heat transfer below the heat flux of 30 kW/m^2 compared with pool boiling. At a heat flux of 15 kW/m^2, the heat transfer performance of the Turbo-B tube in spray evaporation was 2.3 times that in pool boiling, and the performance of the 1575-fpm tube in spray evaporation was 1.2 times as large as the value in pool boiling. While at a heat flux of 30 kW/m^2, the boiling coefficients in these two different heat transfer forms were similar for both the Turbo-B tube and 1575-fpm tube.

In summary, the results of the comparison demonstrate that there are substantial increases in heat transfer provided by the use of the high performance enhanced tubes compared to the plain tube and conventional finned tubes that are currently used with CFC-114 in Navy shipboard chillers.

CHAPTER 3

RECOMMENDATIONS

Recommendations for future research in heat transfer evaluation of alternative refrigerants for CFC-114 or other CFCs are listed as follows,

1. Test the other proposed substitutes for CFC-114 and evaluate their compatibility with the existing systems using the CFC-114.
2. Compare the data for alternative refrigerants with the existing heat transfer correlations and derive new ones. Develop theoretical models to satisfactorily explain the phenomena observed in the two-phase heat transfer occurring on tubes with complex geometries.
3. Investigate the effects of vapor velocity on shell-side condensation and the effects of oil in refrigerant on the pool boiling performance.
4. Test the heat transfer performance of the other enhanced tubes made or suggested by different manufacturers and other researchers.
5. For spray evaporation testing, extend the tested heat flux range to higher values and reduce the occurrence of dry-out phenomenon at high heat fluxes by improving liquid distribution on tubes and pumping power.

CHAPTER 4

EXPERIMENTAL DESCRIPTION

EXPERIMENTAL APPARATUS

Even though all the experiments were performed on the same test rig, different experimental arrangements were required for testing condensation, pool boiling, and spray evaporation. The refrigerant was delivered to the test section through several routes with different auxiliary facilities for the three different tests. The experimental arrangements for testing these three heat transfer forms are illustrated in Figures 4.1 through 4.3, respectively. The main components of the test facility include the test section, test tubes, closed water loop, closed refrigerant loop, glycol/water chiller, and data acquisition system.

The heat transfer experiments were performed in a cylindrical, stainless steel chamber equipped with sight glasses in the front and the rear wall for observation of heat transfer phenomena. On the top of this test section, there are two ports which are passageways for vapor and five threaded ports where spray nozzles could be installed with compression fittings for testing spray evaporation. On the bottom of the test section are two additional ports that serve as liquid paths. Two tube sheets with threaded ports are attached to both ends of the cylindrical chamber so that the tube can be changed by adjusting only the compression fittings.

The tubes tested were copper alloy and had a 19.1-mm (3/4-in.) nominal outside diameter and external enhanced surface geometries. The inner tube surface of the high performance enhanced tubes was originally enhanced by the manufacturer for increasing the in-tube heat transfer coefficient. In addition, a spring-type turbulator was inserted inside each tube tested to promote continuous turbulence and thus balance the thermal resistance on both sides of the tube. The turbulator was provided by the Trane Company located in La Crosse, Wisconsin and made of a wire coil with a coil diameter enabling it to be held at the inner tube surface by the friction fit between the stretched spring and the tube wall. The geometric specifications of the tubes tested are given in Table C.1 in SI units and Table C.2 in English units. All tubes tested were supplied by Wolverine Tube, Inc., Decatur, Alabama. The readers can refer to the company for more detailed information on these tubes.

All the high performance enhanced tubes evaluated have three-dimensional, outward-enhanced geometries. The Turbo-CII tube has short roughened fins, and the Turbo-B and Turbo-BII tubes are characterized by reservoir-type (or re-entrant) cavities with narrow openings constructed by a compressed, doubly cut knurl.

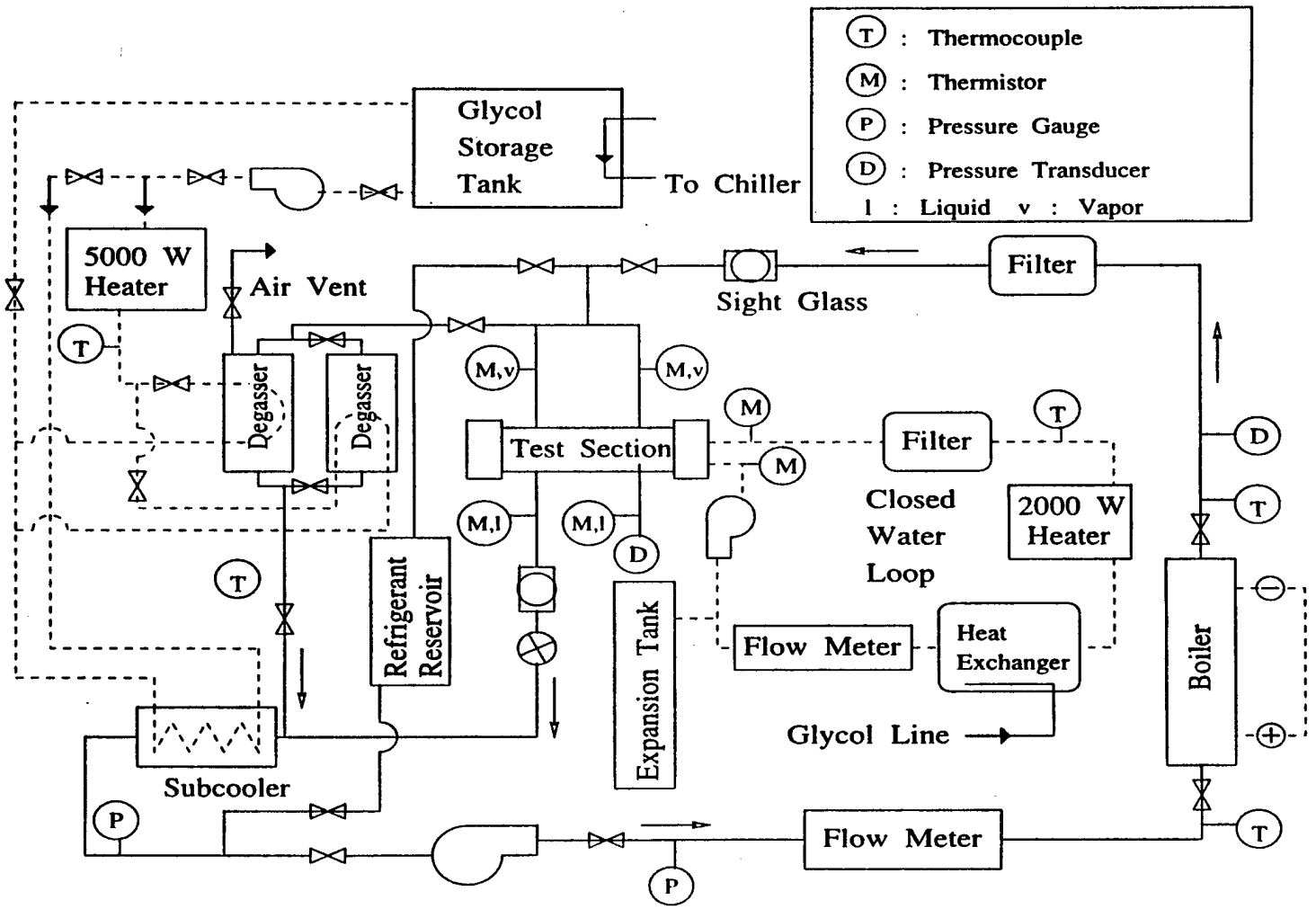

Figure 4.1. Schematic of test facility for condensation tests.

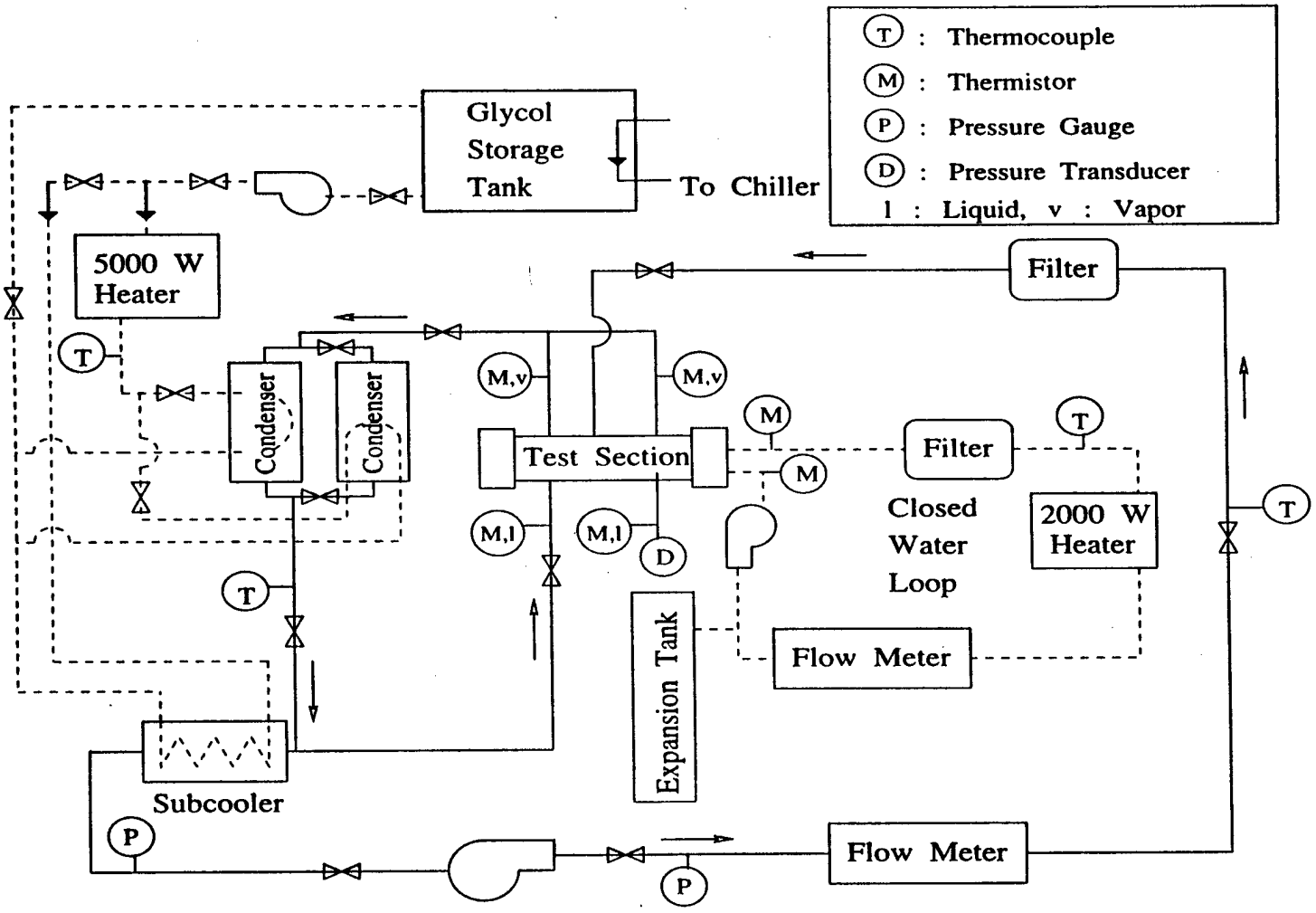

Figure 4.2. Schematic of test facility for pool boiling tests.

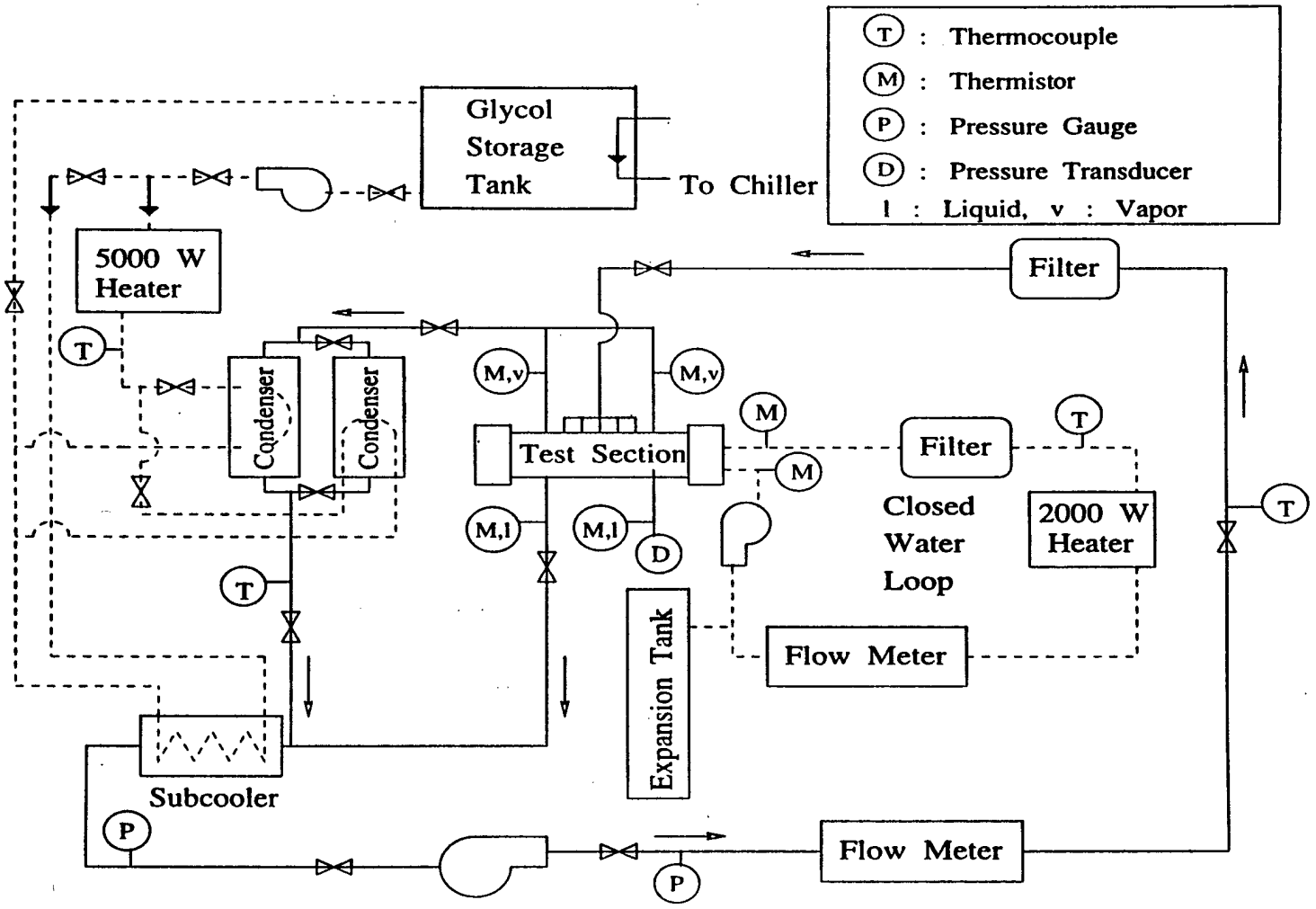

Figure 4.3. Schematic of test facility for spray evaporation tests.

The Turbo-B tube is made based on a 1575-fpm (40-fpi) tube, whereas the Turbo-BII tube is based on a 1969-fpm (50-fpi) tube. The higher fin density of the Turbo-BII tube provides a higher density of nucleation sites. In addition, the boiling sites of the Turbo-BII tube are shape-optimized for specific types of refrigerants, while those of the Turbo-B tube are not.

The closed water loop consists mainly of a storage tank, two triplex diaphragm pumps, a flow meter, an immersion heater, and a dual-tube heat exchanger. The heater and heat exchanger were used to control the water temperature.

The glycol/water mixture was pumped through a chiller of 105-kW (30-ton) cooling capacity and could be supplied through manifolds to a dual-tube heat exchanger, two condensers, and a subcooler.

While water was circulated in the test tube, refrigerant was delivered by a diaphragm pump to the test section through several routes with different auxiliary facilities for different purposes. A stainless steel boiler was used to vaporize refrigerant before it reached the test section for the condensation tests; a subcooler and two condensers were utilized to condense refrigerant after it was boiled in the test section for the evaporation tests. A reservoir was set for adjusting the refrigerant quantity required for the tests.

A detailed description of the apparatus can be found in Huebsch and Pate [2].

INSTRUMENTATION AND CALIBRATION

The temperature necessary for calculating the shell-side heat transfer coefficient was measured by thermistors and compared with the saturation temperature corresponding to the pressure read by a pressure transducer. The acceptable difference in these two temperatures was within ± 0.2°C for the condensation tests and ± 0.1°C for the evaporation tests.

Due to the low pressure of HFC-236ea and the low operating temperatures for the evaporation tests, the strain-gauge pressure transducer which was used to measure the saturation pressure of the test section was sent to the Setra Company for calibration instead of being calibrated in the laboratory with a simple dead-weight tester. The thermistors were also re-calibrated by using a constant temperature bath. Lack of scatter found in the calibration results indicates the consistency of the calibration.

The instrumentation accuracy is ± 0.05°C for the thermistors, ± 0.1% of the full scale for the pressure transducer, and ± 0.20% of the full scale for the water mass flow meter.

EXPERIMENTAL PROCEDURES

Condensation Tests

After the system was verified to be free of leakage, it was evacuated by a vacuum pump for 8 hours. Subsequently, the refrigerant was charged into the system. The noncondensible gas in the system was purged

through the vent valves on the top of the degassers (condensers) while the refrigerant was boiling in the test section. This degassing procedure was repeated until the temperatures registered by the thermistors compared with the saturation temperature corresponding to the pressure transducer reading were within 0.2°C. The condensers were isolated once the purging had been completed.

Liquid refrigerant delivered from the pump was converted to vapor in a boiler and then condensed by the cooler water flowing through the test tube. The refrigerant condensed in the test section flowed back to the pump and was recirculated. In the meantime, the water and refrigerant flow rates along with the temperatures of the refrigerant in the boiler and water were adjusted to meet the required energy rate balance and maintain the refrigerant saturation temperature of 40°C in the test section. Meanwhile, the temperature change of water through the test section was controlled at 2°C. Temperatures of water flowing inside the test tube were controlled by a heater and heat exchanger using a glycol/water mixture (coolant).

The flow rates of the two fluids (water and refrigerant) and the temperatures of the boiler fluid and water were varied to meet the different requirements of the energy rate balance until the whole range of heat fluxes had been tested.

Pool Boiling and Spray Evaporation Tests

Refrigerant was boiled by the circulating warm water in the test section and condensed in the condensers by the circulating glycol/water mixture (coolant) and then returned to the pump. The refrigerant temperature was maintained at a steady state value of 2°C by controlling the flow rates and temperatures of the water and condenser coolant. The circulating water was heated by a heater, and the water temperature difference between the inlet and outlet of the test section was controlled at 2°C. The two condensers were adjusted to work in parallel or independently for the different heat transfer duties.

Adjustment of the flow rates and temperatures of the water and condenser coolant to meet the different requirements of the energy rate balance was repeated until the whole range of heat fluxes had been tested.

Spray evaporation testing was operated in a similar way as pool boiling testing except that the refrigerant was distributed to the test section through a set of nozzles, and the tube was not immersed in a pool of liquid refrigerant.

A detailed description of experimental procedures for condensation and pool boiling is given by Huebsch and Pate [2].

DATA REDUCTION

The average shell-side heat transfer coefficient (h) for a single-row tube with two passes was determined using the heat transfer rate balance between the two fluids (refrigerant and water), where a log mean temperature difference (LMTD) method was applied. The measured parameters for calculating the shell-side heat transfer coefficient were the temperatures of water entering and leaving the test section, the refrigerant saturation temperature and pressure in the test section, and the flow rates of water and refrigerant.

The heat flux was controlled throughout the experiments to obtain the average shell-side heat transfer coefficient. The heat flux during tests ranged from 15 kW/m^2 to 40 kW/m^2 for condensation and pool boiling, and 10 kW/m^2 to 30 kW/m^2 for spray evaporation.

A modified Wilson plot was used to obtain the in-tube (tube-side) heat transfer coefficient, and then the average shell-side heat transfer coefficient was extracted from the UA value by applying the LMTD approach. Under steady state conditions, the heat transfer rate between refrigerant and water is formulated as,

$$q = U_o \cdot A_o \cdot LMTD \tag{4.1}$$

where the heat transfer rate (q, W) was calculated from the measured inlet and outlet temperatures of water ($T_{i,in}$ and $T_{i,out}$, °C); specific heat of water (Cp_i, J/kg·K); and water flow rate ($\dot{m}_i$, kg/s),

$$q = \dot{m}_i \cdot Cp_i \cdot (T_{i,out} - T_{i,in}) \tag{4.2}$$

The log mean temperature difference (LMTD, °C) in Equation 4.1, defined by Equation 4.3, was calculated from the measured refrigerant saturation temperature (T_{sat}, °C) in the test section and the water temperatures entering and leaving the test section.

$$LMTD = \frac{(T_{i,out} - T_{i,in})}{\ln \dfrac{(T_{sat} - T_{i,in})}{(T_{sat} - T_{i,out})}} \tag{4.3}$$

Obtaining q from Equation 4.2 and LMTD from Equation 4.3, and re-arranging Equation 4.1, the overall heat transfer coefficient (U_o, $W/m^2 \cdot K$) based on the outer heat transfer surface area of the tube (A_o, m^2) was solved.

$$U_o = \frac{q}{A_o \times LMTD} \tag{4.4}$$

The shell-side heat transfer coefficient (h, W/m^2·K) was then determined from the overall heat transfer coefficient by subtracting the tube-wall thermal resistance (R_w, K/W) and the forced convective heat transfer coefficient (h_i, W/m^2·K) on the water side,

$$h = \frac{1}{\frac{1}{U_o} - \frac{A_o}{A_i}\frac{1}{h_i} - A_o R_w} \tag{4.5}$$

The tube wall thermal resistance in Equation 4.5 is given by

$$R_w = \frac{\ln(D_o / D_i)}{2\pi k_w L} \tag{4.6}$$

and the in-tube heat transfer coefficient (h_i) was calculated by the familiar Sieder-Tate equation listed below and deduced by a modified Wilson plot technique.

$$h_i = STC \cdot \frac{k_i}{D_i} Re_i^{0.8} Pr_i^{0.33} \left(\frac{\mu_i}{\mu_w}\right)^{0.14} \tag{4.7}$$

The thermal conductivity of tube wall (k_w, W/m·K) in Equation 4.6 and the viscosity of water (μ_w, N·s/m^2) in Equation 4.7 were calculated using the tube wall temperature ($T_w = (T_{sat}+T_{i,bulk})/2$, °C). The Reynolds number (Re_i), Prandtl number (Pr_i), thermal conductivity (k_i, W/m·K), and dynamic viscosity (μ_i, N·s/m^2) in Equation 4.7 were based on the average bulk temperature ($T_{i,bulk} = (T_{i,in}+T_{i,out})/2$, °C) and properties of water. The remaining parameters in the equations above: L (m), D_i (m), D_o (m), and A_i, (m^2) are the tube length, inside tube diameter, outside tube diameter, and inner surface area of the tube, respectively.

Based on the modified Wilson plot technique, the constant STC (Sieder-Tate coefficient) required in Equation 4.7 was determined by boiling refrigerant at a constant heat load of 1.5 kW and maintaining a constant saturation temperature of 2°C on the outside of the tube under test but varying the water flow rate in the tube.

The following equation was generalized by substituting Equation 4.7 for h_i into the equation of thermal resistance (Equation 4.5):

$$Y = \frac{1}{STC} \cdot X + \frac{1}{h} \tag{4.8}$$

where

$$Y = \frac{1}{U_o} - A_o R_w \tag{4.9}$$

$$X = \frac{A_o / A_i}{\frac{k_i}{D_i} Re_i^{0.8} Pr_i^{0.33} \left(\frac{\mu_i}{\mu_w} \right)^{0.14}} \tag{4.10}$$

The Reynolds number of water for the tests ranged from 2800 to 18000. Corresponding to the different water flow rates, the Y ($m^2 \cdot K/W$) values versus X ($m^2 \cdot K/W$) values used in Equation 4.8 were plotted in Figure 4.4 for the Turbo-CII, Turbo-B, and Turbo-BII tubes. As indicated in Equation 4.8, the STC is the inverse of the slope of the X-Y curve. The constant STC value was found to be 0.131 for the Turbo-B tube, 0.108 for the Turbo-BII tube, and 0.1138 for the Turbo-CII tube.

The numerical values for all the data obtained in this study are tabulated in Appendix D.

EXPERIMENTAL UNCERTAINTY OF DATA

The estimate of the uncertainty for the shell-side heat transfer coefficients calculated in this study, following the uncertainty analysis described in the Phase I report [2], is listed in Table 4.1 for the condensation data, Table 4.2 for the pool boiling data, and Table 4.3 for the spray evaporation data. Appendix E presents the derivation of uncertainty analysis equations for the calculated shell-side heat transfer coefficients.

The Turbo-CII tube was tested twice for condensation and spray evaporation. Results for the first test show that the Turbo-CII tube produced relatively high shell-side heat transfer coefficients at low heat loads, and the overall heat transfer coefficients were dominated by the tube-side resistance. In other words, the relatively low thermal resistance on the shell side caused a large uncertainty in the shell-side heat transfer coefficients.

The large uncertainty produced by the Turbo-CII tube for condensation at low heat loads is in accordance with that reported by Huber et al. [4] who found that the maximum experimental uncertainty was ± 36% for the average bundle heat transfer coefficients and ± 53% for the average row heat transfer coefficients.

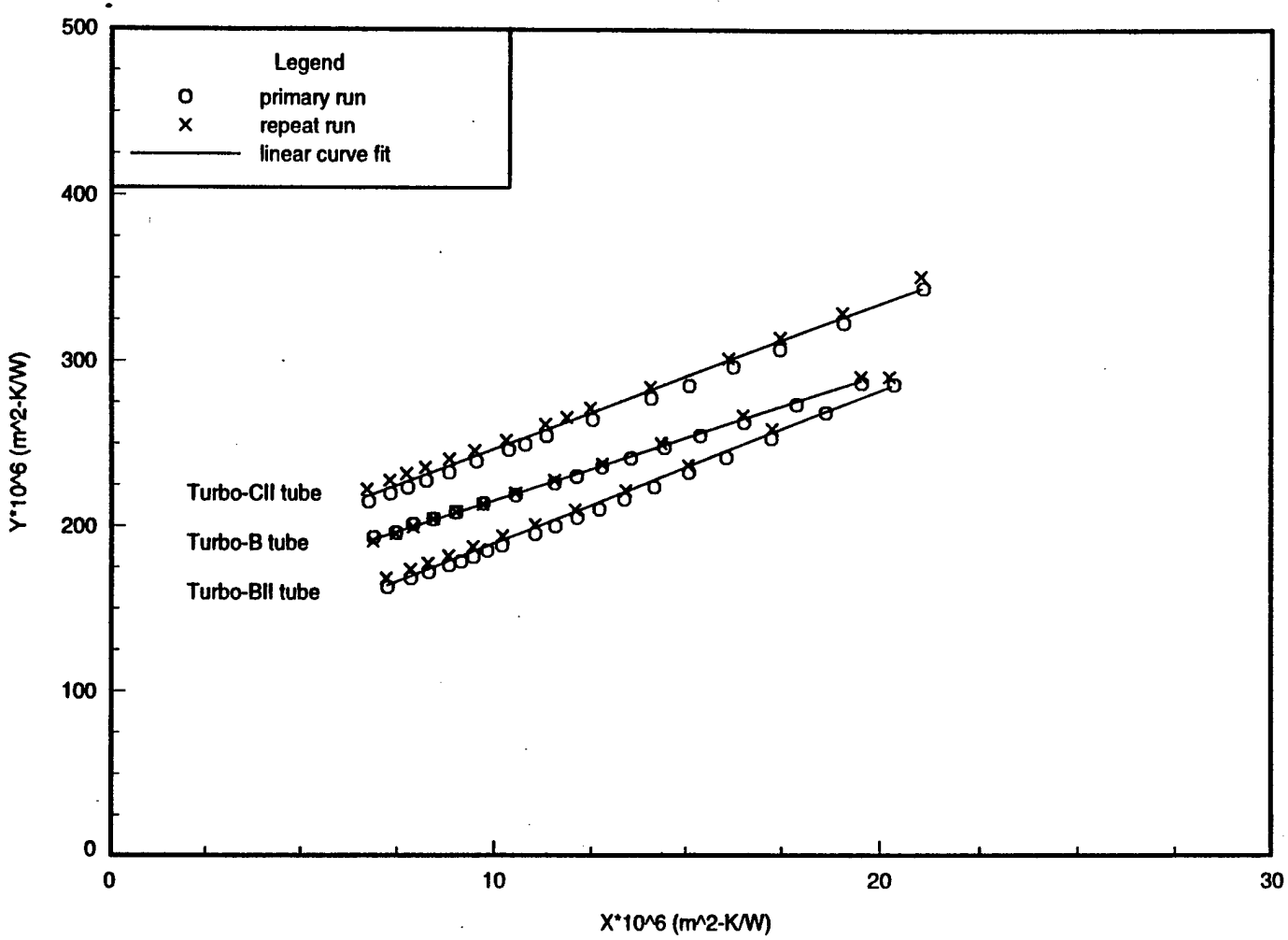

Figure 4.4. Wilson plot data for a Turbo-CII, a Turbo-B, and a Turbo-BII tube (D =19.1 mm) with turbulators installed.

TABLE 4.1: UNCERTAINTY IN THE SHELL-SIDE HEAT TRANSFER COEFFICIENTS FOR CONDENSATION

Heat flux	15 kW/m^2	30 kW/m^2	40 kW/m^2
Uncertainty for the Turbo-CII tube	± 8%	± 6%	± 6%

TABLE 4.2: UNCERTAINTY IN THE SHELL-SIDE HEAT TRANSFER COEFFICIENTS FOR POOL BOILING

Heat flux	15 kW/m^2	30 kW/m^2	40 kW/m^2
Uncertainty for the Turbo-B tube	± 9%	± 7%	± 7%
Uncertainty for the Turbo-BII tube	± 14%	± 9%	± 8%

TABLE 4.3: UNCERTAINTY IN THE SHELL-SIDE HEAT TRANSFER COEFFICIENTS FOR SPRAY EVAPORATION

Uncertainty (±%)	Refrigerant flow rate (kg/min)	Heat flux (kW/m^2)		
		10	20	30
Uncertainty for the Turbo-B tube	2.6	± 25%	± 13%	± 6%
	2.8	± 27%	± 14%	± 7%
	3.0	N/A	± 14%	± 8%
	3.2	± 29%	± 14%	± 8%
Uncertainty for the Turbo-CII tube	2.6	± 25%	± 11%	± 6%
	2.8	± 24%	± 12%	± 7%
	3.0	± 24%	± 12%	± 7%
	3.2	N/A	± 13%	± 8%
Uncertainty for the 1575-fpm tube	2.6	± 16%	± 9%	± 6%
	2.8	± 17%	± 10%	± 6%
	3.0	± 17%	± 11%	± 7%
	3.2	± 17%	± 11%	± 7%

In order to improve the single-phase heat transfer coefficient of water flowing inside the tube for balancing the thermal resistance on both sides of the tube, the Wilson data plot was generated again for the tube, this time with a denser turbulator inserted to create greater turbulence in the tube. The Sieder-Tate coefficient for the Turbo-CII tube was substantially increased from 0.0484 to 0.1138. As shown in Equation 4.7, the STC is in direct proportion to the in-tube heat transfer coefficient (h_i); thus, a large STC value means a large h_i value.

It was also found that a linear curve could fit the data for a Wilson plot better when the tube side had a denser turbulator inserted. In addition to the Turbo-CII tube, the Turbo-B tube was also re-tested by installing a denser in-tube turbulator in order to reduce the uncertainty in the shell-side heat transfer coefficients. The Sieder-Tate coefficient for the Turbo-B tube was almost doubled from 0.067 to 0.131. Another reason for a re-test of these tube types was that the tubes were found to be contaminated with oil, which might have been due to the lubricant applied to the tubes when they were made. The tubes were cleaned before they were tested by using a solvent, CFC-113.

Results of the spray-evaporation tests show that a larger uncertainty occurred at low heat fluxes. This larger uncertainty was attributed to the low operating temperatures of water, which resulted in small LMTD values.

CHAPTER 5

CONDENSATION RESULTS

OVERVIEW

Condensation is defined as the removal of latent heat from a system in such a way that vapor is transformed into liquid. Condensation on horizontal tubes is mainly affected by the combined forces of surface tension and gravity, which play key roles in the removal of condensate. When refrigerant vapor contacts cooler tubes that are below its saturation temperature, condensate formed on the tubes is a resistance to heat transfer on the tube surface. The liquid condensed on a rough surface is drawn from the fins or ridges into the grooves by surface tension forces that act to retain the condensate between fins. The liquid is removed from the tubes by either aerodynamic drag forces or by gravitational forces when the grooves are flooded with the condensate.

Enhanced condensation tubes were developed to promote more rapid removal of condensate as well as to increase the available area for heat transfer. The high performance Turbo-CII tube that has been suggested for improving heat transfer in shell-side condensation was tested in this study. The removal mechanism for condensate strongly depends on the geometrical characteristics of the tube surface, which significantly affect surface tension forces. Proper surface curvature can effectively drain condensate, avoid condensate inundation and reduce the film thickness on the tubes, and hence, increase the condensation rate. The effects of fin density and geometries on condensation were investigated by Briggs et al. [5] and Sukhatme et al. [6]. In addition, Ullmann and Letan [7] studied the influence of noncondensable gases in the condensing vapor, which can degrade the heat transfer rates.

RESULTS AND DISCUSSION

Condensation Performance for the Turbo-CII Tube

Figure 5.1 shows that the heat transfer coefficient for the Turbo-CII tube increased as heat flux increased. Condensation data published by Huber [8] for CFC-11 and by Huebsch and Pate [2] for CFC-114 and HFC-236ea showed similar trends.

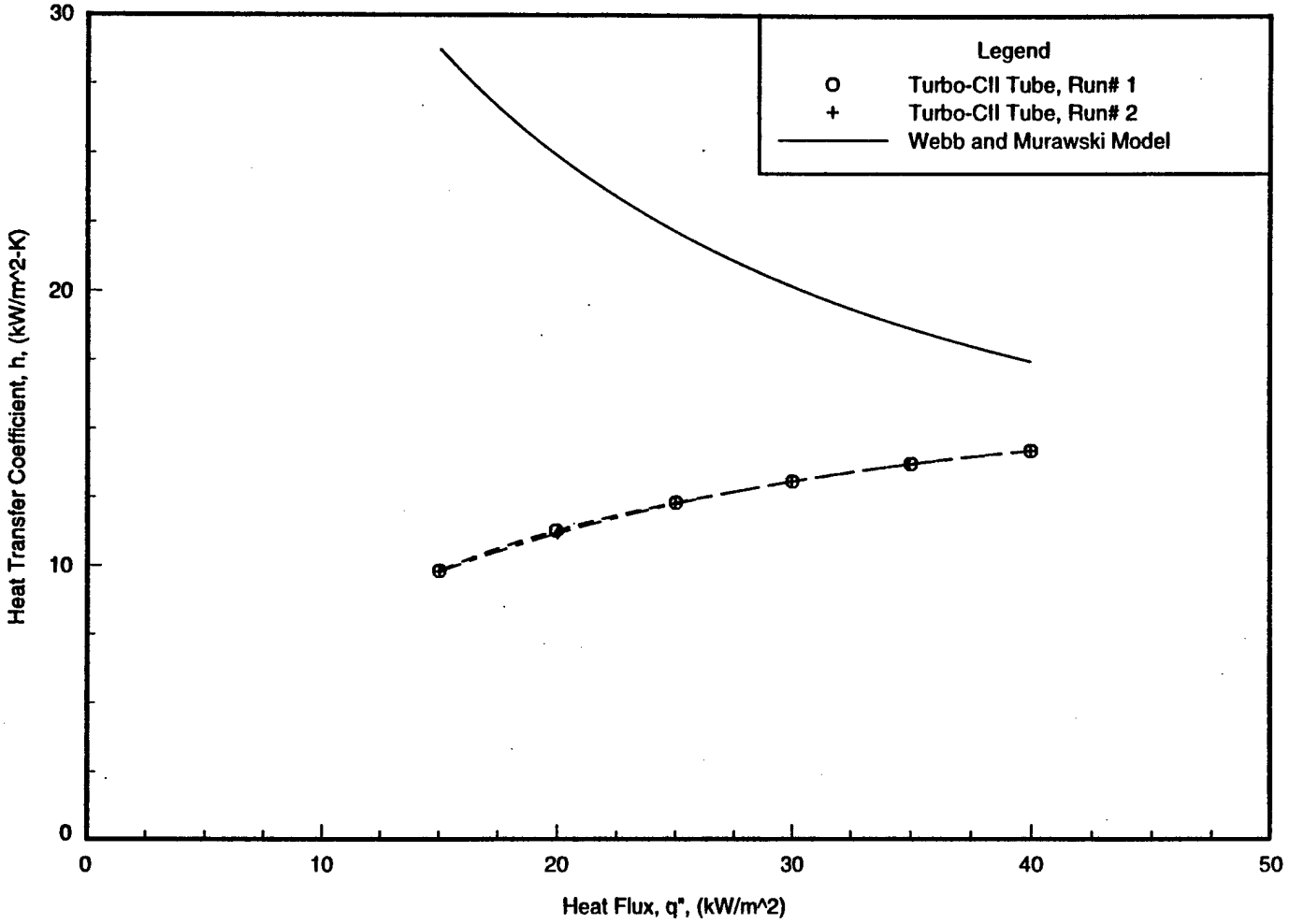

Figure 5.1. Condensation heat transfer coefficients of HFC-236ea on a Turbo-CII tube (D = 19.1 mm) at T_{sat} = 40°C.

As mentioned in Chapter 4, the Turbo-CII tube was tested twice, using different in-tube turbulators in the two tests. In the first test, the heat transfer coefficients dropped markedly as the heat flux increased. These results are consistent with those obtained by and Huber et al. [4]. However, as previously mentioned the first tests had large uncertainty and therefore were considered to be erroneous.

In addition, the large uncertainty accompanying the shell-side heat transfer coefficients determined from the first tests is consistent with that obtained by Huber et al. [4]. However, the heat transfer coefficients calculated from the second tests increased as the heat flux increased, and the uncertainty in the shell-side heat transfer coefficients was substantially reduced by increasing the in-tube (tube-side) heat transfer coefficients.

The different in-tube turbulators caused a substantial difference in results between the two sets of tests. Each different in-tube turbulator was found to affect not only the in-tube heat transfer coefficients but also the operating temperatures of water through the test section. In fact, from the equations mentioned before, Equation 4.1,

$$q = U_o \cdot A_o \cdot LMTD \tag{4.1}$$

and Equation 4.5,

$$\frac{1}{h} = \frac{1}{U_o} - \frac{A_o}{A_i}\frac{1}{h_i} - A_o R_w \tag{4.5}$$

the in-tube and shell-side heat transfer coefficients (h_i and h) and log mean temperature difference (LMTD) can be seen to be mutually related, where the coefficients are related to the overall heat transfer coefficient (U_o) and the LMTD is related to the operating temperatures of water. Once the in-tube heat transfer coefficient, h_i, is changed due to the installation of different in-tube turbulators, the other two variables, h and LMTD, will also change. As shown in Equation 4.5, the different values of the heat transfer coefficients for the two fluids (i.e., h and h_i) will change the resistance to heat transfer ($1/U_o$). It is therefore important to properly equalize the two coefficients.

The data for the repeatability run can be seen in Figure 5.1. The experiment is shown to be repeatable by comparing the data points for the "primary run" and the "repeat run". Both runs were taken in steps from low heat flux to high heat flux, but on two different days.

Comparison with an Existing Correlation

The condensation data obtained in the current study for the Turbo-CII tube were compared to the existing correlation presented by Webb and Murawski [9]. The equations derived by Webb and Murawski were based on the condensation heat transfer coefficients of CFC-11 for five enhanced tube types, including one two-dimensional

finned tube and four three-dimensional enhanced tubes. The heat transfer coefficient for the Nth tube row (h_{NR}, $W/m^2 \cdot K$) was found to be only a function of the condensate Reynolds number leaving the Nth tube row (Re_{NR}),

$$h_{NR} = a \cdot Re_{NR}^{-n} \tag{5.1}$$

The average condensation coefficient (h_N, $W/m^2 \cdot K$) for a bundle was obtained by integrating Equation 5.1 from the first row to the Nth row,

$$h_N = [\frac{a}{1-n}(Re_{NR} - Re_1)][(Re_{NR})^{1-n} - (Re_1)^{1-n}] \tag{5.2}$$

where the Reynolds number for film condensation on tubes is defined as,

$$Re = \frac{4 \cdot \Gamma}{\mu} \tag{5.3}$$

The parameters Re_1, Re_{NR}, Γ, and μ are the condensate Reynolds number leaving the first row and the Nth row, respectively, condensate mass flow rate per unit tube length (kg/m-s), and dynamic viscosity of condensate (kg/m-s). The constants a and n shown in Equations 5.1 and 5.2 correspond to 257800 $W/m^2 \cdot K$ and 0.507, which were obtained for the Turbo-C tube. These constants were obtained by curve fitting the experimental data for h_{NR} versus Re_{NR}. The constants for the other tubes studied can be found in the original paper [9].

As shown in Figure 5.1, the model values obtained from Equation 5.1 are higher than the experimental results. The heat transfer coefficients predicted by the Webb–Murawski correlation are 20% to 1.9 times larger than the measured values.

The average heat transfer coefficients measured by Huber et al. [4] for the Turbo-CII tube were found to be greater than the predicted values based on Equation 5.2 with the same constants (a and n) given above. The measured values were three to four times higher than the predicted values for HFC-134a and 20% higher for HCFC-123 in their study. The authors attributed the poor agreement between the empirical and predicted results to the different refrigerants tested. This implies that the refrigerant properties, such as in the Prandtl number, affect heat transfer and should be included in the correlation to predict results.

It should be noted that the constant a and n used here were derived for the Turbo-C tube by Webb and Murawski [9]; not the Turbo-CII tube tested in this study and the research investigated by Huber et al. [4]. So far, no published correlation for a Turbo-CII tube has been found.

Comparison with Results of Phase I (Finned Tubes)

Figure 5.2 shows that the condensation heat transfer coefficient was a function of heat flux for the Turbo-CII tube as well as for the plain, 1024-fpm, and 1575-fpm tubes which were tested earlier [2]. As the heat flux increased, the heat transfer coefficient increased for the Turbo-CII tube as well as for the 1024-fpm and 1575-fpm tubes, while the coefficient decreased for the plain tube.

The Turbo-CII tube performed better than the plain, 1024-fpm, and 1575-fpm tubes. The Turbo-CII tube provided 1.9 times the heat transfer coefficients of the 1024-fpm and 1575-fpm tubes and 5.4 to 10.1 times the values of the plain tube.

Figure 5.3 shows the variation of heat transfer coefficient with the temperature difference between the saturated refrigerant and the tube wall for the existing shell-side condensation data of HFC-236ea over the heat flux range from 15 kW/m^2 to 40 kW/m^2. The Turbo-CII tube produced the smallest temperature difference among the tube types tested for a given heat flux, meaning that it provided the highest heat transfer coefficients.

Figure 5.3 also shows that the heat transfer coefficient depended on the temperature difference between the saturated refrigerant and the tube wall. As the temperature difference increased, the heat transfer coefficient increased for the Turbo-CII tube as well as for the 1024-fpm and 1575-fpm tubes, while it decreased for the plain tube.

All the theoretical models developed predict that the heat transfer coefficients should decrease as the temperature difference or heat load increase. With an increase in these variables, the heat transfer performance drops because more vapor is condensed and a thicker liquid film is formed so that the resistance on the tubes increases with increasing heat load. The more effective condensate removal provided by the Turbo-CII and two finned tubes relative to the plain tube was thought to affect the experimental results for these three tubes which is in opposition to current theory. The three tubes (Turbo-CII, 1024-fpm, and 1575-fpm) were not more severely inundated with condensate as the heat load increased, which results in a falling heat transfer coefficient during condensation.

Huber et al. [4] reported that the Turbo-CII tubes produced around two to three times larger heat transfer coefficients with HFC-134a than the 1024-fpm and 1575-fpm tubes based on the average bundle data. The results for the Turbo-CII tubes were around four times those for the 1024-fpm tubes and three times those for the 1575-fpm tubes based on the first-row data.

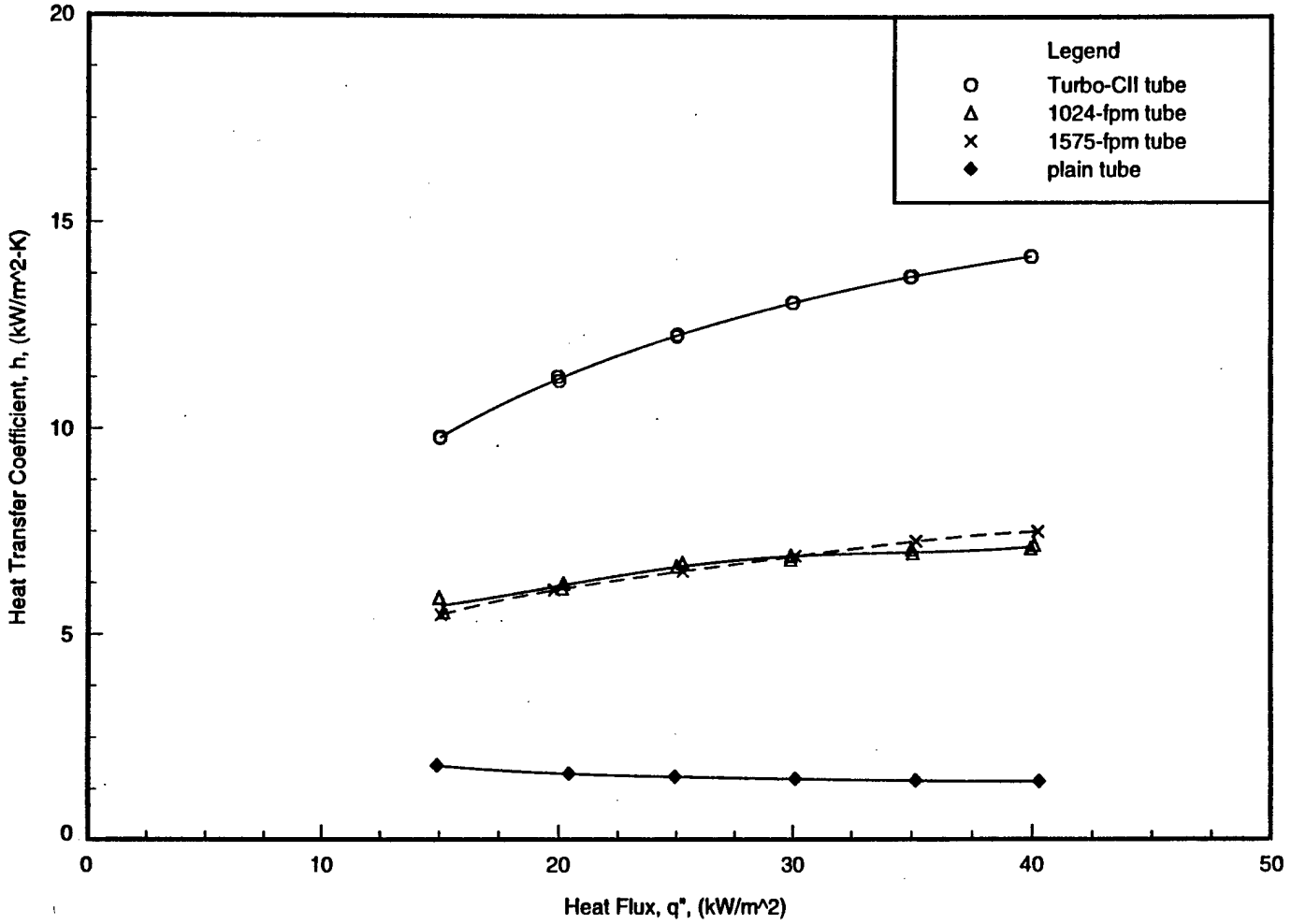

Figure 5.2. Condensation heat transfer coefficients of HFC-236ea using Turbo-CII, 1024-fpm, 1575-fpm, and plain tubes at T_{sat} = 40° C.

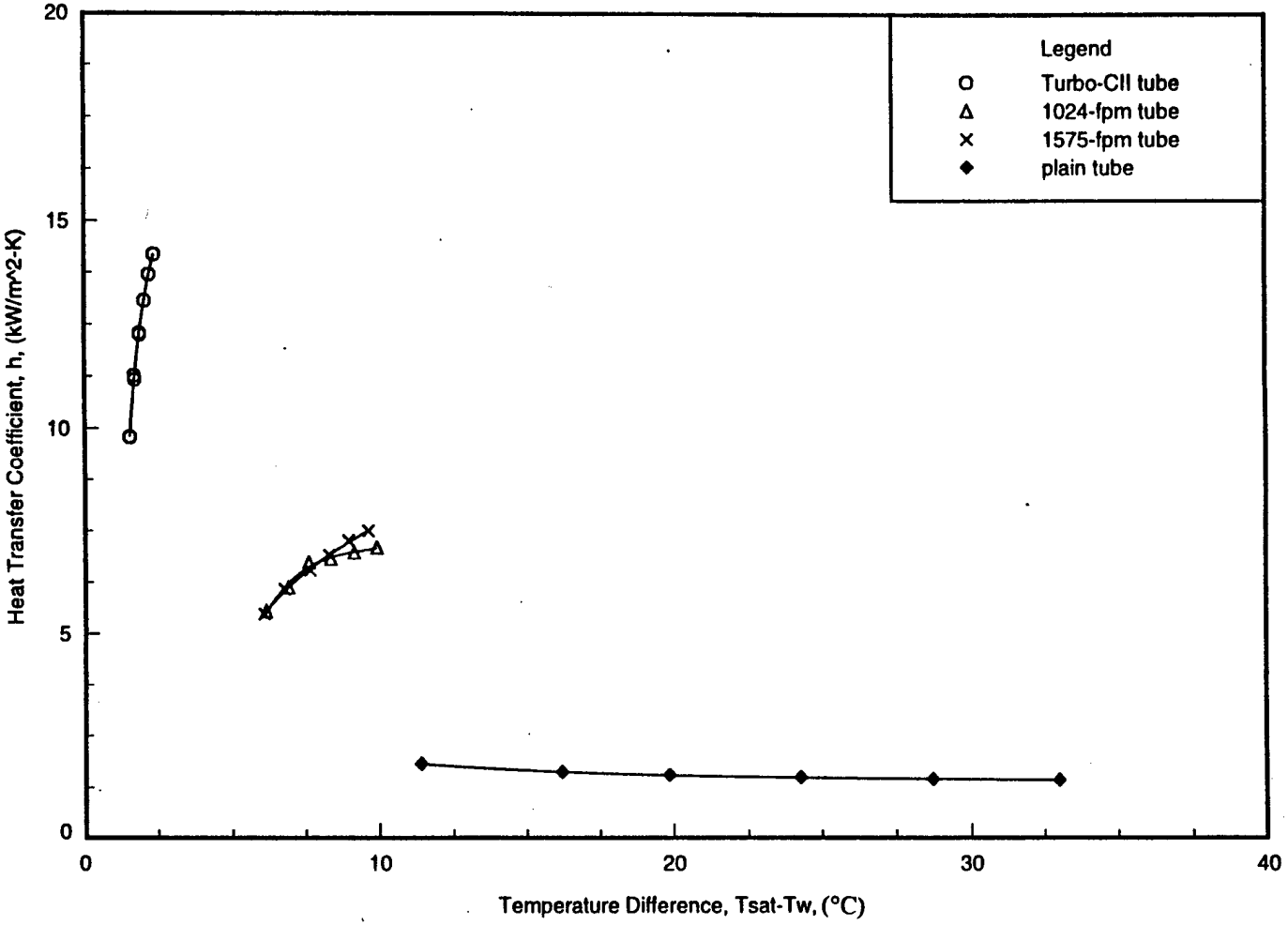

Figure 5.3. Effects of temperature difference on condensation heat transfer coefficients of HFC-236ea at T_{sat} = 40° C.

Applicability of Single-Tube Data to the Design of a Shell-Side Condenser

Row heat transfer coefficients were tested by Webb and Murawski [9], Cheng and Wang [10], and Honda et al. [11], for CFC-11, HFC134a, and CFC-113, respectively. Their results indicated that the row effects on the heat transfer coefficients were negligible for the tubes with integral low fins, but more significant for the tubes with complex fins. The heat transfer coefficients for the complex finned tubes were found to decline noticeably at the lower rows in a bundle where the tubes were arranged vertically with flow entering at the top.

Nguyen and Orozco [12] condensed CFC-113 on a vertical tier of four horizontal tube rows and investigated the effects of the row spacing between the enhanced tubes on the average heat transfer coefficient. The condensation heat transfer coefficient for the test tubes was found to be inversely proportional to the spacing between tube rows.

Condensation on a tube bundle in vertically downward flow is different from condensation on a single tube, because the heat transfer coefficients decrease at the lower tubes in a vertical bundle due to the increase in the film thickness for each successive tube from the top of the bundle. In general, the coefficients for the top tubes (first tube row) of a bundle are comparable to those predicted for single-row tubes, while the condensate falling through a bundle increases the film thickness for each successive tube and reduces the condensation coefficients for the lower-row tubes substantially. If the coefficient for the top tube row of a bundle (h_1) is known, the average heat transfer coefficient (h_N) for the bundle of N tube rows can be then determined from the empirical relationship, such as the Webb–Murawski correlation mentioned earlier, derived for the heat transfer coefficients between tube rows.

In addition to the Webb–Murawski correlation, a well-known relationship between the average heat transfer coefficient (h_N, $W/m^2 \cdot K$) for a vertical rank of N horizontal tube rows and a single horizontal tube row (h_1, $W/m^2 \cdot K$) was proposed by Nusselt [13]. The equation is given by

$$h_N / h_1 = N^{-0.25} \tag{5.4}$$

Equation 5.4 was derived assuming a constant wall temperature and laminar film condensation. The exponent in this equation differs according to Cheng and Wang [10] and Kern [14].

No published data regarding condensation of HFC-236ea on tube bundles were available for comparison of the single-tube data taken in this study.

CHAPTER 6

POOL BOILING RESULTS

OVERVIEW

Boiling is defined as evaporation of liquid that occurs at the interface of a solid surface and a liquid when the temperature of the heated surface exceeds the saturation temperature of the liquid. Pool boiling is boiling from a heated surface immersed in a pool of stationary liquid whose motion near the surface is due to free convection and bubble motion. The pool boiling curve is usually plotted in terms of the surface heat flux against the heater surface temperature or wall superheat, and it is composed of four main regimes— free convection, nucleate boiling, transition boiling, and film boiling— in ascending order of wall superheat [15]. The four regimes are sketched in the boiling curve for water in Figure 6.1.

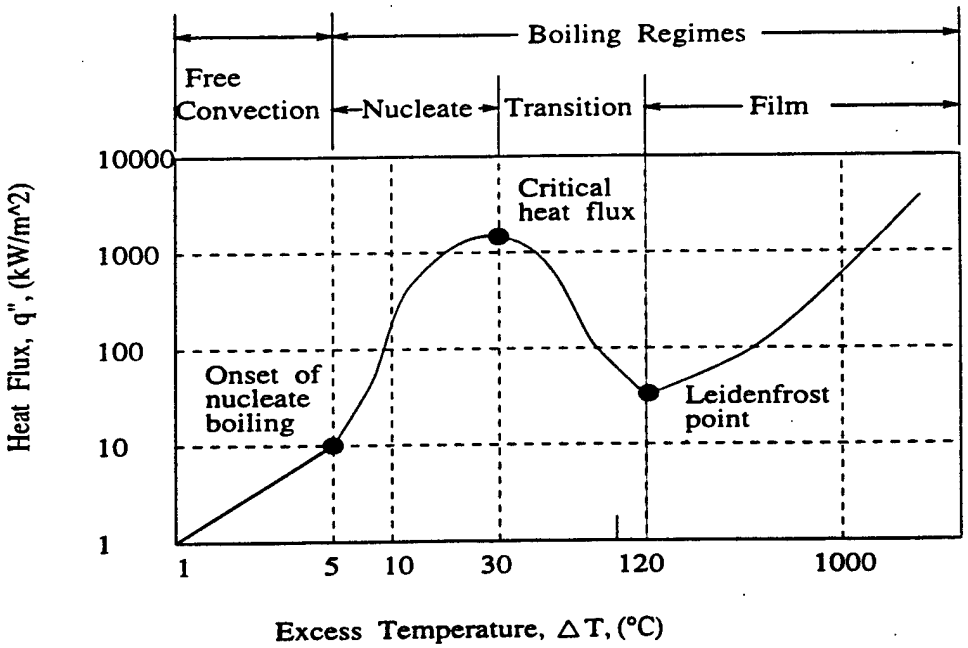

Figure 6.1. Typical boiling curve for water at 1 atmosphere.

The pool boiling investigated here is saturated pool boiling where the temperature through most of the bulk liquid remains at or slightly above the saturation temperature (i.e., boiling point) and is nucleate boiling where the wall superheat is sufficient to cause vapor nucleation from the imperfections of the heating surface, but not too large to cause a vapor film on the surface.

Nucleate pool boiling is characterized by a high heat transfer rate associated with a relatively small wall superheat (excess temperature). Its favorable effect on boiling can also be seen in Figure 6.1, where the nucleate boiling curve exhibits the steepest slope or highest heat transfer coefficient. Although Figure 6.1 was sketched for water, other fluids show similar trends. The process of nucleate pool boiling combines the mechanisms of bubble motion, thermal boundary layer stripping, and evaporation [16]. None of the plentiful theoretical models developed or phenomena observed can explain satisfactorily the great improvement in heat transfer in this region.

Since the shell-side boiling mechanism consists of both nucleate boiling and forced convection vaporization, the heat transfer coefficient for nucleate pool boiling is required for predicting chiller performance. However, knowledge of the mechanisms associated with nucleate boiling as well as convective evaporation on enhanced tubes is limited.

The configuration of the heated surface for boiling has definite effects on the boiling rate. A surface with the proper geometrical shape of its cavities can provide effective nucleation sites and, thus, requires lower superheat to initiate and sustain boiling. A number of papers concerning the boiling mechanism on different surface geometries has been published. The evolution of enhanced surface geometries for nucleate boiling was surveyed by Webb [17]. A detailed discussion on enhanced boiling surfaces was provided by Thome [3]. Later, a comprehensive literature survey of 61 references concerning pool boiling on enhanced surfaces was published by Pais and Webb [18].

Other parameters that can affect pool boiling, such as gravitational field and liquid subcooling, were reported to be negligible for nucleate pool boiling [15].

The Turbo-B and Turbo-BII tubes that have been suggested by manufacturers and researchers for the heat transfer enhancement in pool boiling were tested in this study.

RESULTS AND DISCUSSION

Pool Boiling Performance for the Turbo-B and Turbo-BII Tubes

The heat transfer coefficients shown in Figures 6.2 and 6.3 indicate a direct relationship with heat flux, and they increased as the heat flux increased. More bubbles were created as the active nucleation sites increased with increasing heat flux, and hence resulted in the increase of the heat transfer coefficients.

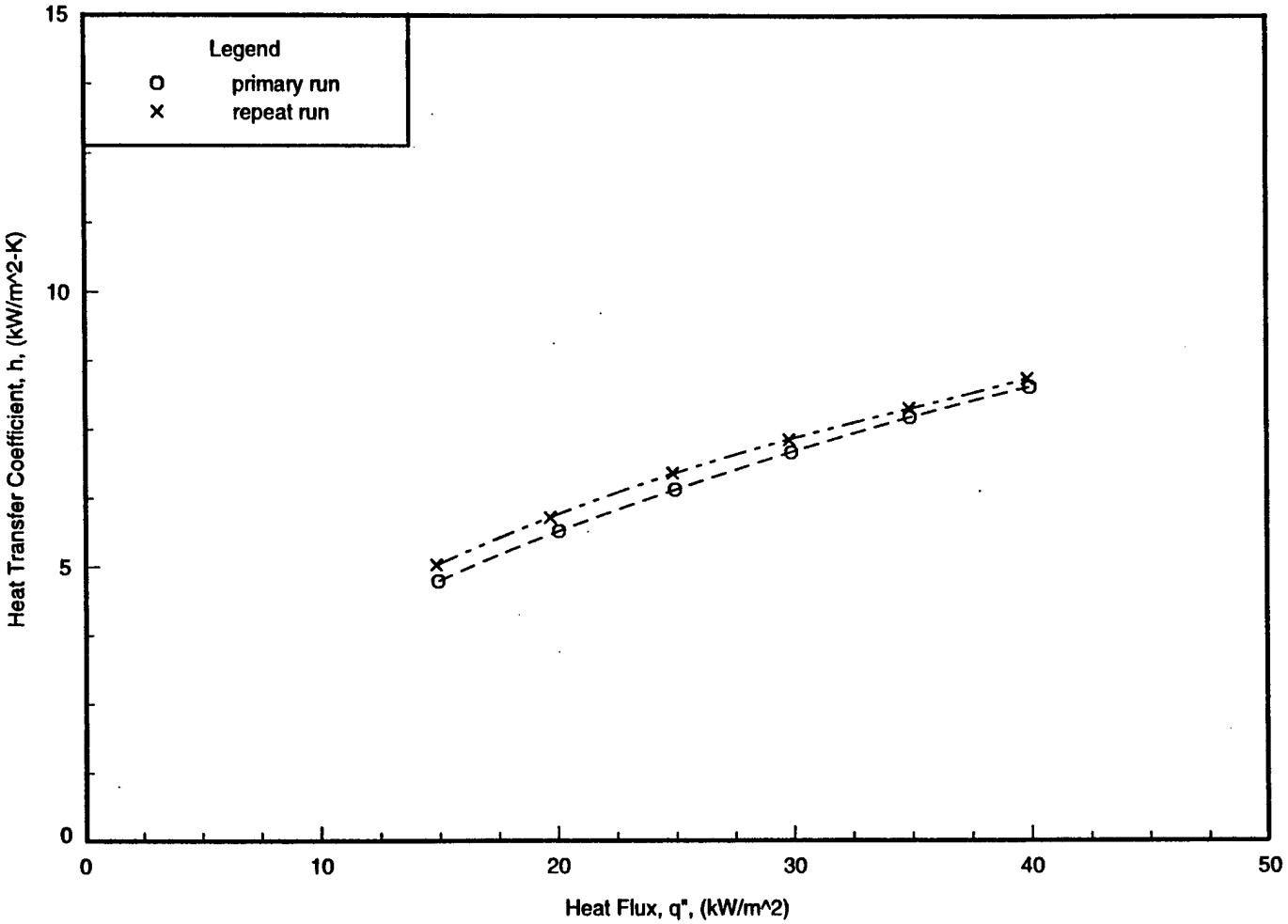

Figure 6.2. Pool boiling of HFC-236ea on a Turbo-B tube (D = 19.1 mm) at T_{sat} = 2°C.

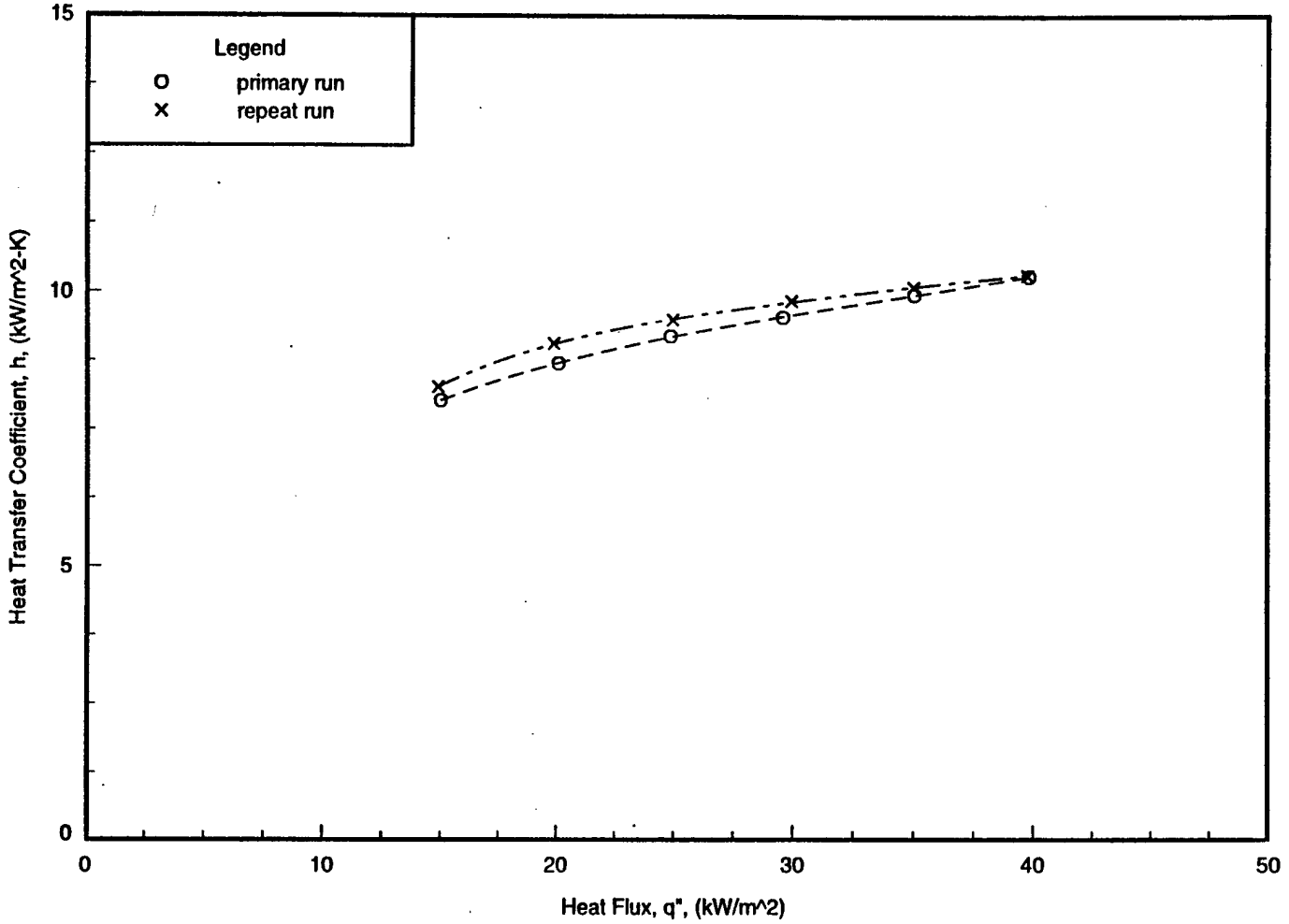

Figure 6.3. Pool boiling of HFC-236ea on a Turbo-BII tube (D = 19.1 mm) at T_{sat} = 2°C.

On the other hand, Barthau [19] developed a simple optical method for counting active nucleation sites on a horizontal plain tube using CFC-114. Even though the active nucleate site density was observed to be directly proportional to the heat flux, the heat transfer contribution of an individual active site was found to decrease strongly with increasing heat flux, based on his experimental results and theoretical assumptions.

After almost all the nucleation sites were activated (i.e., nucleation was fully developed), the increase in heat transfer slowed down even though the heat flux increased. Figure 6.4 indicates that most of the h-q" curves tend to flatten out at higher heat fluxes.

Two high performance enhanced tubes provided by the manufacturer, the Turbo-B tube and Turbo-BII tube, were tested for pool boiling. The Turbo-BII tube was found to provide heat transfer coefficients 1.2 to 1.7 times of those for the Turbo-B tube.

In the literature searches reported by Barthau [19] and by Hahne et al. [20], the hysteresis effects were avoided by running all the experiments in order of decreasing heat loads. All the experiments performed here for pool boiling were in order of decreasing heat flux. The repeatability of the present experiments is shown in Figures 6.2 and 6.3.

Comparison with Results of Phase I (Finned Tubes)

The data of the present study concerning the Turbo-B and Turbo-BII tubes were compared with those of Phase I [2] concerning the plain, 1024-fpm, and 1575-fpm tubes in Figures 6.4 and 6.5. Results were plotted in terms of the heat transfer coefficient versus the heat flux and versus the excess temperature, respectively.

The Turbo-B tube yielded heat transfer coefficients approximately 1.1 to 1.3 times of those for the 1024-fpm tube, 1.4 to 1.5 times of those for the 1575-fpm tube, and 1.8 to 2.2 times of those for the plain tube. The Turbo-BII tube yielded higher heat transfer coefficients than the Turbo-B tube, values approximately 1.6 to 1.8 times of those for the 1024-fpm tube, 1.9 to 2.4 times of those for the 1575-fpm tube, and 2.8 to 3.0 times of those for the plain tube.

Webb and Pais [21] presented pool-boiling data on three tube types using single tube tests. The Turbo-B tube outperformed the 1024-fpm tube by 35% for HCFC-123 and 30% for HFC-134a.

Figure 6.5 shows that the heat transfer coefficients for all the tube types tested depended on the temperature difference between the heated surface and the saturated refrigerant (excess temperature), and they increased as the excess temperatures increased for the high performance enhanced tubes— Turbo-B and Turbo-BII tubes— as well as for the conventional finned tubes and plain tube. The specified heat transfer rate was accomplished with a smaller temperature difference by using the high performance enhanced tubes rather than the conventional finned tubes or plain tube.

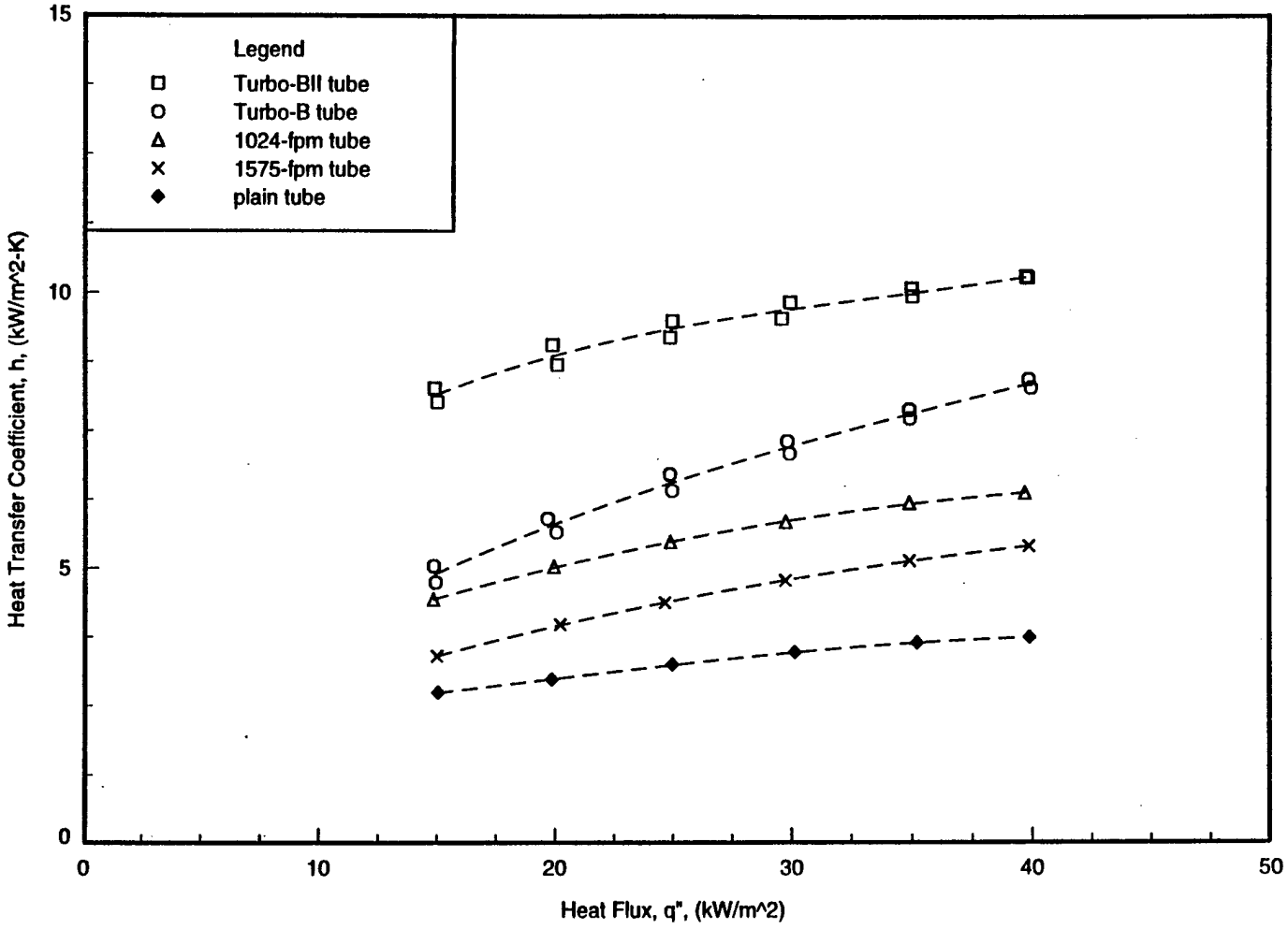

Figure 6.4. Heat transfer coefficients of HFC-236ea for Turbo-B, Turbo-BII, 1024-fpm, 1575-fpm, and plain tubes in pool boiling at T_{sat} = 2°C.

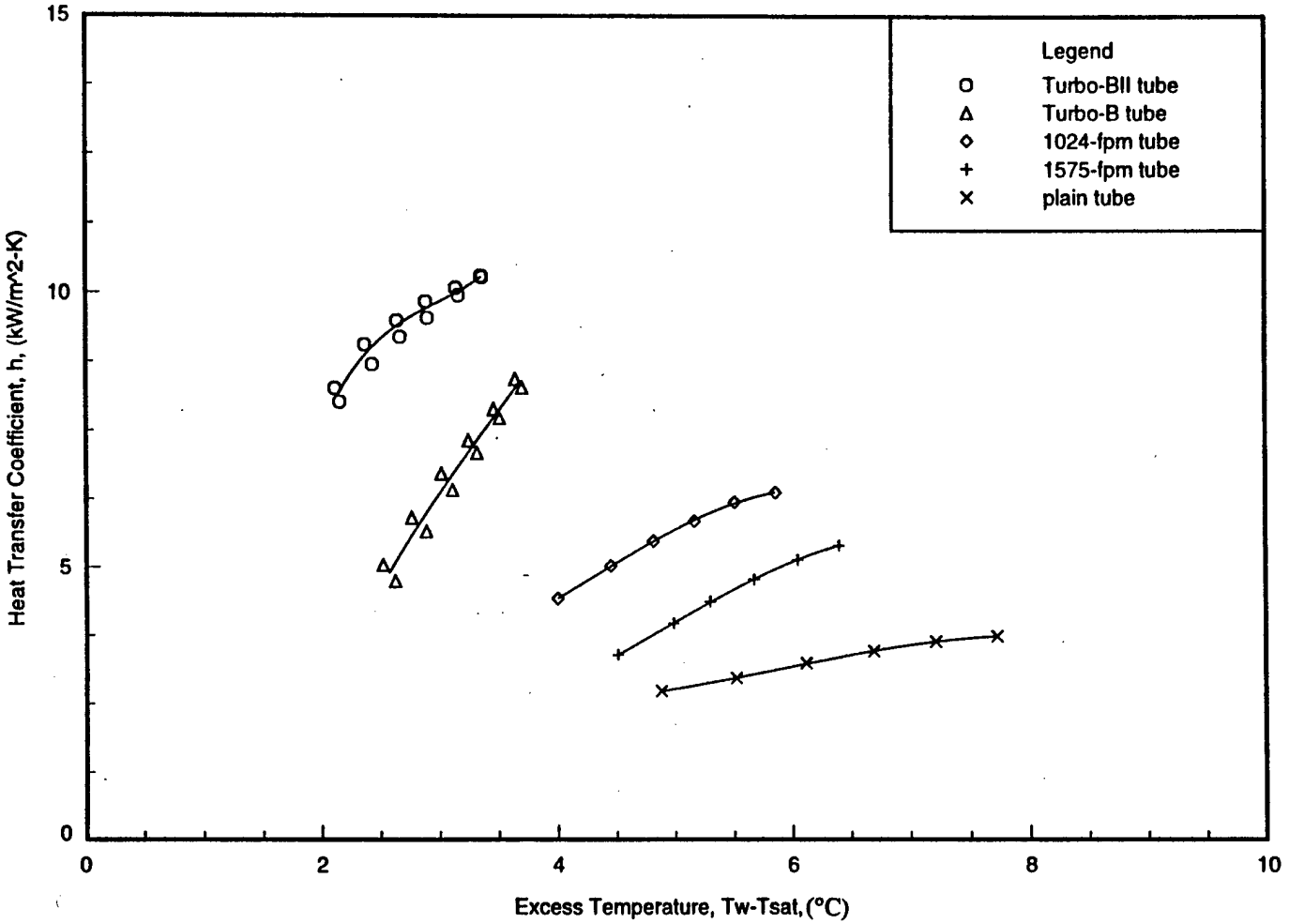

Figure 6.5. Heat transfer coefficients of HFC-236ea as a function of excess temperature for Turbo-B, Turbo-BII, 1024-fpm, 1575-fpm tubes in pool boiling at T_{sat} = 2°C.

It stands to reason that the Turbo-B tube and the Turbo-BII tube, which were especially designed for the enhancement of nucleate boiling, performed better than the traditional finned tubes in pool boiling. However, these three-dimensional, enhanced tube types could not be concluded to have higher overall heat transfer because the overall shell-side heat transfer is affected by both nucleate boiling and forced convection as mentioned earlier. The results compared here only indicate that the high performance enhanced tubes performed better during nucleate boiling than the finned tubes. Webb et al. [22] reported that forced convection tended to dominate the process of forced convection boiling when standard integral finned tubes were used.

Applicability of Single-Tube Data to the Design of a Flooded Evaporator

The effects of finned tube pitch on the pool-boiling heat transfer of CFC-11 were investigated by Hahne et al. [20]. Two tube types, namely a single tube and a twin tube, were tested at a saturation pressure of 10^5 Pa (1 bar). The tube pitch was observed to have no effect on heat transfer coefficients once fully developed boiling had been reached, while larger tube pitches produced higher heat transfer coefficients when boiling was not fully developed.

Webb [17] reported that a tube bundle had approximately the same boiling coefficients as a single tube if enhanced tubes were tested, but had substantially higher boiling coefficients if plain or standard finned tubes in bundles were tested.

An experimental study was conducted by Hahne and Müller [23] to measure heat transfer coefficients for a single tube, twin tubes, and a bundle in flooded evaporators operated at a saturation state of 10^5 Pa (1 bar) and 23.3 °C with CFC-11. The bundle tubes were in an aligned-tube arrangement with a square tube pitch which is twice the root diameter of the tubes, while the twin tubes were arranged vertically and had the same tube pitch as the bundle. Heat transfer coefficients for the finned tubes in the bundle were found to be in agreement with those in the twin-tube arrangement.

In general, the boiling coefficients for the bottom tubes of a bundle are comparable to those predicted by a single-row tube, while the two-phase fluid circulating up through a bundle enhances the boiling coefficients for the upper tubes substantially. Heat transfer coefficients for a single tube may coincide with those for a tube bundle if nucleate boiling rather than forced convection dominates the heat transfer process.

Since boiling coefficients vary over the bundle depth, the amount of refrigerant charge in a realistic flooded evaporator should be determined by experimental tests to give the highest evaporator performance. Overcharge will invoke a hydrostatic head penalty across the rows, while insufficient charge will cause dry-out phenomenon occurring on the upper tubes.

No published data regarding nucleate boiling of HFC-236ea on tube bundles were available for comparison of the single-tube data taken in this study.

CHAPTER 7

SPRAY EVAPORATION RESULTS

OVERVIEW

Falling-film evaporators using water or ammonia as the working fluid are commonly employed in the wine and poultry industries for processing distillation and desalination. However, the use of has been restricted to spray evaporators.

Two passes of a single horizontal tube were subjected to liquid refrigerant sprayed from a set of nozzles located above the tube. The nozzles had an orifice diameter of 1.58 mm (1/16 in.). When liquid drops impinged on the tube surface, intensive droplets integrated together and formed a thin film on the surface through shear forces. Then heat was transferred through evaporation and boiling of the liquid film on the tube. Droplets that missed hitting the tube, together with those that were not evaporated on the tube before falling due to gravitational and aerodynamic drag forces, returned to the pump and were recirculated to the spray nozzles.

The recirculation rate (RR) of refrigerant in the test section is defined as the ratio of the mass flow rate of refrigerant distributed to the test section to the mass flow rate of refrigerant vapor leaving the test section. The mass and energy rate balances across the test section were used to obtain this parameter since the facility was not able to measure the mass flow rates of refrigerant exiting the test section as liquid ($\dot{m}_{liq}$, kg/s) and as vapor ($\dot{m}_{vap}$, kg/s).

Under steady state conditions, the mass rate balance across the test section is formulated as,

$$\dot{m}_{spr} = \dot{m}_{liq} + \dot{m}_{vap} \tag{7.1}$$

and the energy rate balance across the test section is given as,

$$q + \dot{m}_{spr} \cdot i_{spr} = \dot{m}_{liq} \cdot i_{liq} + \dot{m}_{vap} \cdot i_{vap} \tag{7.2}$$

where the heat transfer rate (q, W) was obtained from Equation 4.2; the total spray rate ($\dot{m}_{spr}$, kg/s) was measured; the enthalpies (J/kg), i_{spr}, i_{liq}, and i_{vap}, were calculated based on the measured temperatures of the manifold, the liquid outlet of the test section, and the vapor outlets of the test section, respectively.

The fraction of the total refrigerant flow leaving the test section as vapor, y, was calculated by substituting it into Equations 7.1 and 7.2 and resulted in

$$q + \dot{m}_{spr} \cdot i_{spr} = (1 - y) \cdot \dot{m}_{spr} \cdot i_{liq} + y \cdot \dot{m}_{spr} \cdot i_{vap} \tag{7.3}$$

The recirculation rate (RR) was then determined by simply inverting y,

$$RR = \frac{\dot{m}_{spr}}{\dot{m}_{vap}} = \frac{1}{y} \tag{7.4}$$

The values of recirculation rates corresponding to the heat fluxes are listed in Table 7.1. Recirculation rates depend on the tube arrangements as well as the flow rates. The recirculation rates for air-conditioning systems are generally low; however, tests using a single tube yield higher recirculation rates than those using a tube bundle, since the liquid which is not evaporated from the top tubes may fall onto the lower row tubes in a bundle and then be evaporated, while for a single tube test the liquid returns directly to the pump.

TABLE 7.1: TEST-SECTION RECIRCULATION RATIOS

Heat flux (kW/m^2)	Total spray rate (kg/min)			
	2.6	2.8	3.0	3.2
10	14.3	15.4	16.5	17.6
15	9.5	10.2	11.0	11.8
20	7.1	7.7	8.2	8.7
25	5.7	6.1	6.6	7.0
30	4.8	5.1	5.5	5.8

The characteristics for sprayed fluid flowing through a tube bundle were studied by Zeng et al. [24]. The local performance of water distribution on the tubes, which is affected by the tube surface geometry and tube bundle pattern, was investigated. Among the three tube types tested, the grooved tube performed similar to the plain tube, while the 1575-fpm tube provided the worst liquid distribution because the longitudinal liquid

movement was restricted by the fins. A bundle with tubes arranged in a triangular pitch was observed to require a higher total flow rate in order to prevent the tubes from overheating than that in a square pitch.

Tests of spray-film evaporation, along with the comparative tests of pool boiling on a plain tube, were conducted by Moeykens and Pate [25]. The effects of nozzle type, liquid flow rate, and tube diameter on heat transfer coefficients of HFC-134a were evaluated. Their results showed that nozzles producing higher pressure drop and tubes with a smaller diameter yielded higher heat transfer coefficients. The heat transfer coefficients were observed to be strongly dependent on the flow rates at high heat fluxes where dry-out became dominant, but were only weakly dependent on the flow rates at low heat fluxes.

RESULTS AND DISCUSSION

Tests were performed at several flow rates in order to find the flow rates for optimum heat transfer. Heat transfer coefficients were found to vary according to surface geometries and flow conditions. The critical flow rate which maximizes the heat transfer performance without causing dry-out or overfeed problems varies with the design and operating conditions of heat exchangers [25].

Spray Evaporation Performance for Three Tube Types

1. Effects of Heat Fluxes--

The effects of heat fluxes on the heat transfer coefficient are exhibited in Figures 7.1 through 7.3 for the Turbo-B tube, Turbo-CII tube, and 1575-fpm tube, respectively.

These figures indicate that the heat transfer coefficients depended on the heat flux throughout the entire range of heat loads tested. For any tube type at any feed rate except for relatively low feed rates, the general trend revealed in these figures is that as the heat flux increased, the heat transfer coefficient increased until a critical (maximum) heat flux was reached, and then decreased beyond this critical value. In general, the critical heat flux varies with different flow rates as well as different tube types and working fluids.

Dry-out phenomenon occurred after the critical heat flux was reached and became progressively significant beyond this critical value with increasing heat loads, and hence, resulted in decreasing heat transfer.

2. Effects of Flow Rates--

The effects of flow rates on the heat transfer behavior at various heat fluxes can be observed in Figures 7.4 through 7.6 for the Turbo-B tube, Turbo-CII tube, and 1575-fpm tube, respectively.

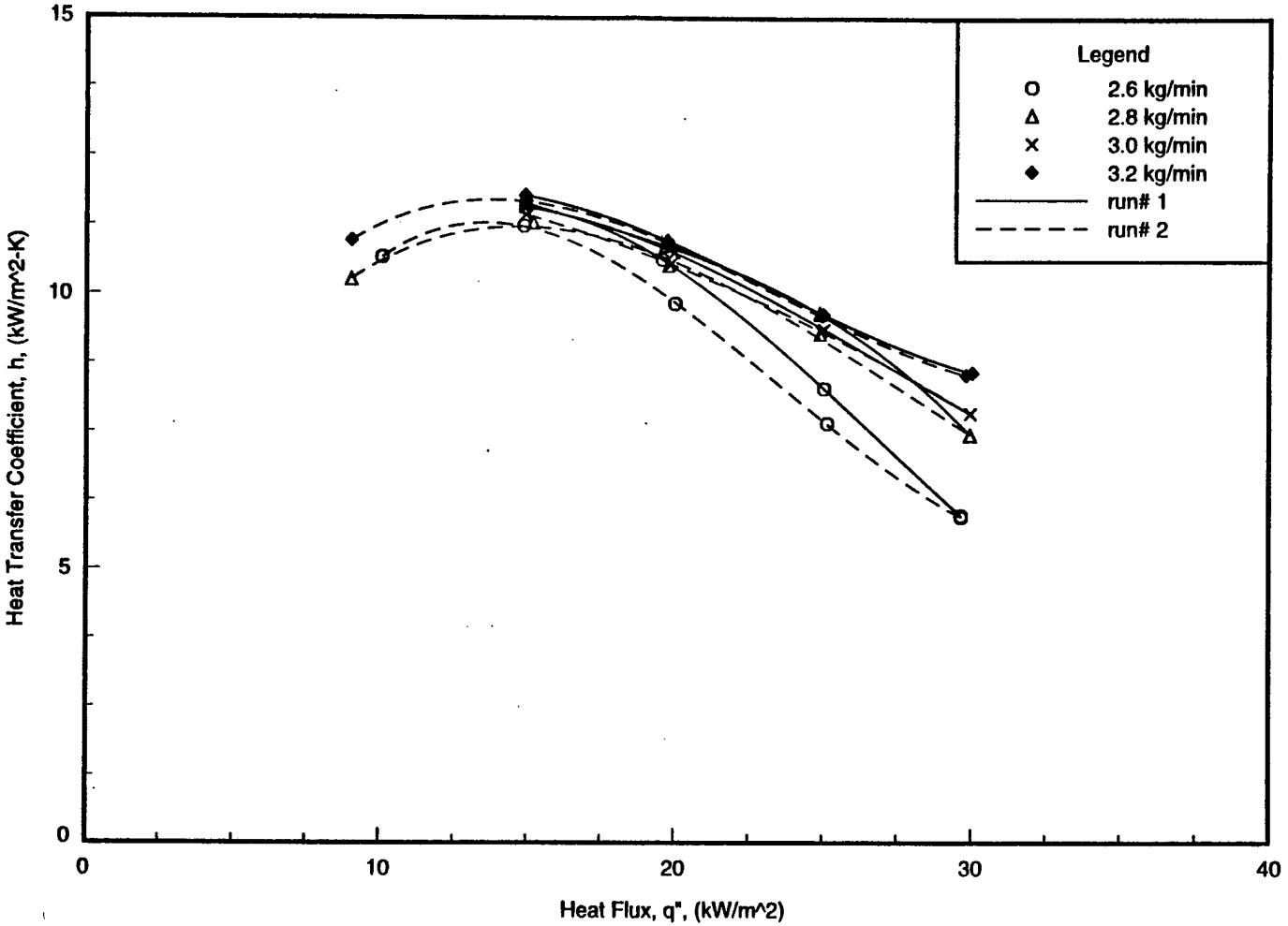

Figure 7.1. Spray evaporation of HFC-236ea on a Turbo-B tube (D = 19.1 mm) at T_{sat} = 2°C.

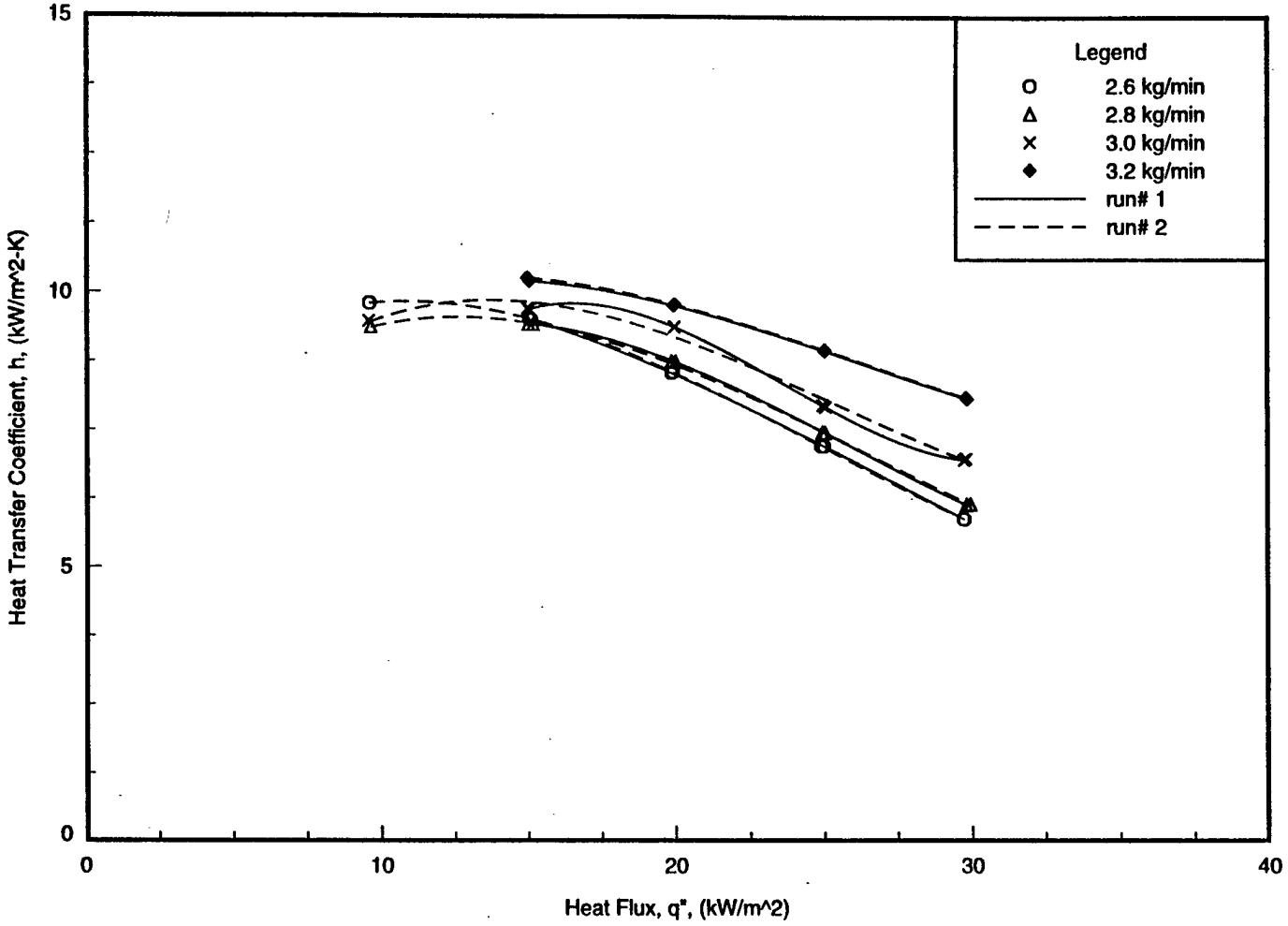

Figure 7.2. Spray evaporation of HFC-236ea on a Turbo-CII tube (D = 19.1 mm) at T_{sat} = 2°C.

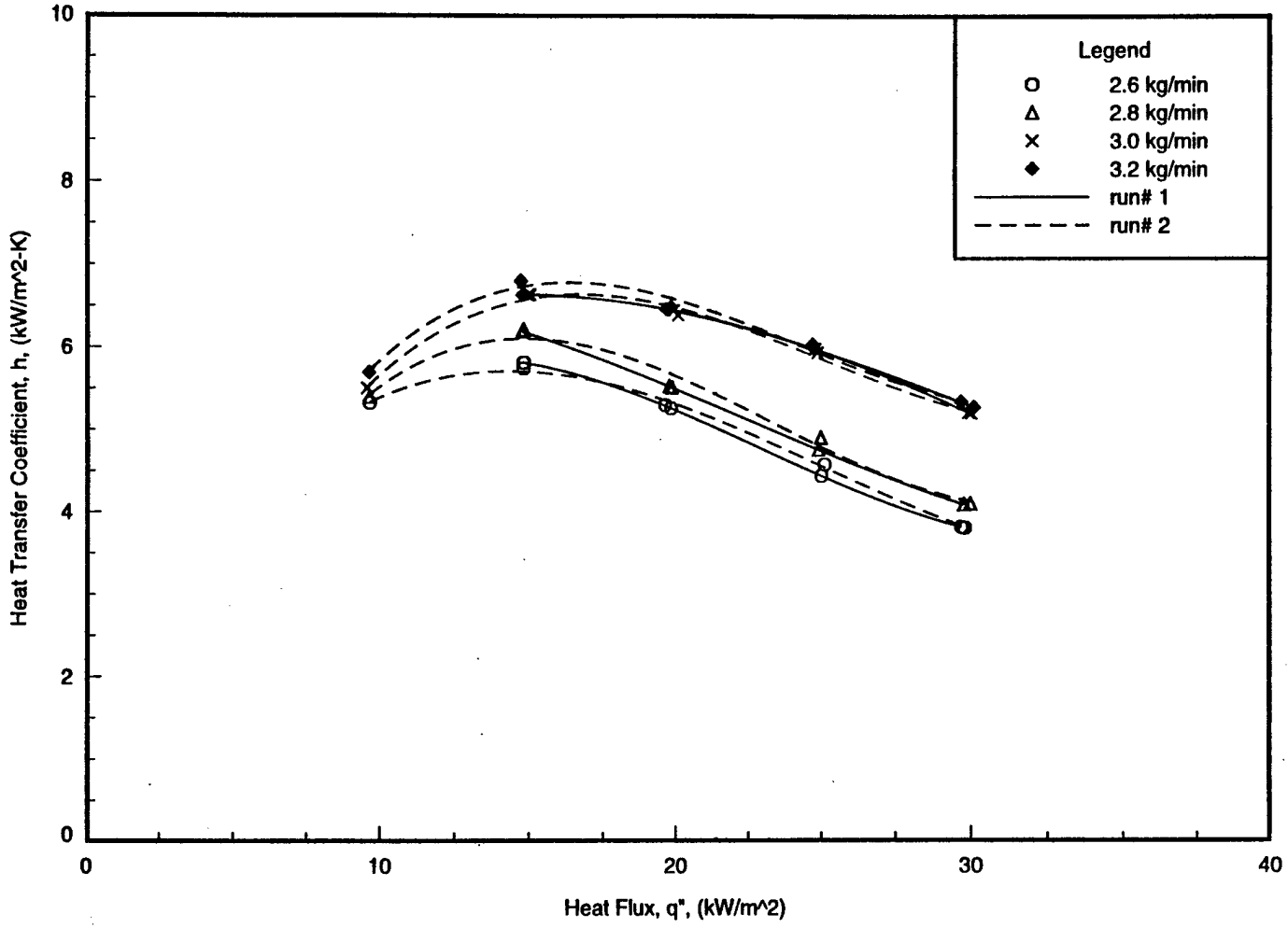

Figure 7.3. Spray evaporation of HFC-236ea on a 1575-fpm tube (D = 19.1 mm) at T_{sat} = 2°C.

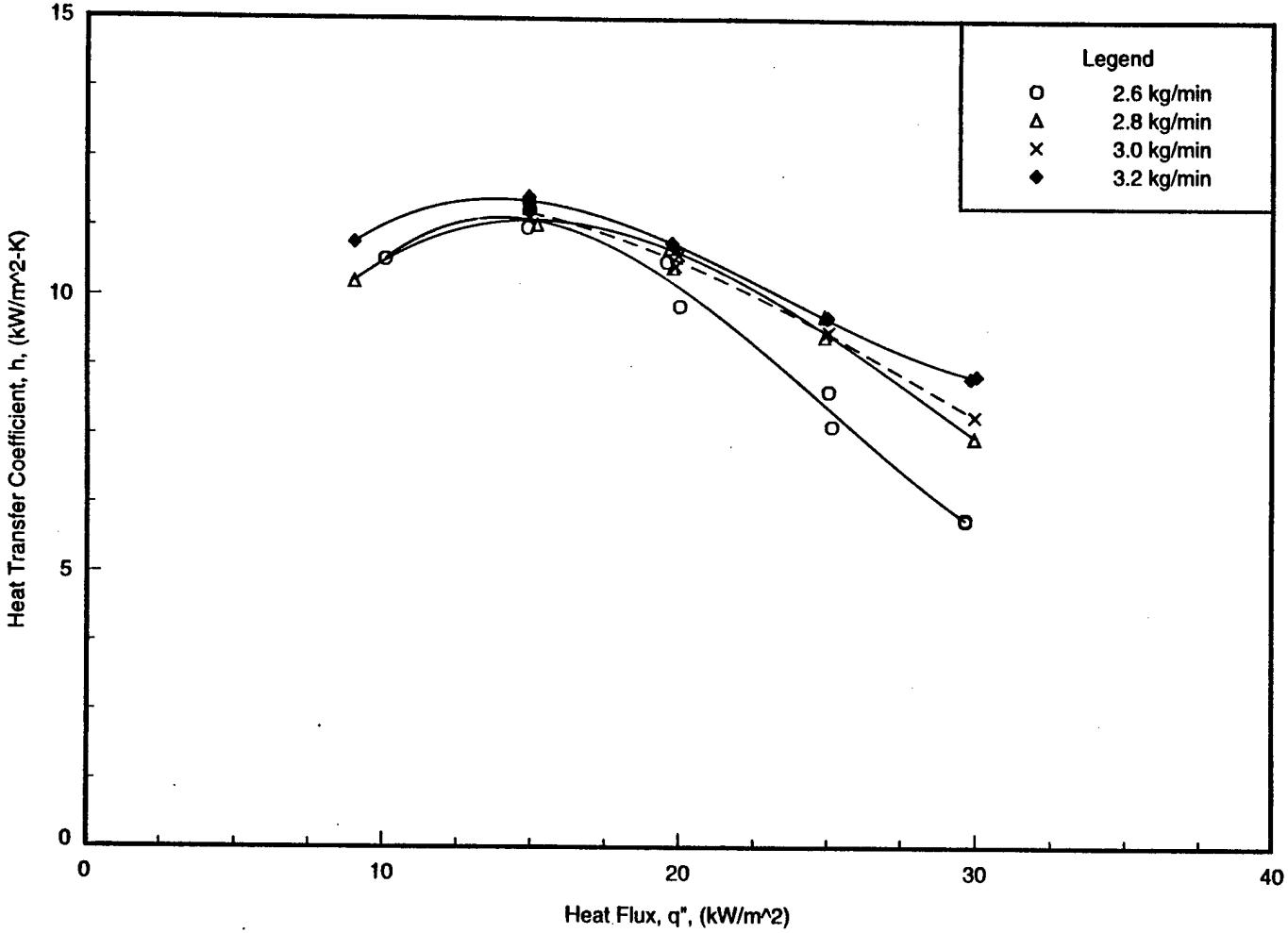

Figure 7.4. Effects of HFC-236ea flow rate on heat transfer coefficients of HFC-236ea for spray evaporation on a Turbo-B tube (D = 19.1 mm) at T_{sat} = 2°C.

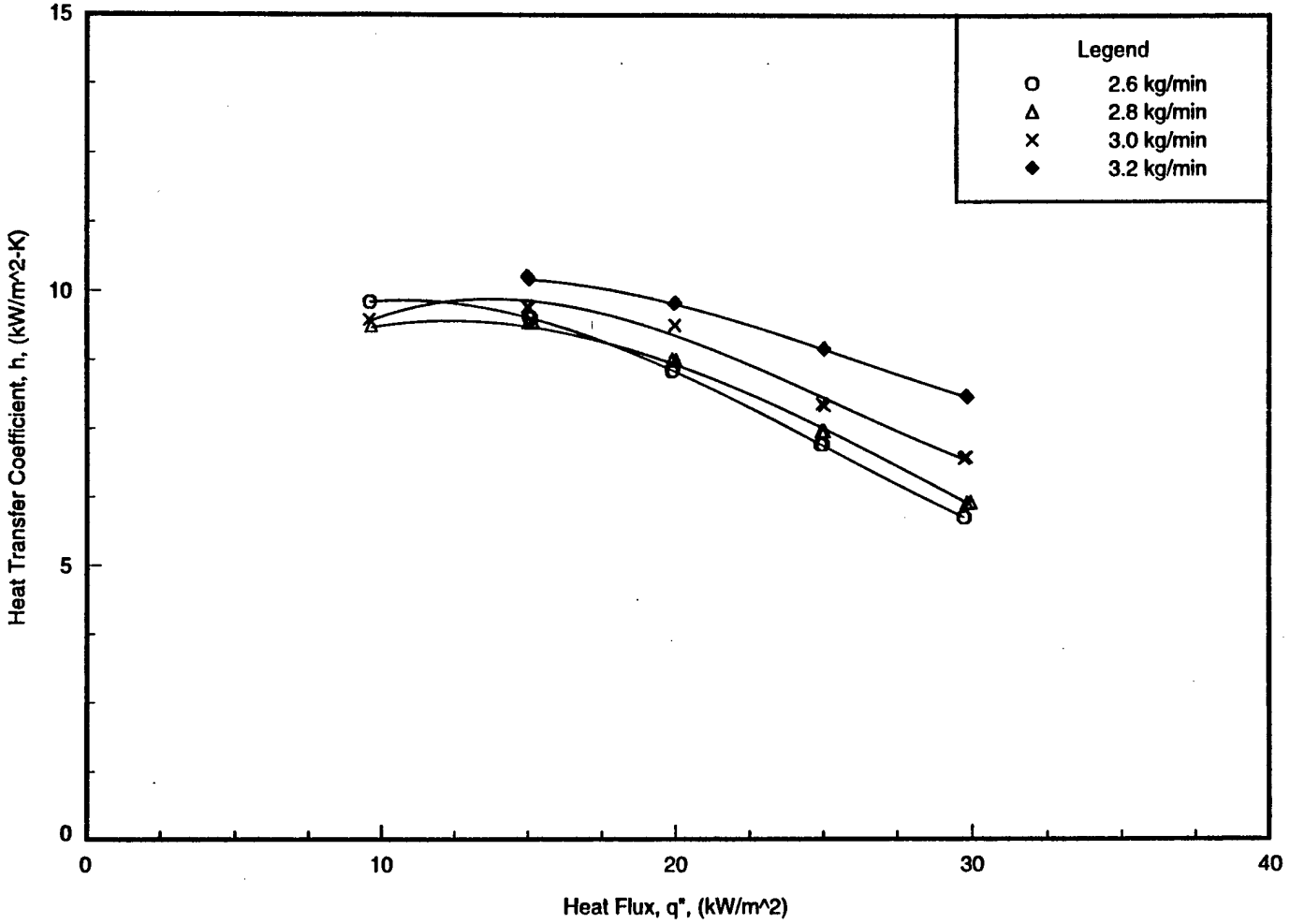

Figure 7.5. Effects of HFC-236ea flow rate on heat transfer coefficients of HFC-236ea for spray evaporation on a Turbo-CII tube (D = 19.1 mm) at T_{sat} = 2°C.

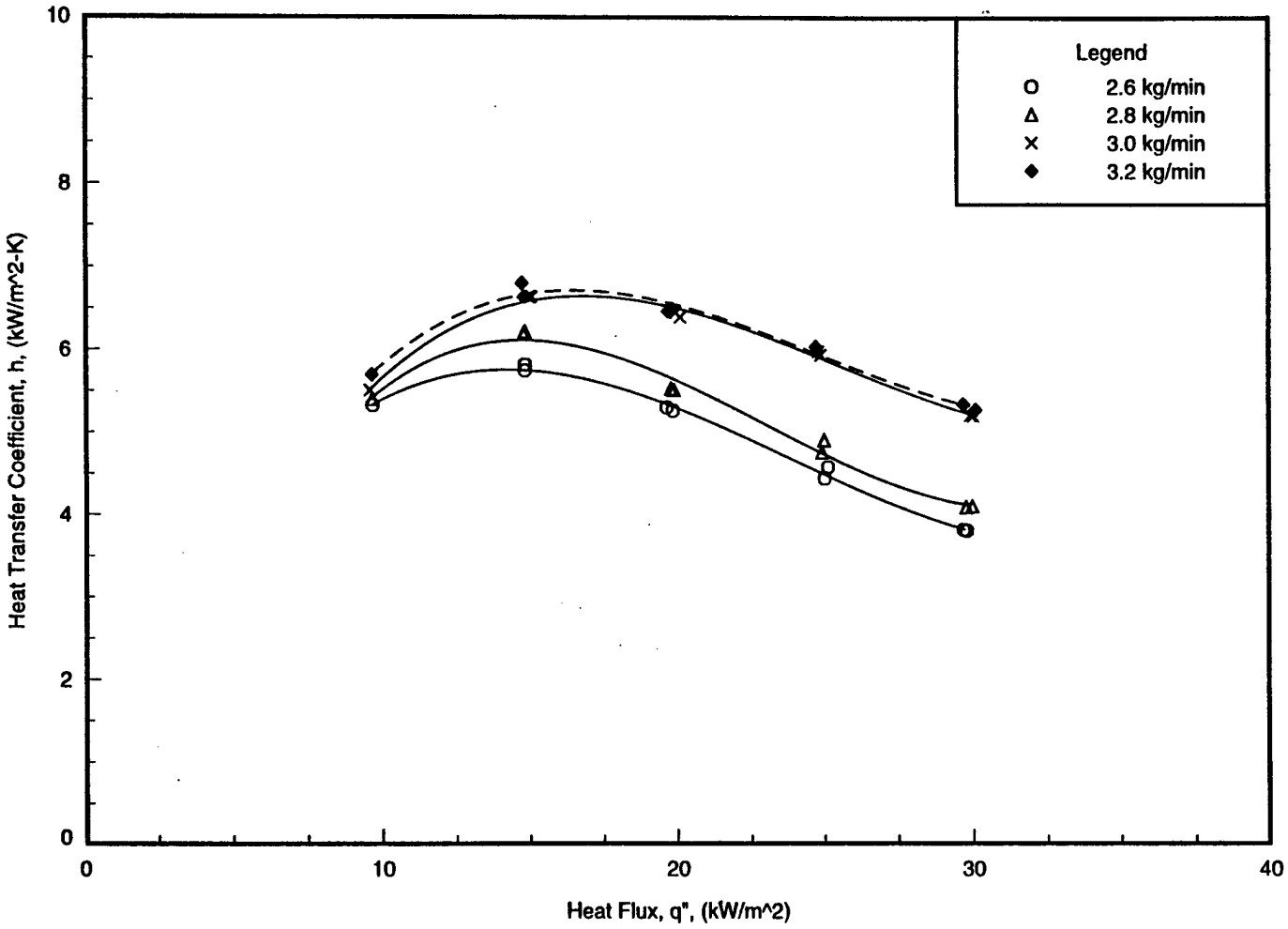

Figure 7.6. Effects of HFC-236ea flow rate on heat transfer coefficients of HFC-236ea for spray evaporation on a 1575-fpm tube (D = 19.1 mm) at T_{sat} = 2°C.

Heat transfer coefficients were observed to weakly depend on the feed rates below the critical heat flux, but strongly on them beyond this critical value. In other words, feed rates had almost no effect on the heat transfer coefficients before dry-out phenomenon occurred, but had significant influence on them afterwards. The heat transfer coefficient generally increased as the feed rate increased at a given heat flux. Higher heat transfer coefficients are expected at higher feed rates. These results are consistent with those observed by Moeykens and Pate [25].

Figures 7.4 through 7.6 also indicate that the dry-out phenomenon occurred earlier when the tube was subjected to a lower flow rate at a given heat flux. Figure 7.6 for the 1575-fpm tube shows that there was no significant improvement in the heat transfer as the feed rate increased from 3 kg/min to 3.2 kg/min.

3. Effects of tube types--

The effects of tube type on heat transfer are presented in Figure 7.7 which is plotted in terms of heat transfer coefficient versus heat flux at the flow rate of 3.0 kg/min.

The three tube types tested had the similar trend in the change of heat transfer coefficient with varying heat flux. The Turbo-B tube produced 1.0 to 1.2 times the heat transfer coefficients of the Turbo-CII tube, and 1.5 to 2.0 times those of the 1575-fpm tube. The heat transfer enhancement of the Turbo-B tube over the Turbo-CII tube and over the 1575-fpm tube under different feed rates and different heat fluxes is listed in Table 7.2.

TABLE 7.2: HEAT TANSFER ENHANCEMENT FOR SPRAY EVAPORATION TEST

Flow rate (kg/min)	Heat transfer enhancement	Heat flux (kW/m^2)		
		15	20	30
2.6	Turbo-B / Turbo-CII	1.2	1.2	1.0
	Turbo-B / 1575-fpm	2.0	1.9	1.6
2.8	Turbo-B / Turbo-CII	1.2	1.2	1.2
	Turbo-B / 1575-fpm	1.9	1.9	1.8
3.0	Turbo-B / Turbo-CII	1.2	1.1	1.1
	Turbo-B / 1575-fpm	1.7	1.7	1.5
3.2	Turbo-B / Turbo-CII	1.2	1.1	1.1
	Turbo-B / 1575-fpm	1.8	1.7	1.6

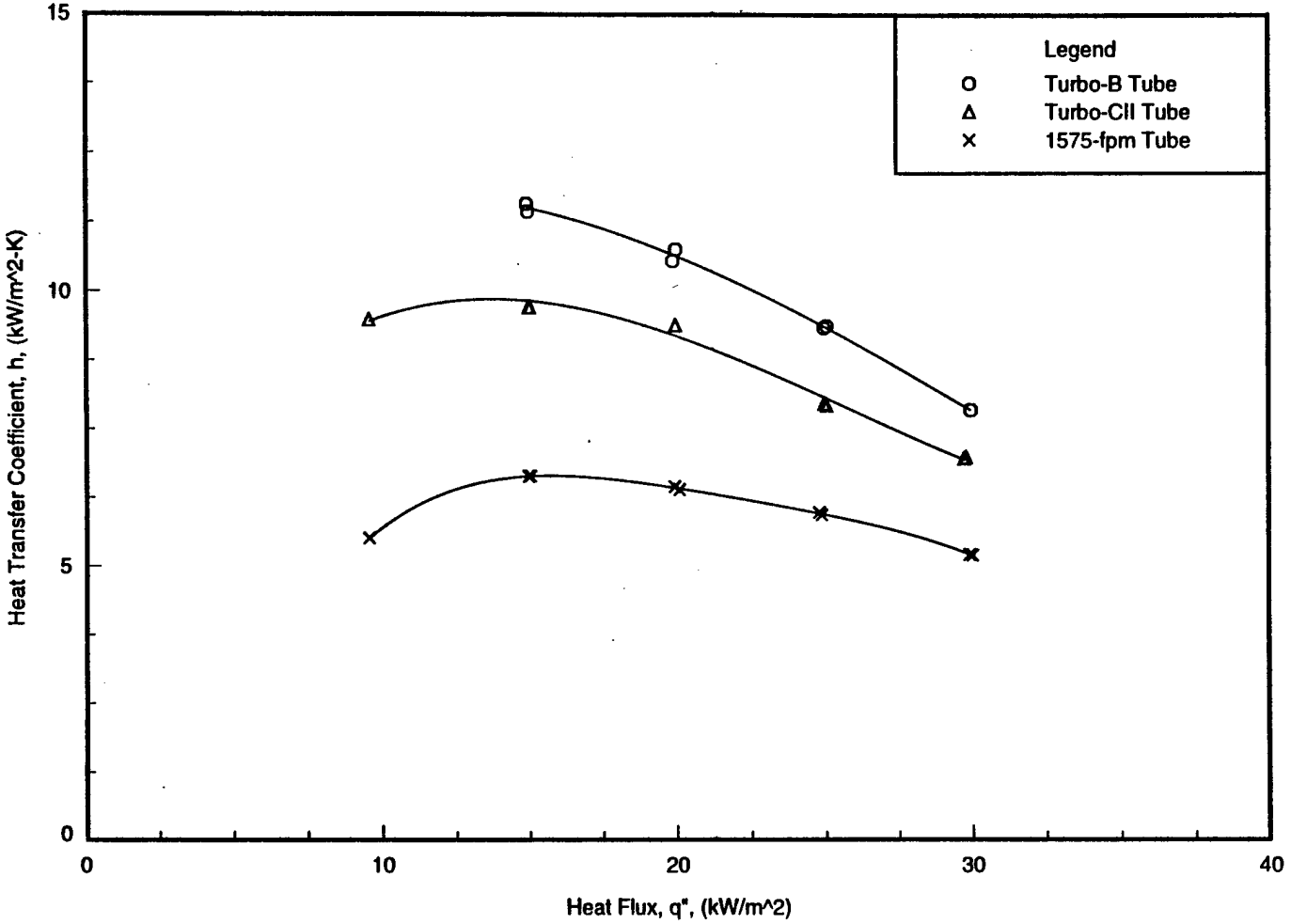

Figure 7.7. Effects of tube type on heat transfer coefficients of HFC-236ea for spray evaporation at a flow rate = 3.0 kg/min, T_{sat} = 2°C.

The Turbo-B tube which is designed for pool boiling provided the highest performance for spray evaporation among the tube types tested, followed by the enhanced condensation Turbo-CII tube. The 1575-fpm tube performed the worst, which was expected because the circular fins restricted and prevented the longitudinal movement of liquid. Thus, the cumulated liquid between fins could not stay on the tube for a long time and dripped easily due to gravity. Repeatability runs at the flow rate of 3.0 kg/min are shown in Figures 7.8 and 7.9 for the Turbo-B tube, Figures 7.10 and 7.11 for the Turbo-CII tube, and Figure 7.12 for the 1575-fpm tube.

4. Effects of temperature difference--

The effects of temperature difference on the heat transfer coefficient are presented in Figure 7.13 which is plotted in terms of heat transfer coefficient versus excess temperature at the feed rate of 3.0 kg/min.

Figure 7.13 indicates that the Turbo-B tube gave larger heat transfer coefficients than the Turbo-CII tube and 1575-fpm tube at the same excess temperature. In other words, the Turbo-B tube produced the smallest temperature difference among the three tubes tested at a given heat flux. It provided the highest heat transfer coefficients, while the 1575-fpm tube having the worst performance produced the largest temperature difference at a given heat flux.

Comparison of Spray Evaporation with Pool Boiling

The comparative performance of spray evaporation with pool boiling for the Turbo-B tube and 1575-fpm tube is shown in Figure 7.14 and Figure 7.15, respectively.

For both tube types, spray-film evaporation resulted in higher heat transfer and was more efficient than pool boiling at the lower heat loads. The turbulent environment generated by the spray and impingement of the droplets was beneficial to the heat transfer of spray evaporation, while in pool boiling the quiescent liquid was not stirred much by low bubble density at low heat loads. Moreover, the external force of droplet impingement increased the energy of liquid molecules on the tubes sufficiently to overcome their binding energy, and thus contributed to increase the evaporation rate of spray evaporation.

However, the superiority of performance of spray evaporation over that of pool boiling disappeared when nucleate boiling was completely established in pool boiling at high heat fluxes, while dry-out phenomenon appeared and became significant for spray evaporation with increasing heat loads.

The phenomena observed here are consistent with the results published by Moeykens and Pate [25]. Their results also indicated that the superiority in heat transfer for spray evaporation over pool boiling only existed at low heat loads.

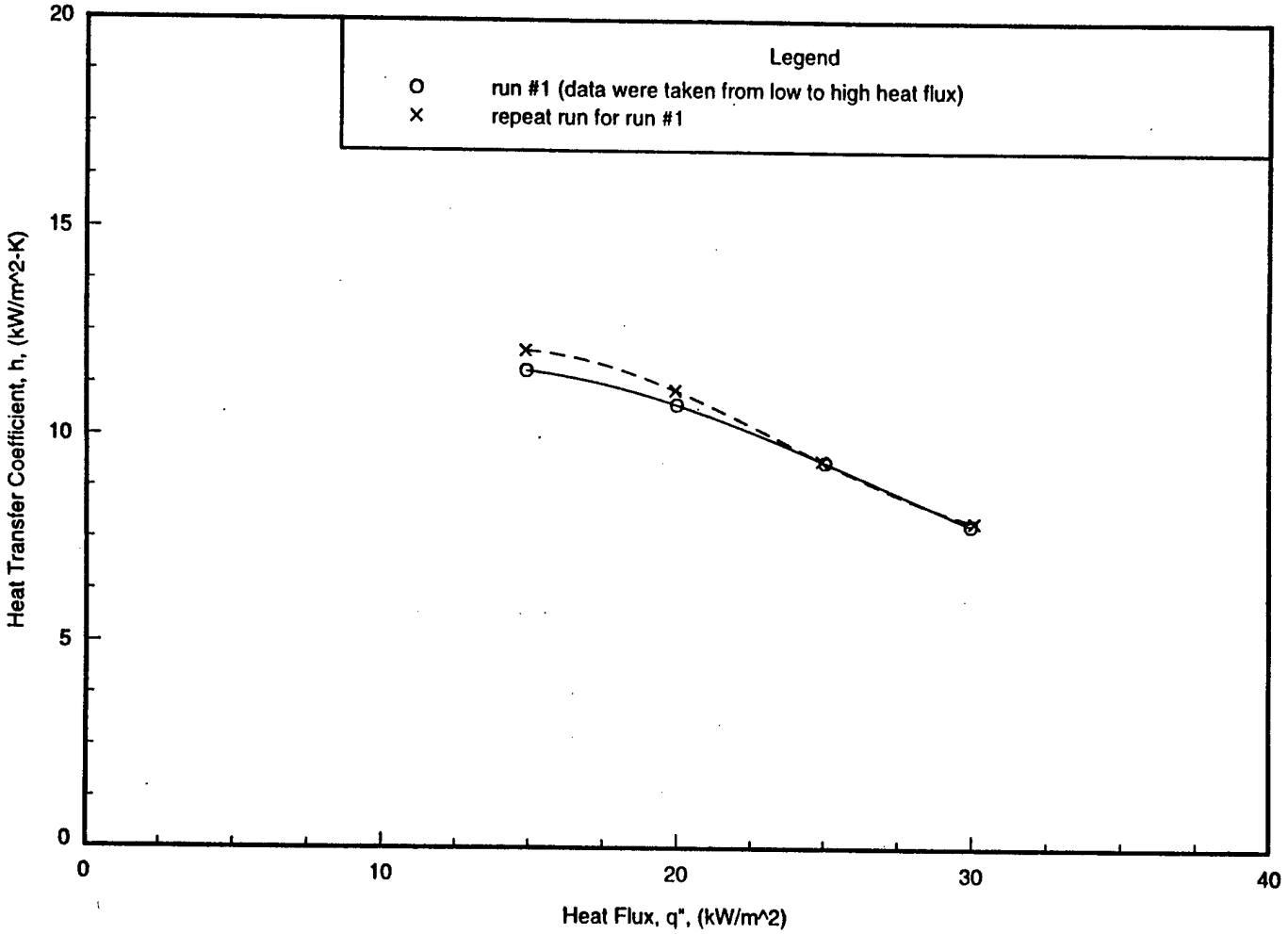

Figure 7.8. Repeatability of heat transfer coefficients for spray evaporation of HFC-236ea on a Turbo-B tube (D = 19.1 mm) at a flow rate = 3 kg/min (data were taken from low to high heat flux).

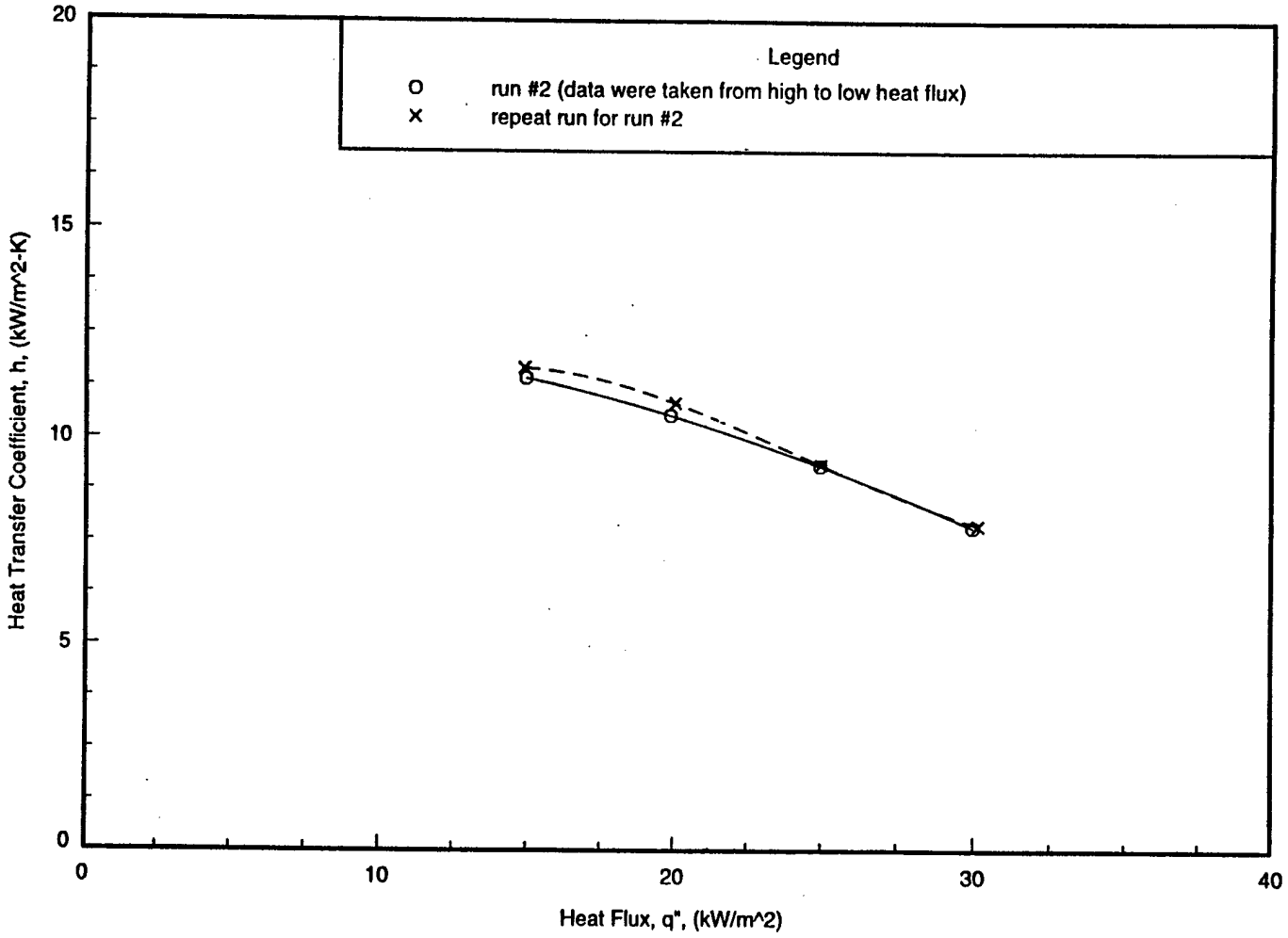

Figure 7.9. Repeatability of heat transfer coefficients for spray evaporation of HFC-236ea on a Turbo-B tube (D = 19.1 mm) at a flow rate = 3 kg/min (data were taken from high to low heat flux).

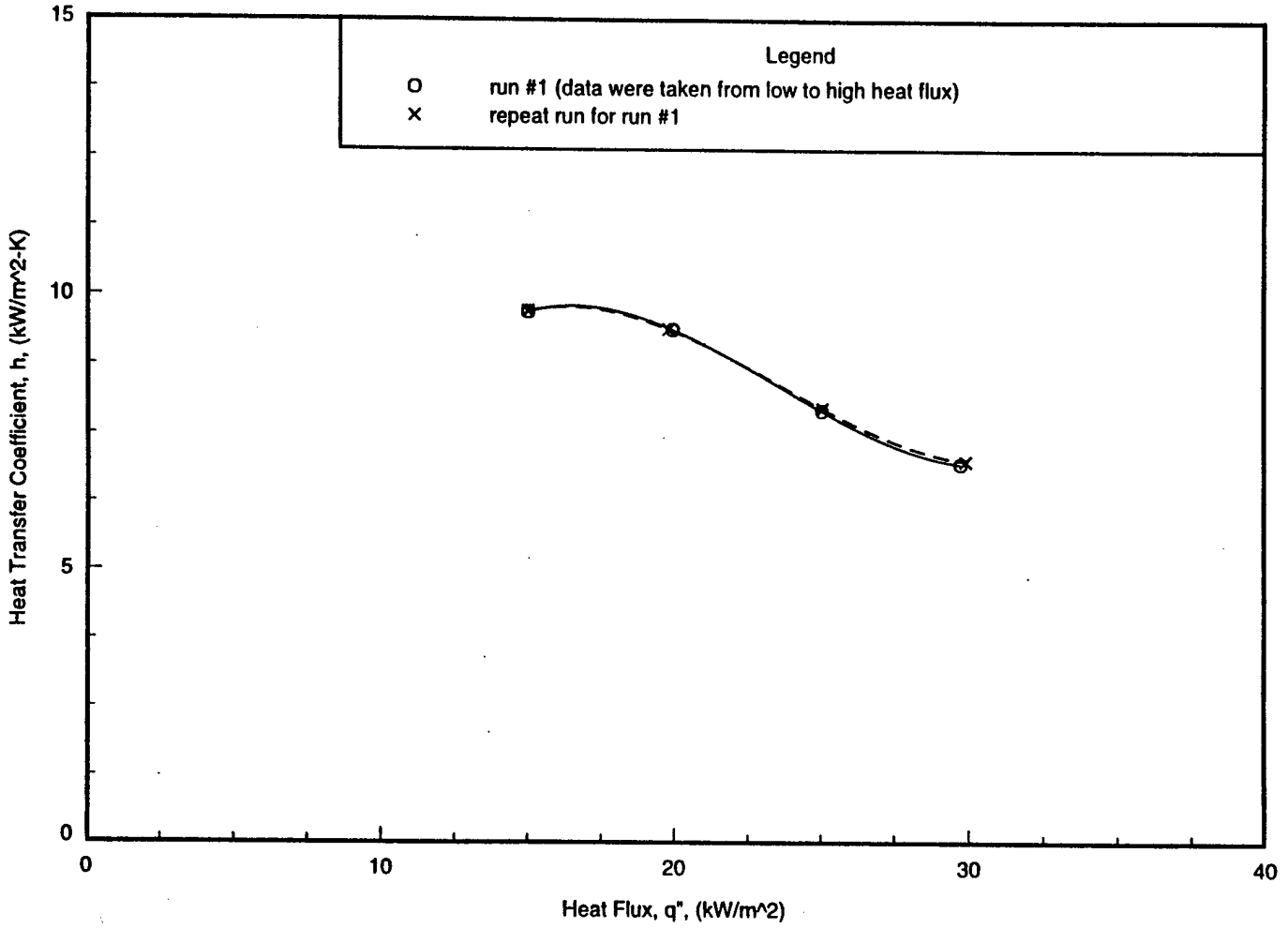

Figure 7.10. Repeatability of heat transfer coefficients for spray evaporation of HFC-236ea on a Turbo-CII tube (D = 19.1 mm) at a flow rate = 3 kg/min (data were taken from low to high heat flux).

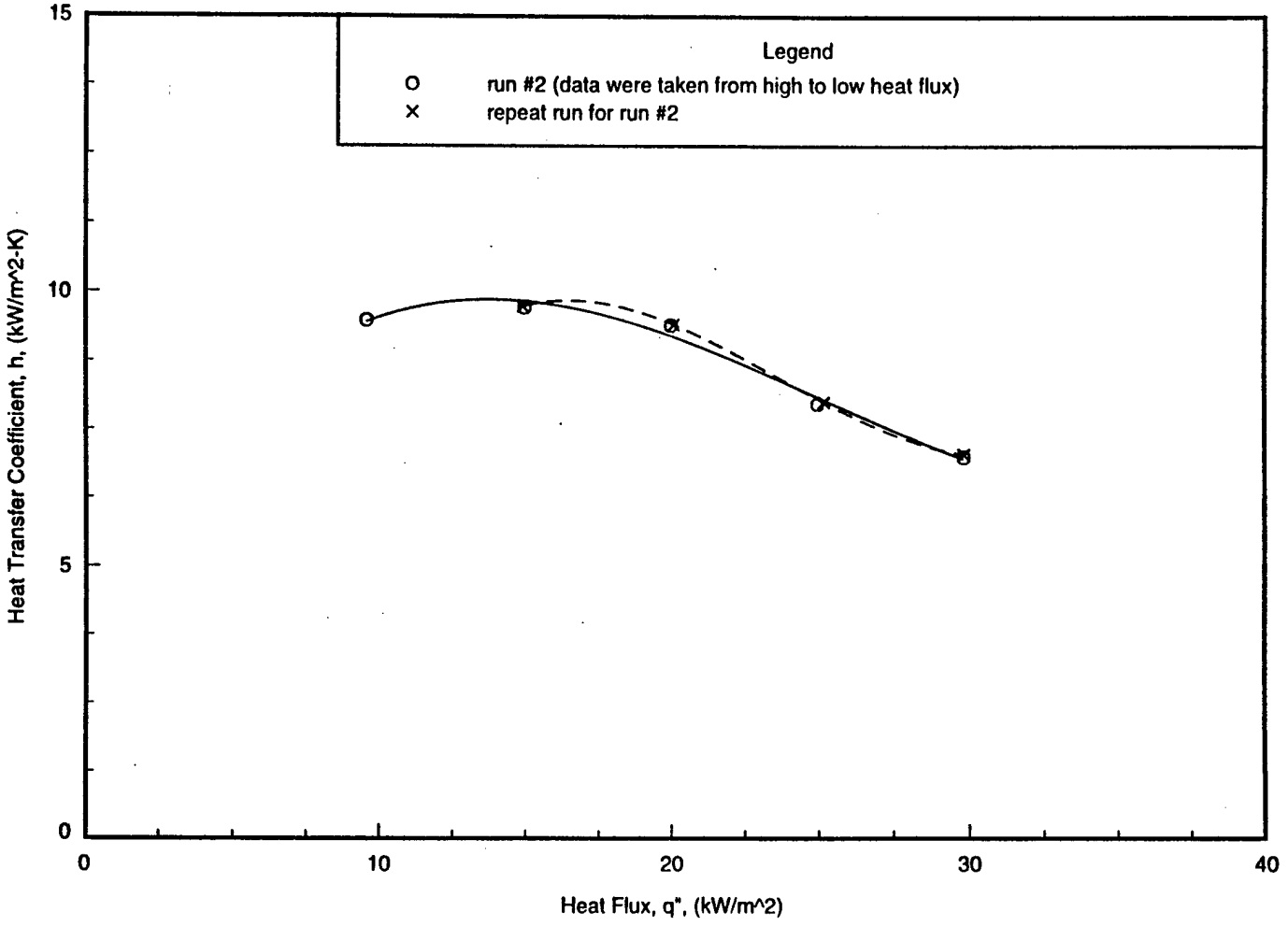

Figure 7.11. Repeatability of heat transfer coefficients for spray evaporation of HFC-236ea on a Turbo-CII tube (D = 19.1 mm) at a flow rate = 3 kg/min (data were taken from high to low heat flux).

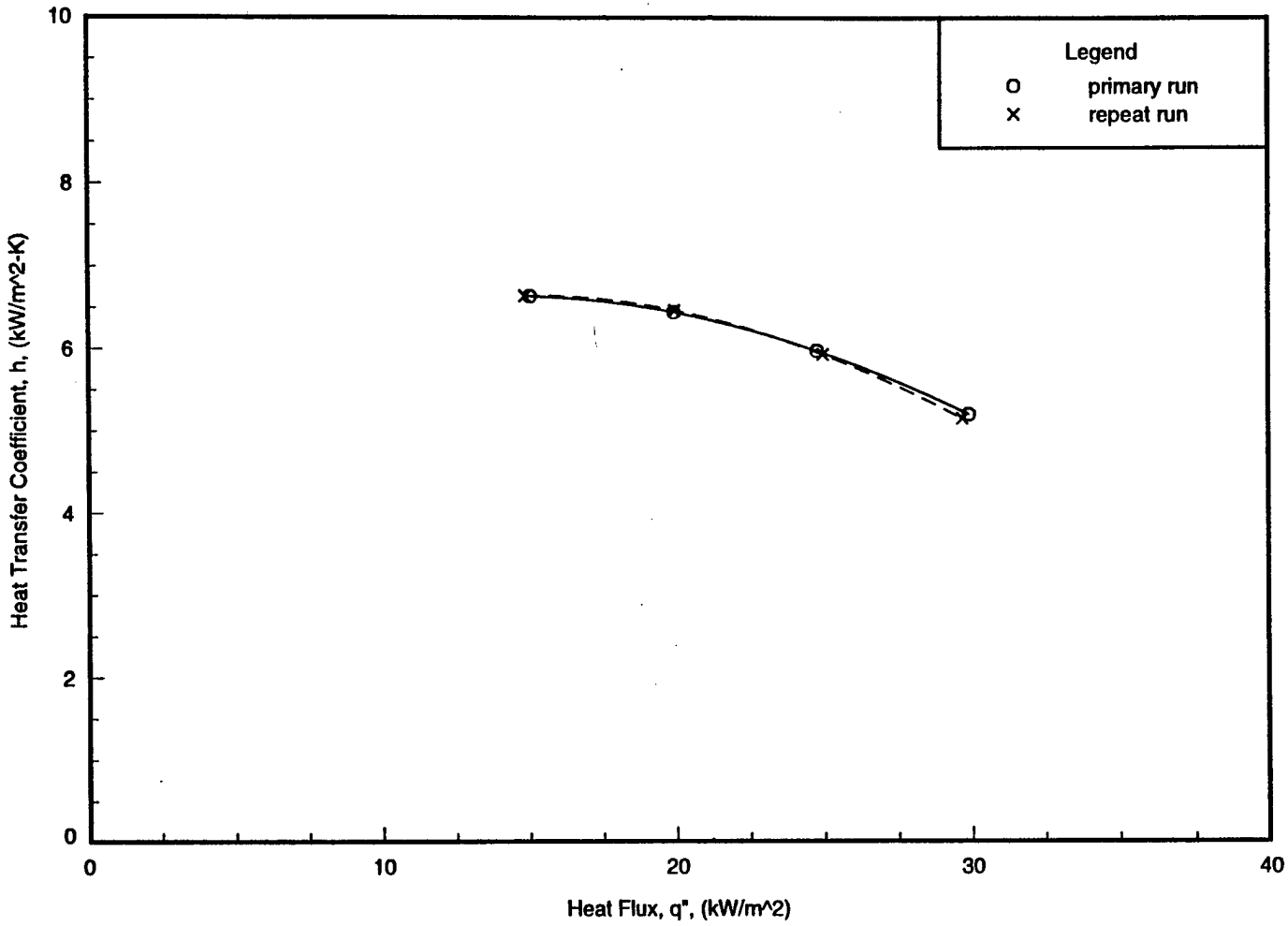

Figure 7.12. Repeatability of heat transfer coefficients for spray evaporation of HFC-236ea on a 1575-fpm tube (D = 19.1 mm) at a flow rate = 3 kg/min (data were taken from low to high heat flux).

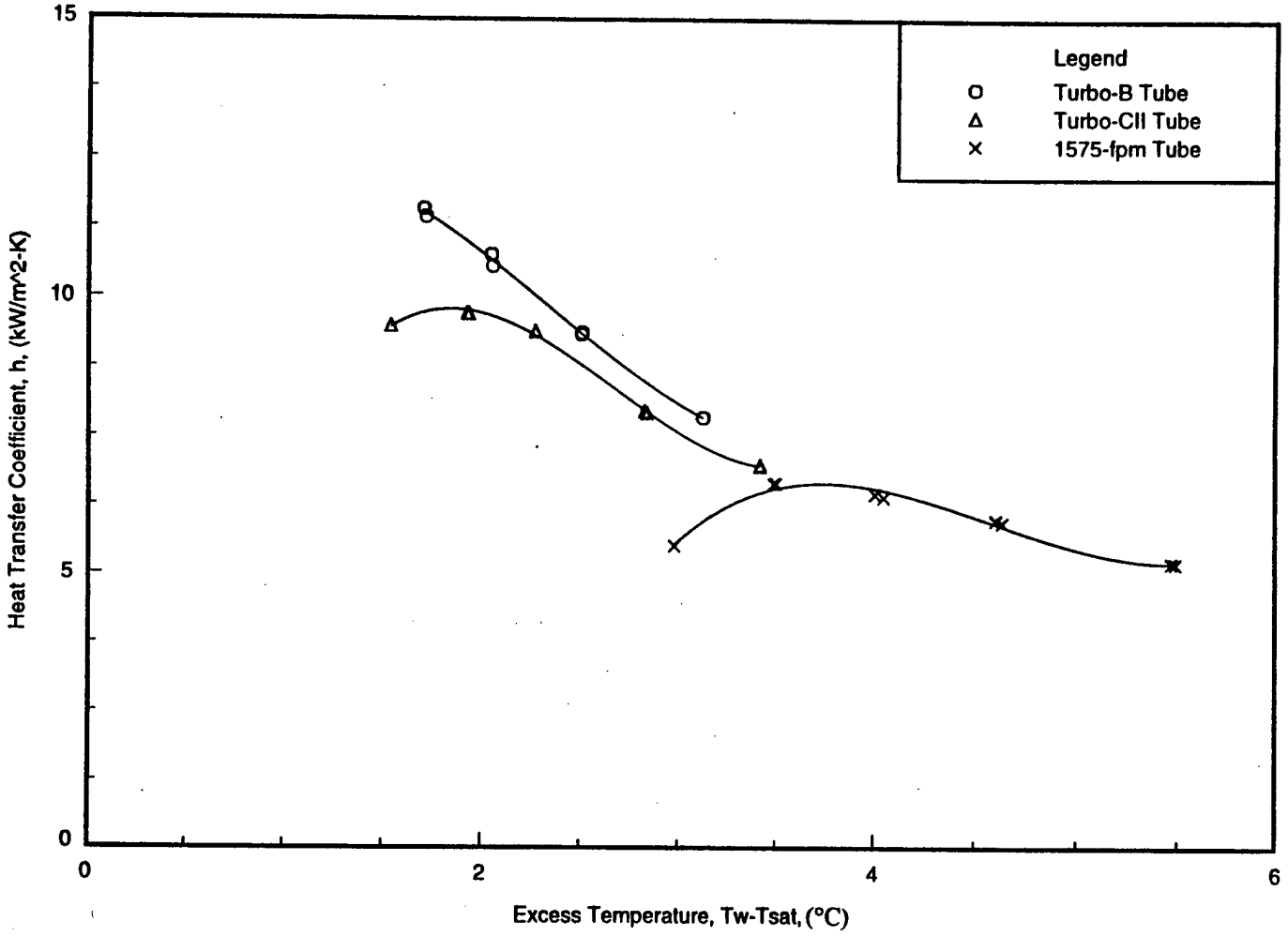

Figure 7.13. Effects of temperature difference on heat transfer coefficients of HFC-236ea for spray evaporation on Turbo-B, Turbo-CII, and 1575-fpm tubes at a flow rate = 3 kg/min and T_{sat} = 2°C.

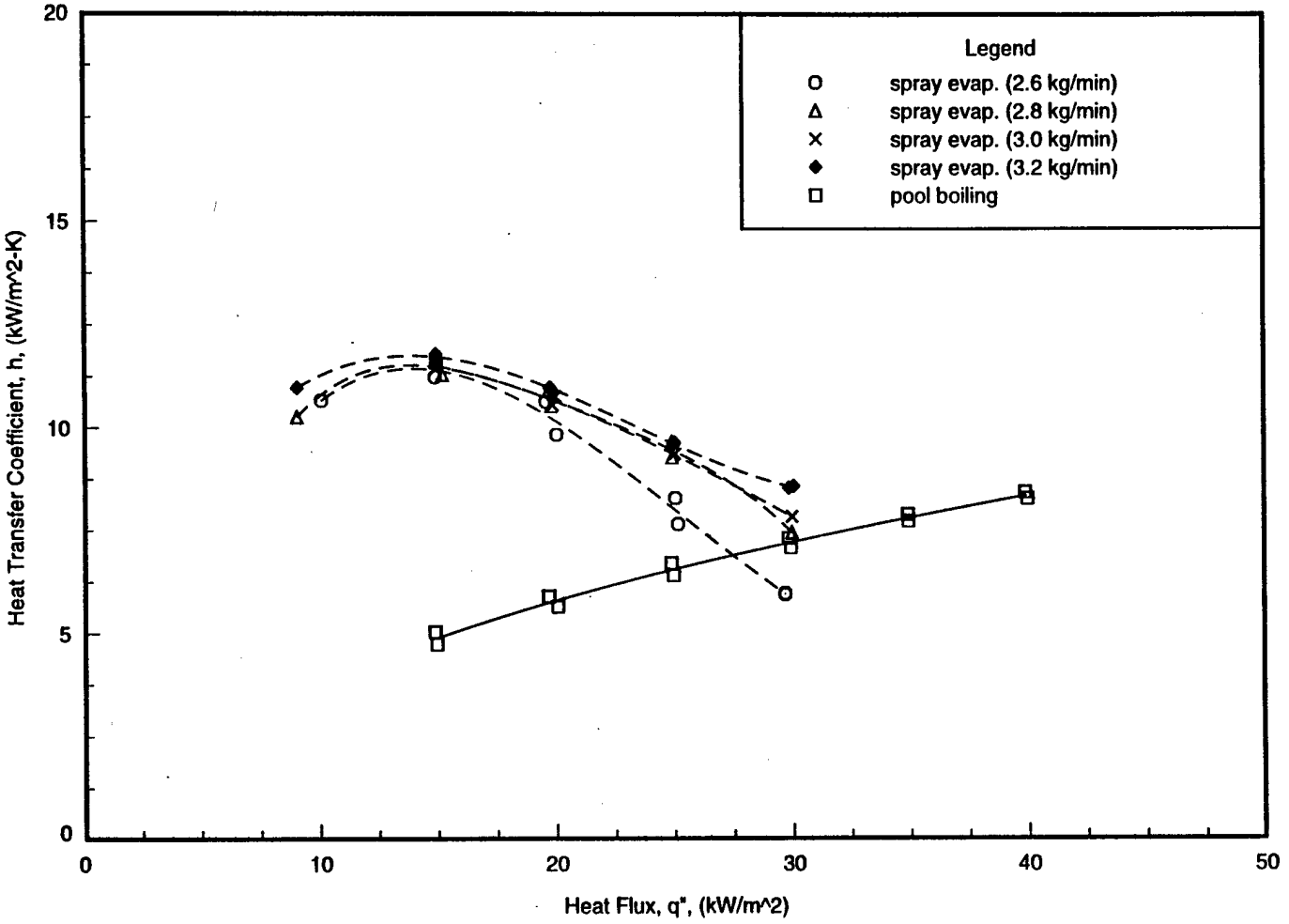

Figure 7.14. Comparison of pool boiling and spray evaporation of HFC-236ea using a Turbo-B tube (D = 19.1 mm) at T_{sat} = 2°C.

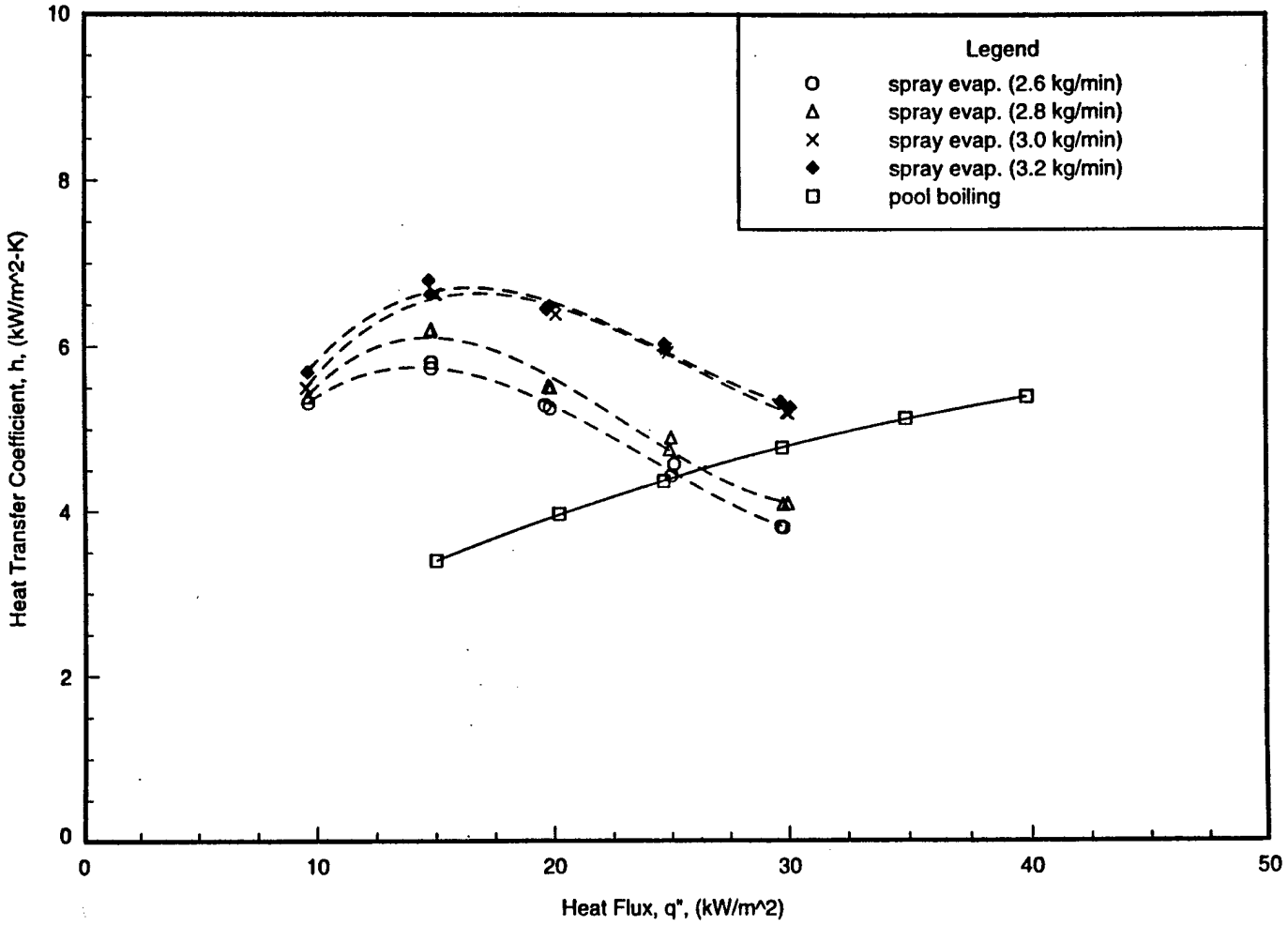

Figure 7.15. Comparison of pool boiling and spray evaporation of HFC-236ea using a 1575-fpm tube (D = 19.1 mm) at T_{sat} = 2°C.

Effects of Nouniform Liquid Distribution on The Tubes

Nonuniform liquid distribution along the tubes degrades the overall performance of spray evaporators. The portions of tube surface which are subjected to insufficient liquid dry out due to the breakdown of the film, while the portions with a dense spray are exposed to a thick liquid layer.

The dry-out phenomenon may not be a severe problem in the evaporators of refrigerating and air-conditioning systems, because the systems will not be overheated by the low wall superheat that commonly occurs in them.

A method mentioned by Zeng et al. [24] was developed for designing a spray system spraying a full solid cone. The optimal dimensions of a spray system are summarized as follows. As shown in Figure 7.16, in order to reduce the pumping power, the surrounding portion of a tube bundle in the spray zone (A1) and the overlapped area between two neighboring spray cones (A2) should be minimized. Based on this criterion, for a spray system with a tube bundle of width, bw, the optimal distance (OL) between two neighboring nozzles is 1.41*bw, and the corresponding height (d) of nozzles above tubes is $0.866 \times bw \times \cot(\beta/2)$, where β is the angle of a spray cone.

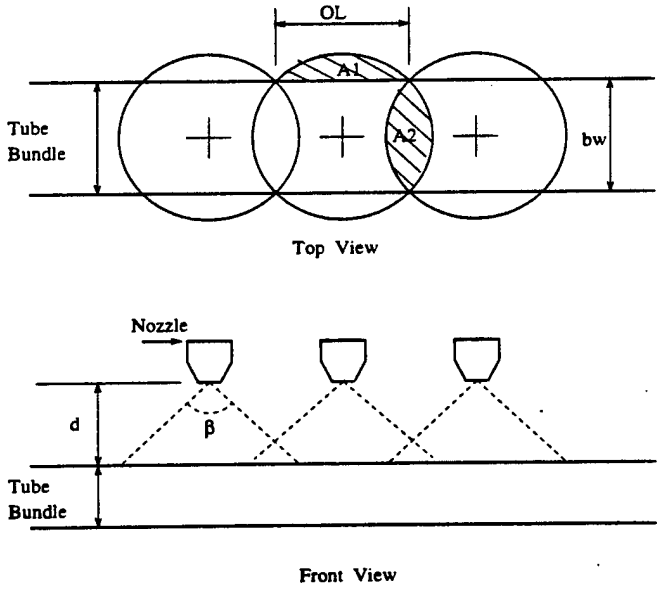

Figure 7.16. Schematic of nozzle spray system design.

However, the angle of a spray cone (β) varies with the spray flow rate, the higher spray rate producing the smaller angle, and thus, the optimal height (d) varies with the spray flow rate. Also, the overlapped area (A2) tends to be greater than the minimum value mentioned above in order to wet the tube surface enough. Thus, fluids of lower surface tension may require higher feed rates.

Heat Transfer Performance at High Loads

Dry patches occur when the liquid feed rate is relatively low compared to the high heat load present, and they first appear on the top surface of tubes where the film is the thinnest. If the sprayed fluid has low surface tension, the liquid is not allowed to remain long on the tube surface and falls off before being evaporated because the gravitational effects easily overcome the surface tension effects.

Since the effective flow rate was limited by the pumping power in the present study, data were not taken at high heat flux where dry-out phenomenon was significant. The dry-out problem at high heat flux can be avoided by techniques which improve the effective liquid distribution onto the tube. For instance, the liquid can be distributed directly onto the tube.

Applicability of Single-Tube Data to the Design of a Spray Evaporator

The applicability of single-tube data to the design of large-scale evaporators was investigated by Lorenz and Yung [26]. Below the critical Reynolds number of 300, the single tube was found to have higher heat transfer coefficients than the tube bundle where dry-out spots occurred on its tubes. Beyond the critical Reynolds number of 300, the average heat transfer coefficients of the bundle were equal to that of the single tube when the Reynolds number was large enough so that all the tubes were fully wetted. Nevertheless, these results were based on the low operating heat flux of 4 to 8 kW/m^2 in tests with ammonia. The critical Reynolds number might be raised under the higher heat flux conditions.

No published data regarding spray evaporation of HFC-236ea on tube bundles were available for comparison of the single-tube data taken in this study.

REFERENCES

1. Bare, J. C. 1993. "Simulation of performance of chlorine-free fluorinated ethers and fluorinated hydrocarbons to replace CFC-11 and CFC-114 in chillers." ASHRAE Transactions, Vol. 99(1), pp. 397-407.
2. Huebsch, W. W. and Pate, M. B. 1996. "Heat transfer evaluation of HFC-236ea and CFC-114 in condensation and evaporation." EPA-600/R-96-070 (NTIS PB96-183900), U. S. Environmental Protection Agency, Research Triangle Park, NC.
3. Thome, J. R. 1990. In Enhanced Boiling Heat Transfer, New York: Hemisphere Publishing Co.
4. Huber, J. B., Rewerts, L. E., and Pate, M. B. 1994. "Shell-side condensation heat transfer of R-134a— Part II: Enhanced tube performance." ASHRAE Transactions, Vol. 100(2), pp. 248-256.
5. Briggs, A., Baichoo, S., and Rose, J. W. 1994. "Condensation of steam and CFC113 on commercially available integral-fin tubes." Fundamentals of Phase Change: Boiling and Condensation, ASME, Heat Transfer Division, New York, NY. HTD, Vol. 273, pp. 41-47.
6. Sukhatme, S. P., Jagadish, B. S., and Prabhakaran, P. 1990. "Film condensation of R-11 vapor on single horizontal enhanced condenser tubes." Journal of Heat Transfer, Vol. 112, pp. 229-234.
7. Ullmann, A. and Letan, R. 1989. "Effect of noncondensibles on condensation and evaporation of bubbles." Journal of Heat Transfer, Vol. 111, pp. 1060-1067.
8. Huber, J. B. 1994. "Experimental determination of shell-side condenser bundle heat transfer design factors for refrigerants R-123 and R-134a." Ph.D. Dissertation, Iowa State University.
9. Webb, R. L. and Murawski, C. G. 1990. "Row effect for R-11 condensation on enhanced tubes." Journal of Heat Transfer, Vol. 112, pp. 768-776.
10. Cheng, W. Y. and Wang, C. 1994. "Condensation of R-134a on enhanced tubes." ASHRAE Transactions, Vol. 100(2), pp. 809-817.
11. Honda, H., Uchima, B., Nozu, S., Torigoe, E., and Imai, S. 1992. "Film condensation of R-113 on staggered bundles of horizontal finned tubes." Journal of Heat Transfer, Vol. 114, pp. 442-449.
12. Nguyen, T.-N. and Orozco, J. A. 1994. "Condensation of R-113 on enhanced surfaces." ASHRAE Transactions, Vol. 100(1), pp. 736-743.
13. Nusselt, W. 1916. "Die Oberflachenkondensation des Wasserdampfes." Z. Ver. Deut. Ing., Vol. 60, pp. 541-569.
14. Kern, K. Q. 1958. "Mathematical development of loading in horizontal condenser." AIChE Journal. Vol. 4, pp. 157-160.

15. Incropera, F. P. and DeWitt, D. P. 1990. In Fundamentals of Heat and Mass Transfer, 3rd ed. New York: Wiley.
16. Collier, J. G. and Thome, J. R. 1994. In Convective Boiling and Condensation, 3rd ed. New York: Oxford University Press, Inc., p. 430.
17. Webb, R. L. 1981. "The evolution of enhanced surface geometries for nucleate boiling." Heat Transfer Engineering, Vol. 2, pp. 46-69.
18. Pais, C. and Webb, R. L. 1991. "Literature survey of pool boiling on enhanced surfaces." ASHRAE Transactions, Vol. 97(1), pp. 79-89.
19. Barthau, G. 1992. "Active nucleation site density and pool boiling heat transfer — an experimental study." Int. J. Heat Mass Transfer, Vol. 35, pp. 271-278.
20. Hahne, E., Chen, Q., and Windisch, R. 1991. "Pool boiling heat transfer on finned tubes — an experimental and theoretical study." Int. J. Heat Mass Transfer, Vol. 34, pp. 2071-2079.
21. Webb, R. L. and Pais, C. 1991. "Pool boiling data for five refrigerants on three tube geometries." ASHRAE Transactions, Vol. 97(1), pp. 72-78.
22. Webb, R. L., Choi, K. D., and Apparao, T. R. 1989. "Prediction of the heat duty in flooded refrigerant evaporators." ASHRAE Transactions, Vol. 95(1), pp. 339-348.
23. Hahne, E. and Müller , J. 1983. "Boiling on a finned tube and finned tube bundle." Int. J. Heat Mass Transfer, Vol. 26, pp. 849-859.
24. Zeng, X., Chyu, M. C., and Ayub, Z. H. 1994. "Characteristic study of sprayed fluid flow in a tube bundle." ASHRAE Transactions, Vol. 100(1), pp. 63-72.
25. Moeykens, S. A. and Pate, M. B. 1994. "Spray evaporation heat transfer of R-134a on plain tubes." ASHRAE Transactions, Vol. 100(2), pp. 173-184.
26. Lorenz, J. J. and Yung, D. 1982. "Film breakdown and bundle-depth effects in horizontal-tube, falling-film evaporators." Journal of Heat Transfer, Vol. 104, pp. 569-571.

APPENDIX A

REFRIGERANT PROPERTIES

TABLE A.1: PROPERTIES OF HFC-236ea

Temperature (°C)	Pressure (kPa)	Enthalpy (kJ/kg)	Density (kg/m^3)	Viscosity (mPa s)	Thermal Conductivity (W/m K)	Phase
2.0	85.14	213.5	5.920	10.26	0.0109	Vapor
2.0	85.14	48.2	1497.	539.6	0.0803	Liquid
40.0	337.6	239.8	22.19	11.92	0.0139	Vapor
40.0	337.6	94.6	1377.	313.6	0.0665	Liquid

APPENDIX B

PROJECT SUMMARY OF HEAT TRANSFER EVALUATION OF HFC-236ea AND CFC-114 IN CONDENSATION AND EVAPORATION

A copy of the project summary for the Phase I report, which was prepared by Huebsch and Pate [2], is presented here.

United States
Environmental Protection
Agency
Research and Development

National Risk Management
Research Laboratory
Research Triangle Park, NC 27711
EPA/600/SR-96/070 August 1996

EPA

Project Summary

Heat Transfer Evaluation of HFC-236ea and CFC-114 in Condensation and Evaporation

W. W. Huebsch and M. B. Pate

With the mandatory phaseout of chlorofluorocarbons (CFCs), as dictated by the Montreal Protocol and the Clean Air Act Amendments, it is imperative for the Navy to find a replacement for 1,1,2,2-dichloro-tetrafluoroethane (CFC-114) that is environmentally safe and possesses similar performance characteristics. Currently, one of the leading candidates to replace CFC-114 is hexafluoropropane (HFC-236ea). This research focuses on comparing the refrigerants not only in condensation and pool boiling, but also with various tube surfaces.

The test facility used in this study was initially used for spray evaporation testing; however, it was redesigned and modified for use with condensation, pool boiling, or spray evaporation testing. During condensation, the rig was capable of producing saturated or superheated vapor. During pool boiling or spray evaporation, the test facility was capable of testing pure refrigerants or refrigerant/lubricant mixtures. The test facility is described in detail in the full report.

The two refrigerants produced similar performance characteristics in condensing vapor on integral-fin tubes, so that the transition to HFC-236ea should be accomplished without major modifications to existing condensers. The results also showed that the condensation of superheated vapor had negligible effects on the shell-side heat transfer coefficient as compared to condensation of saturated vapor results. The superheated vapor data for the 26 and 40 fpi (fins per inch) tubes were within 5 and 3%, respectively, of the saturated vapor results for the same tube surface.

HFC-236ea produced higher boiling coefficients than CFC-114 for all tubes tested. In addition, the 26 fpi tube outperformed the 40 fpi tube by 18% and the plain tube by 41% for HFC-236ea. The maximum increase in boiling with HFC-236ea was 39% for the 26 fpi tube and 34% for the 40 fpi tube.

The mineral oil used with CFC-114 showed a general improvement in the heat transfer performance, while the polyol-ester oil consistently degraded the performance of HFC-236ea. Even then the boiling performance of HFC-236ea was either equal to or greater than the performance of CFC-114 for all tested parameters.

This Project Summary was developed by EPA's National Risk Management Research Laboratory's Air Pollution Prevention and Control Division, Research Triangle Park, NC, to announce key findings of the research project that is fully documented in a separate report of the same title (see Project Report ordering information at back).

Introduction

The U.S. Navy presently uses CFC-114 as the working refrigerant in shipboard and submarine chiller units. With the mandatory phaseout of CFCs dictated by the Montreal Protocol, it is imperative for the Navy to find a replacement that is environmentally safe and possesses similar performance characteristics to CFC-114. Currently, one of the leading candidates to replace CFC-114 is HFC-236ea. This

alternative refrigerant is the focus of the results presented here. There are several reasons for choosing this refrigerant to replace CFC-114. First, there is currently a commercial production route available for acquiring the refrigerant. Of special importance, the operating capacities, pressures, and temperatures are very similar to those of CFC-114, and initial modeling indicates that the performance is within 1% of that of CFC-114.

This research focuses on comparing the refrigerants not only in condensation and pool boiling but also with various tube surfaces. Horizontal, integral finned tubes have been in service for over 40 years, and these tubes are widely used because of their higher performance compared to plain tubes.

The scope of this project was:

- Modify an existing spray evaporation test facility so it can perform condensation and pool boiling tests using a two-pass single-tube setup.
- Test alternative refrigerant HFC-236ea and compare its performance to CFC-114 as the reference fluid.
- Evaluate the plain and 26 and 40 fpi tubes for condensation.
- Evaluate the plain and 26 and 40 fpi tubes for flooded evaporation.
- Investigate oil effects in pool boiling on the shell-side heat transfer performance by varying the oil concentration from 0 to 3%.
- Compare results to published correlations for condensation and pool boiling.

Experimental Apparatus

The test facility used in this study was initially used for spray evaporation testing; however, it was redesigned and modified for use with condensation, pool boiling, or spray evaporation testing. During condensation, the rig was capable of producing saturated or superheated vapor. During pool boiling or spray evaporation, the test facility was capable of testing pure refrigerants or refrigerant/lubricant mixtures. The test facility is described in detail in the full report.

During some boiling experiments, lubricant was mixed with the refrigerant. Miscibility and solubility testing for CFC-114 and HFC-236ea were performed previous to this research in another portion of the project. These results along with other criteria such as material compatibility determined which lubricants would be used in the refrigerant/lubricant mixtures. The mineral oil used with CFC-114 was York "C" with a viscosity of 315 SUS (68 cSt--centistoke-- at 40°C). The miscibility data also showed that a synthetic ester refrigerant oil was to be used with HFC-236ea. This lubricant is a polyol-ester oil with a viscosity of 340 SUS. The trade name is Castrol Icematic SW-68. The two lubricants were miscible with the corresponding refrigerants over the entire range of conditions tested in this research.

Results and Discussion

The main objective of this study was to conduct an experimental heat transfer evaluation comparing the performance of CFC-114 and HFC-236ea in the condensation and pool boiling environments. The condensation testing included an investigation of saturated and superheated vapor on fin-tube surfaces. The pool boiling research involved nucleate boiling of pure refrigerant and refrigerant/lubricant mixtures on fin-tube surfaces.

All of the tubes used in this study had a nominal outside diameter of 19.1 mm (0.75 in.) and a length of 838.2 mm (33 in.). The shell-side heat transfer coefficients presented in this study were based on the outside surface area of a corresponding smooth tube, with the outer diameter measured over the surface enhancement. Therefore, the calculated heat transfer coefficient takes into account the area enhancement, fin efficiency, and surface enhancement of the tubes tested.

Condensation Heat Transfer

The refrigerants CFC-114 and HFC-236ea were evaluated in the condensation environment on the plain and 26 and 40 fpi tube surfaces. In addition, the effects on the heat transfer performance from condensing superheated vapor were investigated with CFC-114. During saturated vapor testing, the saturation temperature was held constant at 40°C. For condensation of superheated vapor, the saturation temperature was also 40°C, but the incoming vapor was 3 to 5°C higher than T_{sat}.

For condensation of both refrigerants, the integral-fin tubes yielded heat transfer coefficients approximately four times those produced from the plain tube. In addition, all combinations of the finned tubes and refrigerants produced similar shell-side condensation coefficients in the heat flux range tested, with a maximum deviation of 9%.

The results also showed that the condensation of superheated vapor had negligible effects on the shell-side heat transfer coefficient with respect to saturated vapor results. The superheated vapor data for the 26 and 40 fpi tubes were within 5 and 3%, respectively, of the saturated vapor results for the same tube surface.

The correlation comparison made with the plain tube results showed excellent agreement with the Nusselt correlation. The CFC-114 and HFC-236ea data were predicted within ±3 and ±10%, respectively. The Beatty and Katz correlation was able to predict the 26 fpi tube data for both refrigerants with a maximum deviation of 15%. The predictions for the 40 fpi tube resulted in larger deviations. The Beatty and Katz correlation predicted the 40 fpi tube data within 18 and 21% for CFC-114 and HFC-236ea, respectively.

The two refrigerants produced similar performance characteristics in condensing vapor on integral-fin tubes, so the transition to HFC-236ea should be accomplished without major modifications to existing condensers. Overall, the above information shows that HFC-236ea is a valid replacement for CFC-114 in the condensation environment.

Pool Boiling Heat Transfer

CFC-114 and HFC-236ea were evaluated in the pool boiling environment on plain and 26 and 40 fpi tube surfaces. In addition, this study investigated the effects of small concentrations of oil on the heat transfer performance. The concentrations tested were 1 and 3% by mass using a 68 cSt mineral oil for CFC-114 and a 340 SUS polyol-ester oil for HFC-236ea. During pool boiling, data were taken at a constant saturation temperature of 2°C for both pure refrigerant and refrigerant/lubricant mixtures.

The pool boiling results for the pure refrigerants show that the tube performance for CFC-114 and HFC-236ea fall in the following order from high to low: 26 fpi, 40 fpi, and plain tube. The 26 fpi tube produced boiling coefficients for CFC-114 that were 12 and 30% higher than for the 40 fpi tube and the plain tube, respectively. For HFC-236ea, the 26 fpi tube outperformed the 40 fpi tube by 18% and the plain tube by 41%. In addition, HFC-236ea produced higher boiling coefficients than CFC-114 for all tubes tested. The maximum increase in boiling with HFC-236ea was 39% for the 26 fpi tube and 34% for the 40 fpi tube.

The lubricant addition with CFC-114 produced enhancements in the boiling coefficients for the three tubes tested with oil. The maximum enhancement occurred at a 3% oil concentration for each tube. The addition of oil at a 1% concentration improved the heat transfer coefficients for the 26 fpi tube by 27%, while the 3% oil

concentration only showed minor improvement over the 1% results. The 40 fpi tube produced similar trends to the 26 fpi tube at both oil concentrations.

Pool boiling of HFC-236ea with the polyol-ester oil produced consistent decreases in the heat transfer performance at both concentrations. The 26 fpi tube showed a decrease in performance of 6 and 17% at oil concentrations of 1 and 3%, respectively. The 40 fpi tube had only a 10% decrease in the boiling coefficients at a 3% concentration with respect to the pure refrigerant. At an oil concentration of 1%, the 40 fpi tube showed negligible oil effects in the low heat flux range. It is evident that the oil enhancement gained from the turbulent mixing within the foaming layer is dependent upon the type of oil. The mineral oil used with CFC-114 showed a general improvement in the heat transfer performance, while the polyol-ester oil consistently degraded the performance of HFC-236ea.

It is also worth noting that, even though the pure HFC-236ea results are higher than those for CFC-114, the oil effects on both refrigerants cause the boiling coefficients to be within 12% for the 26 fpi tube at an oil concentration of 3%. Therefore, the addition of oil decreased the deviation in the heat transfer coefficients between the two refrigerants. CFC-114 consistently produced higher boiling coefficients than HFC-236ea for both finned tubes at a 3% oil concentration.

A review of the above information shows that HFC-236ea is a valid replacement for CFC-114 in the nucleate boiling environment. The boiling performance of HFC-236ea was either equal to or greater than the performance of CFC-114 for all testing parameters. With the similar boiling characteristics, transition to HFC-236ea in a flooded evaporator would be relatively simple.

Summary

The two refrigerants produced similar performance characteristics in condensing vapor on integral-fin tubes, so that the transition to HFC-236ea should be accomplished without major modifications to existing condensers. The results also showed that the condensation of superheated vapor had negligible effects on the shell-side heat transfer coefficient with respect to the saturated vapor results. The superheated vapor data for the 26 and 40 fpi tubes were within 5 and 3%, respectively, of the saturated vapor results for the same tube surface.

HFC-236ea produced higher boiling coefficients than CFC-114 for all tubes tested. In addition, the 26 fpi tube outperformed the 40 fpi tube by 18% and the plain tube by 41% for HFC-236ea. The maximum increase in the boiling heat transfer coefficient with HFC-236ea was 39% for the 26 fpi tube and 34% for the 40 fpi tube. The mineral oil used with CFC-114 produced a general improvement in the heat transfer performance, while the polyol-ester oil consistently degraded the performance of HFC-236ea. Even then, the boiling performance of HFC-236ea was either equal to or greater than the performance of CFC-114 for all testing parameters.

W. W. Huebsch and M. B. Pate are with Iowa State University, Ames, IA 50011.
Theodore G. Brna is the EPA Project Officer (see below).
The complete report, entitled "Heat Transfer Evaluation of HFC-236ea and CFC-114 in Condensation and Evaporation," (Order No. PB96-183900; Cost: $31.00, subject to change) will be available only from:
National Technical Information Service
5285 Port Royal Road
Springfield, VA 22161
Telephone: 703-487-4650
The EPA Project Officer can be contacted at:
Air Pollution Prevention and Control Division
National Risk Management Research Laboratory
U.S. Environmental Protection Agency
Research Triangle Park, NC 27711

APPENDIX C

GEOMETRIC SPECIFICATIONS OF TUBES

TABLE C.1 GEOMETRIC SPECIFICATIONS OF TUBES IN SI UNITS

tube	fin count (fins/m)	D_o nominal (mm)	D_i nominal (mm)	D_r (mm)	fin height (mm)	A_o/L nominal (m^2/m)	A_o/L actual (m^2/m)	A_r/L nominal (m^2/m)
1024-fpm	1024	18.8	14.4	15.9	1.45	0.0588	0.193	0.0454
1575-fpm	1575	18.8	15.7	17.1	0.86	0.0593	0.179	0.0493
Turbo-CII	N/A	18.90	15.54	17.07	0.91	0.0597	N/A	0.0488
Turbo-B	N/A	18.5	16.1	17.3	0.59	0.0582	N/A	0.0506
Turbo-BII	N/A	18.62	16.05	17.27	0.68	0.0585	N/A	0.0504

TABLE C.2 GEOMETRIC SPECIFICATIONS OF TUBES IN ENGLISH UNITS

tube	fin count (fins/in)	D_o nominal (in)	D_i nominal (in)	D_r (in)	fin height (in)	A_o/L nominal (ft^2/ft)	A_o/L actual (ft^2/ft)	A_r/L nominal (ft^2/ft)
26-fpi	26	0.739	0.568	0.625	0.057	0.193	0.634	0.149
40-fpi	40	0.743	0.622	0.675	0.034	0.195	0.586	0.163
Turbo-CII	N/A	0.744	0.612	0.672	0.036	0.196	N/A	0.160
Turbo-B	N/A	0.730	0.632	0.682	0.024	0.191	N/A	0.165
Turbo-BII	N/A	0.733	0.632	0.680	0.027	0.192	N/A	0.165

APPENDIX D

TABULATED DATA

The experimental data obtained in this study are presented in this appendix.

TABLE D.1 CONDENSATION OF HFC-236ea ON THE TURBO-CII TUBE AT A SATURATION TEMPERATURE OF 40°C (PRIMARY RUN)

h (W/m^2K)	9.79E+03	1.13E+04	1.23E+04	1.31E+04	1.37E+04	1.42E+04
q" (W/m^2)	1.50E+04	2.00E+04	2.50E+04	3.00E+04	3.50E+04	4.00E+04
q (Watts)	7.54E+02	1.00E+03	1.26E+03	1.51E+03	1.76E+03	2.01E+03
LMTD (°C)	3.02E+00	3.35E+00	3.71E+00	4.06E+00	4.38E+00	4.72E+00
Δ T (°C)	1.57E+00	1.72E+00	1.90E+00	2.07E+00	2.23E+00	2.39E+00
h_i (W/m^2K)	1.29E+04	1.63E+04	1.93E+04	2.22E+04	2.51E+04	2.78E+04
Re_i	1.08E+04	1.44E+04	1.77E+04	2.10E+04	2.45E+04	2.77E+04
U_o (W/m^2K)	5.05E+03	6.05E+03	6.84E+03	7.51E+03	8.12E+03	8.61E+03
UN (± %)	7.63E+00	7.00E+00	6.46E+00	6.10E+00	5.78E+00	5.51E+00

TABLE D.2 CONDENSATION OF HFC-236ea ON THE TURBO-CII TUBE AT A SATURATION TEMPERATURE OF 40°C (REPEAT RUN)

h (W/m^2K)	9.77E+03	1.12E+04	1.22E+04	1.31E+04	1.37E+04	1.42E+04
q" (W/m^2)	1.50E+04	2.00E+04	2.50E+04	3.00E+04	3.50E+04	4.00E+04
q (Watts)	7.54E+02	1.00E+03	1.25E+03	1.50E+03	1.75E+03	2.01E+03
LMTD (°C)	3.03E+00	3.38E+00	3.73E+00	4.05E+00	4.38E+00	4.71E+00
Δ T (°C)	1.57E+00	1.74E+00	1.91E+00	2.07E+00	2.23E+00	2.39E+00
h_i (W/m^2K)	1.29E+04	1.62E+04	1.92E+04	2.22E+04	2.51E+04	2.78E+04
Re_i	1.08E+04	1.43E+04	1.76E+04	2.11E+04	2.44E+04	2.77E+04
U_o (W/m^2K)	5.05E+03	6.02E+03	6.81E+03	7.52E+03	8.11E+03	8.61E+03
UN (± %)	7.63E+00	6.92E+00	6.43E+00	6.07E+00	5.77E+00	5.52E+00

TABLE D.3 POOL BOILING OF HFC-236ea ON THE TURBO-B TUBE AT A SATURATION TEMPERATURE OF 2°C (PRIMARY RUN)

h (W/m^2K)	8.27E+03	7.72E+03	7.08E+03	6.40E+03	5.65E+03	4.74E+03
q" (W/m^2)	4.00E+04	3.49E+04	2.99E+04	2.50E+04	2.01E+04	1.50E+04
q (Watts)	2.00E+03	1.75E+03	1.50E+03	1.25E+03	1.01E+03	7.50E+02
LMTD (°C)	7.36E+00	6.97E+00	6.59E+00	6.17E+00	5.73E+00	5.19E+00
Δ T (°C)	3.70E+00	3.51E+00	3.32E+00	3.11E+00	2.89E+00	2.63E+00
h_i (W/m^2K)	2.11E+04	1.89E+04	1.66E+04	1.43E+04	1.19E+04	9.40E+03
Re_i	1.43E+04	1.24E+04	1.05E+04	8.69E+03	6.86E+03	5.07E+03
U_o (W/m^2K)	5.60E+03	5.16E+03	4.68E+03	4.17E+03	3.61E+03	2.97E+03
UN (± %)	6.46E+00	6.72E+00	7.02E+00	7.39E+00	7.87E+00	8.56E+00

TABLE D.4 POOL BOILING OF HFC-236ea ON THE TURBO-B TUBE AT A SATURATION TEMPERATURE OF 2°C (REPEAT RUN)

h (W/m^2K)	8.42E+03	7.88E+03	7.30E+03	6.70E+03	5.89E+03	5.03E+03
q" (W/m^2)	3.99E+04	3.49E+04	2.98E+04	2.49E+04	1.97E+04	1.49E+04
q (Watts)	2.00E+03	1.75E+03	1.50E+03	1.25E+03	9.88E+02	7.46E+02
LMTD (°C)	7.25E+00	6.87E+00	6.44E+00	5.98E+00	5.48E+00	4.98E+00
Δ T (°C)	3.65E+00	3.46E+00	3.25E+00	3.02E+00	2.77E+00	2.52E+00
h_i (W/m^2K)	2.12E+04	1.89E+04	1.66E+04	1.43E+04	1.19E+04	9.36E+03
Re_i	1.43E+04	1.24E+04	1.05E+04	8.62E+03	6.81E+03	5.03E+03
U_o (W/m^2K)	5.67E+03	5.23E+03	4.77E+03	4.29E+03	3.70E+03	3.08E+03
UN (± %)	6.57E+00	6.82E+00	7.20E+00	7.67E+00	8.28E+00	9.04E+00

TABLE D.5 POOL BOILING OF HFC-236ea ON THE TURBO-BII TUBE AT A SATURATION TEMPERATURE OF 2°C (PRIMARY RUN)

h (W/m^2K)	1.03E+04	9.94E+03	9.53E+03	9.19E+03	8.69E+03	8.02E+03
q" (W/m^2)	3.98E+04	3.50E+04	2.96E+04	2.49E+04	2.01E+04	1.50E+04
q (Watts)	2.00E+03	1.76E+03	1.48E+03	1.25E+03	1.01E+03	7.53E+02
LMTD (°C)	6.68E+00	6.27E+00	5.75E+00	5.28E+00	4.80E+00	4.23E+00
Δ T (°C)	3.36E+00	3.16E+00	2.90E+00	2.67E+00	2.43E+00	2.16E+00
h_i (W/m^2K)	1.72E+04	1.54E+04	1.35E+04	1.16E+04	9.69E+03	7.61E+03
Re_i	1.41E+04	1.22E+04	1.03E+04	8.47E+03	6.70E+03	4.93E+03
U_o (W/m^2K)	5.94E+03	5.56E+03	5.13E+03	4.69E+03	4.17E+03	3.53E+03
UN (± %)	7.96E+00	8.50E+00	9.36E+00	1.04E+01	1.18E+01	1.40E+01

TABLE D.6 POOL BOILING OF HFC-236ea ON THE TURBO-BII TUBE AT A SATURATION TEMPERATURE OF2°C (REPEAT RUN)

h (W/m^2K)	1.03E+04	1.01E+04	9.83E+03	9.48E+03	9.05E+03	8.26E+03
q" (W/m^2)	3.98E+04	3.50E+04	2.99E+04	2.50E+04	1.99E+04	1.49E+04
q (Watts)	2.00E+03	1.76E+03	1.50E+03	1.25E+03	9.98E+02	7.48E+02
LMTD (°C)	6.66E+00	6.23E+00	5.72E+00	5.22E+00	4.67E+00	4.15E+00
Δ T (°C)	3.36E+00	3.14E+00	2.89E+00	2.64E+00	2.37E+00	2.11E+00
h_i (W/m^2K)	1.72E+04	1.53E+04	1.35E+04	1.16E+04	9.66E+03	7.60E+03
Re_i	1.41E+04	1.21E+04	1.03E+04	8.44E+03	6.67E+03	4.91E+03
U_o (W/m^2K)	5.95E+03	5.60E+03	5.22E+03	4.76E+03	4.24E+03	3.58E+03
UN (± %)	7.98E+00	8.58E+00	9.48E+00	1.06E+01	1.23E+01	1.45E+01

TABLE D.7 SPRAY EVAPORATION OF HFC-236ea ON THE TURBO-B TUBE AT A SATURATION TEMPERATURE OF 2°C (FLOW RATE = 2.6 kg/min, RUN 1)

h (W/m^2K)	1.16E+04	1.06E+04	8.28E+03	5.97E+03
q" (W/m^2)	1.50E+04	1.96E+04	2.50E+04	2.97E+04
q (Watts)	7.50E+02	9.82E+02	1.26E+03	1.49E+03
LMTD (°C)	3.32E+00	3.96E+00	5.30E+00	7.32E+00
Δ T (°C)	1.71E+00	2.02E+00	2.68E+00	3.68E+00
h_i (W/m^2K)	9.18E+03	1.17E+04	1.42E+04	1.68E+04
Re_i	4.82E+03	6.55E+03	8.48E+03	1.07E+04
U_o (W/m^2K)	4.65E+03	5.10E+03	4.87E+03	4.18E+03
UN (± %)	1.88E+01	1.36E+01	8.98E+00	6.30E+00

TABLE D.8 SPRAY EVAPORATION OF HFC-236ea ON THE TURBO-B TUBE AT A SATURATION TEMPERATURE OF 2°C (FLOW RATE = 2.6 kg/min, RUN 2)

h (W/m^2K)	5.94E+03	7.65E+03	9.82E+03	1.12E+04	1.07E+04
q" (W/m^2)	2.97E+04	2.52E+04	2.00E+04	1.49E+04	1.01E+04
q (Watts)	1.49E+03	1.26E+03	1.00E+03	7.47E+02	5.06E+02
LMTD (°C)	7.34E+00	5.57E+00	4.20E+00	3.35E+00	2.83E+00
Δ T (°C)	3.69E+00	2.82E+00	2.14E+00	1.72E+00	1.47E+00
h_i (W/m^2K)	1.68E+04	1.42E+04	1.17E+04	9.18E+03	6.58E+03
Re_i	1.08E+04	8.54E+03	6.60E+03	4.82E+03	3.16E+03
U_o (W/m^2K)	4.16E+03	4.65E+03	4.92E+03	4.59E+03	3.67E+03
UN (± %)	6.28E+00	8.39E+00	1.25E+01	1.84E+01	2.53E+01

TABLE D.9 SPRAY EVAPORATION OF HFC-236ea ON THE TURBO-B TUBE AT A SATURATION TEMPERATURE OF 2°C (FLOW RATE = 2.8 kg/min, RUN 1)

h (W/m^2K)	1.16E+04	1.09E+04	9.64E+03	7.44E+03
q" (W/m^2)	1.49E+04	1.97E+04	2.49E+04	3.00E+04
q (Watts)	7.49E+02	9.88E+02	1.25E+03	1.50E+03
LMTD (°C)	3.31E+00	3.95E+00	4.85E+00	6.40E+00
Δ T (°C)	1.70E+00	2.01E+00	2.46E+00	3.22E+00
h_i (W/m^2K)	9.17E+03	1.16E+04	1.40E+04	1.66E+04
Re_i	4.81E+03	6.51E+03	8.34E+03	1.04E+04
U_o (W/m^2K)	4.65E+03	5.14E+03	5.29E+03	4.83E+03
UN (± %)	1.89E+01	1.39E+01	1.02E+01	7.26E+00

TABLE D.10 SPRAY EVAPORATION OF HFC-236ea ON THE TURBO-B TUBE AT A SATURATION TEMPERATURE OF 2°C (FLOW RATE = 2.8 kg/min, RUN 2)

h (W/m^2K)	7.43E+03	9.27E+03	1.05E+04	1.13E+04	1.03E+04
q" (W/m^2)	3.00E+04	2.49E+04	1.98E+04	1.52E+04	9.04E+03
q (Watts)	1.50E+03	1.25E+03	9.93E+02	7.63E+02	4.53E+02
LMTD (°C)	6.40E+00	4.95E+00	4.02E+00	3.41E+00	2.58E+00
Δ T (°C)	3.23E+00	2.51E+00	2.05E+00	1.75E+00	1.34E+00
h_i (W/m^2K)	1.66E+04	1.41E+04	1.17E+04	9.19E+03	6.53E+03
Re_i	1.04E+04	8.39E+03	6.55E+03	4.82E+03	3.11E+03
U_o (W/m^2K)	4.82E+03	5.19E+03	5.07E+03	4.60E+03	3.61E+03
UN (± %)	7.25E+00	9.89E+00	1.34E+01	1.81E+01	2.71E+01

TABLE D.11 SPRAY EVAPORATION OF HFC-236ea ON THE TURBO-B TUBE AT A SATURATION TEMPERATURE OF 2°C (FLOW RATE = 3.0 kg/min, RUN 1)

h (W/m^2K)	1.16E+04	1.07E+04	9.36E+03	7.83E+03
q" (W/m^2)	1.49E+04	2.00E+04	2.50E+04	3.00E+04
q (Watts)	7.48E+02	1.00E+03	1.26E+03	1.50E+03
LMTD (°C)	3.31E+00	4.02E+00	4.96E+00	6.20E+00
Δ T (°C)	1.71E+00	2.05E+00	2.51E+00	3.13E+00
h_i (W/m^2K)	9.17E+03	1.17E+04	1.41E+04	1.65E+04
Re_i	4.81E+03	6.55E+03	8.38E+03	1.04E+04
U_o (W/m^2K)	4.64E+03	5.12E+03	5.21E+03	4.98E+03
UN (± %)	1.89E+01	1.35E+01	9.91E+00	7.52E+00

TABLE D.12 SPRAY EVAPORATION OF HFC-236ea ON THE TURBO-B TUBE AT A SATURATION TEMPERATURE OF 2°C (FLOW RATE = 3.0 kg/min, RUN 2)

h (W/m^2K)	7.83E+03	9.32E+03	1.05E+04	1.14E+04
q" (W/m^2)	3.00E+04	2.50E+04	1.99E+04	1.49E+04
q (Watts)	1.50E+03	1.25E+03	9.97E+02	7.50E+02
LMTD (°C)	6.20E+00	4.95E+00	4.04E+00	3.34E+00
Δ T (°C)	3.13E+00	2.51E+00	2.06E+00	1.72E+00
h_i (W/m^2K)	1.65E+04	1.41E+04	1.16E+04	9.17E+03
Re_i	1.04E+04	8.37E+03	6.54E+03	4.81E+03
U_o (W/m^2K)	4.98E+03	5.20E+03	5.08E+03	4.62E+03
UN (± %)	7.52E+00	9.92E+00	1.34E+01	1.86E+01

TABLE D.13 SPRAY EVAPORATION OF HFC-236ea ON THE TURBO-B TUBE AT A SATURATION TEMPERATURE OF 2°C (FLOW RATE = 3.0 kg/min, REPEAT RUN FOR RUN 1)

h (W/m^2K)	1.20E+04	1.11E+04	9.40E+03	7.91E+03
q" (W/m^2)	1.49E+04	1.99E+04	2.49E+04	3.01E+04
q (Watts)	7.46E+02	1.00E+03	1.25E+03	1.51E+03
LMTD (°C)	3.25E+00	3.95E+00	4.92E+00	6.19E+00
Δ T (°C)	1.67E+00	2.02E+00	2.49E+00	3.12E+00
h_i (W/m^2K)	9.16E+03	1.16E+04	1.41E+04	1.65E+04
Re_i	4.80E+03	6.53E+03	8.39E+03	1.04E+04
U_o (W/m^2K)	4.72E+03	5.20E+03	5.22E+03	5.01E+03
UN (± %)	1.96E+01	1.40E+01	1.00E+01	7.55E+00

TABLE D.14 SPRAY EVAPORATION OF HFC-236ea ON THE TURBO-B TUBE AT A SATURATION TEMPERATURE OF 2°C (FLOW RATE = 3.0 kg/min, REPEAT RUN FOR RUN 2)

h (W/m^2K)	7.88E+03	9.36E+03	1.08E+04	1.17E+04
q" (W/m^2)	3.01E+04	2.50E+04	2.00E+04	1.49E+04
q (Watts)	1.51E+03	1.25E+03	1.01E+03	7.47E+02
LMTD (°C)	6.20E+00	4.94E+00	4.01E+00	3.29E+00
Δ T (°C)	3.13E+00	2.50E+00	2.05E+00	1.70E+00
h_i (W/m^2K)	1.66E+04	1.41E+04	1.17E+04	9.18E+03
Re_i	1.04E+04	8.38E+03	6.55E+03	4.82E+03
U_o (W/m^2K)	5.00E+03	5.21E+03	5.15E+03	4.66E+03
UN (± %)	7.53E+00	9.93E+00	1.36E+01	1.90E+01

TABLE D.15 SPRAY EVAPORATION OF HFC-236ea ON THE TURBO-B TUBE AT A SATURATION TEMPERATURE OF 2°C (FLOW RATE = 3.2 kg/min, RUN 1)

h (W/m^2K)	1.18E+04	1.10E+04	9.63E+03	8.57E+03
q" (W/m^2)	1.49E+04	1.98E+04	2.50E+04	3.00E+04
q (Watts)	7.49E+02	9.91E+02	1.25E+03	1.51E+03
LMTD (°C)	3.30E+00	3.94E+00	4.87E+00	5.87E+00
Δ T (°C)	1.70E+00	2.01E+00	2.47E+00	2.97E+00
h_i (W/m^2K)	9.16E+03	1.16E+04	1.41E+04	1.65E+04
Re_i	4.80E+03	6.53E+03	8.35E+03	1.03E+04
U_o (W/m^2K)	4.67E+03	5.17E+03	5.29E+03	5.27E+03
UN (± %)	1.91E+01	1.39E+01	1.02E+01	8.04E+00

TABLE D.16 SPRAY EVAPORATION OF HFC-236ea ON THE TURBO-B TUBE AT A SATURATION TEMPERATURE OF 2°C (FLOW RATE = 3.2 kg/min, RUN 2)

h (W/m^2K)	8.52E+03	9.60E+03	1.09E+04	1.17E+04	1.10E+04
q" (W/m^2)	2.98E+04	2.50E+04	1.99E+04	1.50E+04	9.05E+03
q (Watts)	1.50E+03	1.25E+03	9.96E+02	7.50E+02	4.54E+02
LMTD (°C)	5.86E+00	4.88E+00	3.97E+00	3.31E+00	2.51E+00
Δ T (°C)	2.96E+00	2.47E+00	2.03E+00	1.70E+00	1.31E+00
h_i (W/m^2K)	1.65E+04	1.41E+04	1.16E+04	9.17E+03	6.58E+03
Re_i	1.03E+04	8.35E+03	6.53E+03	4.81E+03	3.14E+03
U_o (W/m^2K)	5.25E+03	5.28E+03	5.15E+03	4.66E+03	3.71E+03
UN (± %)	8.06E+00	1.01E+01	1.38E+01	1.90E+01	2.89E+01

TABLE D.17 SPRAY EVAPORATION OF HFC-236ea ON THE TURBO-CII TUBE AT A SATURATION TEMPERATURE OF 2 °C (FLOW RATE = 2.6 kg/min, RUN 1)

h (W/m^2K)	9.50E+03	8.53E+03	7.20E+03	5.87E+03
q" (W/m^2)	1.51E+01	1.99E+01	2.50E+01	2.97E+01
q (Watts)	7.58E+02	9.96E+02	1.25E+03	1.49E+03
LMTD (°C)	3.82E+00	4.66E+00	5.92E+00	7.55E+00
Δ T (°C)	1.96E+00	2.36E+00	2.99E+00	3.80E+00
h_i (W/m^2K)	8.51E+03	1.08E+04	1.31E+04	1.55E+04
Re_i	5.06E+03	6.89E+03	8.91E+03	1.12E+04
U_o (W/m^2K)	4.01E+03	4.33E+03	4.29E+03	4.00E+03
UN (± %)	1.59E+01	1.14E+01	8.27E+00	6.38E+00

TABLE D.18 SPRAY EVAPORATION OF HFC-236ea ON THE TURBO-CII TUBE AT A SATURATION TEMPERATURE OF 2°C (FLOW RATE = 2.6 kg/min, RUN 2)

h (W/m^2K)	5.87E+03	7.20E+03	8.55E+03	9.51E+03	9.79E+03
q" (W/m^2)	2.97E+01	2.49E+01	1.99E+01	1.50E+01	9.59E+00
q (Watts)	1.49E+03	1.25E+03	9.99E+02	7.54E+02	4.81E+02
LMTD (°C)	7.56E+00	5.89E+00	4.67E+00	3.81E+00	2.96E+00
Δ T (°C)	3.80E+00	2.97E+00	2.37E+00	1.95E+00	1.53E+00
h_i (W/m^2K)	1.55E+04	1.31E+04	1.08E+04	8.48E+03	6.06E+03
Re_i	1.12E+04	8.91E+03	6.89E+03	5.03E+03	3.27E+03
U_o (W/m^2K)	3.99E+03	4.29E+03	4.33E+03	4.00E+03	3.29E+03
UN (± %)	6.37E+00	8.30E+00	1.14E+01	1.60E+01	2.49E+01

TABLE D.19 SPRAY EVAPORATION OF HFC-236ea ON THE TURBO-CII TUBE AT A SATURATION TEMPERATURE OF 2°C (FLOW RATE = 2.8 kg/min, RUN 1)

h (W/m^2K)	9.41E+03	8.73E+03	7.44E+03	6.13E+03
q'' (W/m^2)	1.52E+01	2.00E+01	2.50E+01	2.98E+01
q (Watts)	7.61E+02	1.00E+03	1.26E+03	1.50E+03
LMTD (°C)	3.86E+00	4.64E+00	5.81E+00	7.38E+00
ΔT (°C)	1.97E+00	2.36E+00	2.93E+00	3.71E+00
h_i (W/m^2K)	8.50E+03	1.08E+04	1.31E+04	1.54E+04
Re_i	5.05E+03	6.88E+03	8.90E+03	1.11E+04
U_o (W/m^2K)	3.99E+03	4.38E+03	4.37E+03	4.11E+03
UN (± %)	1.57E+01	1.15E+01	8.47E+00	6.54E+00

TABLE D.20 SPRAY EVAPORATION OF HFC-236ea ON THE TURBO-CII TUBE AT A SATURATION TEMPERATURE OF 2°C (FLOW RATE = 2.8 kg/min, RUN 2)

h (W/m^2K)	6.14E+03	7.44E+03	8.74E+03	9.42E+03	9.36E+03
q'' (W/m^2)	3.00E+01	2.49E+01	1.99E+01	1.50E+01	9.64E+00
q (Watts)	1.50E+03	1.25E+03	9.97E+02	7.53E+02	4.84E+02
LMTD (°C)	7.40E+00	5.79E+00	4.61E+00	3.82E+00	3.01E+00
ΔT (°C)	3.72E+00	2.92E+00	2.34E+00	1.95E+00	1.56E+00
h_i (W/m^2K)	1.54E+04	1.31E+04	1.08E+04	8.49E+03	6.08E+03
Re_i	1.11E+04	8.87E+03	6.89E+03	5.04E+03	3.29E+03
U_o (W/m^2K)	4.11E+03	4.37E+03	4.38E+03	3.99E+03	3.25E+03
UN (± %)	6.51E+00	8.50E+00	1.16E+01	1.59E+01	2.38E+01

TABLE D.21 SPRAY EVAPORATION OF HFC-236ea ON THE TURBO-CII TUBE AT A SATURATION TEMPERATURE OF 2°C (FLOW RATE = 3.0 kg/min, RUN 1)

h (W/m^2K)	9.71E+03	9.38E+03	7.95E+03	7.00E+03
q" (W/m^2)	1.50E+01	1.98E+01	2.51E+01	2.99E+01
q (Watts)	7.54E+02	9.94E+02	1.26E+03	1.50E+03
LMTD (°C)	3.78E+00	4.44E+00	5.61E+00	6.80E+00
Δ T (°C)	1.93E+00	2.26E+00	2.84E+00	3.42E+00
h_i (W/m^2K)	8.49E+03	1.08E+04	1.30E+04	1.53E+04
Re_i	5.04E+03	6.86E+03	8.80E+03	1.09E+04
U_o (W/m^2K)	4.04E+03	4.53E+03	4.54E+03	4.47E+03
UN (± %)	1.63E+01	1.24E+01	8.90E+00	7.14E+00

TABLE D.22 SPRAY EVAPORATION OF HFC-236ea ON THE TURBO-CII TUBE AT A SATURATION TEMPERATURE OF 2°C (FLOW RATE = 3.0 kg/min, RUN 2)

h (W/m^2K)	7.02E+03	7.98E+03	9.39E+03	9.72E+03
q" (W/m^2)	2.98E+01	2.52E+01	2.01E+01	1.49E+01
q (Watts)	1.50E+03	1.26E+03	1.01E+03	7.48E+02
LMTD (°C)	6.76E+00	5.62E+00	4.49E+00	3.75E+00
Δ T (°C)	3.40E+00	2.84E+00	2.28E+00	1.92E+00
h_i (W/m^2K)	1.53E+04	1.31E+04	1.08E+04	8.48E+03
Re_i	1.09E+04	8.81E+03	6.86E+03	5.03E+03
U_o (W/m^2K)	4.48E+03	4.55E+03	4.53E+03	4.04E+03
UN (± %)	7.19E+00	8.90E+00	1.23E+01	1.64E+01

TABLE D.23 SPRAY EVAPORATION OF HFC-236ea ON THE TURBO-CII TUBE AT A SATURATION TEMPERATURE OF 2°C (FLOW RATE = 3.0 kg/min, REPEAT RUN FOR RUN 1)

h (W/m^2K)	9.69E+03	9.37E+03	7.91E+03	6.95E+03
q" (W/m^2)	1.50E+01	2.00E+01	2.50E+01	2.97E+01
q (Watts)	7.54E+02	1.00E+03	1.26E+03	1.49E+03
LMTD (°C)	3.79E+00	4.48E+00	5.62E+00	6.79E+00
Δ T (°C)	1.94E+00	2.28E+00	2.84E+00	3.42E+00
h_i (W/m^2K)	8.48E+03	1.08E+04	1.31E+04	1.53E+04
Re_i	5.03E+03	6.86E+03	8.83E+03	1.09E+04
U_o (W/m^2K)	4.03E+03	4.53E+03	4.53E+03	4.45E+03
UN (± %)	1.62E+01	1.23E+01	8.88E+00	7.15E+00

TABLE D.24 SPRAY EVAPORATION OF HFC-236ea ON THE TURBO-CII TUBE AT A SATURATION TEMPERATURE OF 2°C (FLOW RATE = 3.0 kg/min, REPEAT RUN FOR RUN 2)

h (W/m^2K)	6.97E+03	7.94E+03	9.37E+03	9.70E+03	9.47E+03
q" (W/m^2)	2.98E+01	2.50E+01	2.00E+01	1.50E+01	9.57E+00
q (Watts)	1.50E+03	1.25E+03	1.00E+03	7.51E+02	4.80E+02
LMTD (°C)	6.79E+00	5.59E+00	4.47E+00	3.77E+00	2.98E+00
Δ T (°C)	3.42E+00	2.83E+00	2.27E+00	1.93E+00	1.54E+00
h_i (W/m^2K)	1.53E+04	1.30E+04	1.08E+04	8.49E+03	6.06E+03
Re_i	1.09E+04	8.79E+03	6.87E+03	5.03E+03	3.27E+03
U_o (W/m^2K)	4.46E+03	4.53E+03	4.53E+03	4.04E+03	3.25E+03
UN (± %)	7.14E+00	8.94E+00	1.23E+01	1.63E+01	2.42E+01

TABLE D.25 SPRAY EVAPORATION OF HFC-236ea ON THE TURBO-CII TUBE AT A SATURATION TEMPERATURE OF 2°C (FLOW RATE = 3.2 kg/min, RUN 1)

h (W/m^2K)	1.02E+04	9.76E+03	8.93E+03	8.06E+03
q" (W/m^2)	1.50E+01	1.99E+01	2.50E+01	2.99E+01
q (Watts)	7.54E+02	1.00E+03	1.26E+03	1.50E+03
LMTD (°C)	3.71E+00	4.39E+00	5.26E+00	6.24E+00
Δ T (°C)	1.90E+00	2.23E+00	2.66E+00	3.14E+00
h_i (W/m^2K)	8.49E+03	1.08E+04	1.30E+04	1.52E+04
Re_i	5.03E+03	6.83E+03	8.73E+03	1.07E+04
U_o (W/m^2K)	4.12E+03	4.61E+03	4.83E+03	4.86E+03
UN (± %)	1.70E+01	1.28E+01	9.80E+00	7.93E+00

TABLE D.26 SPRAY EVAPORATION OF HFC-236ea ON THE TURBO-CII TUBE AT A SATURATION TEMPERATURE OF 2°C (FLOW RATE = 3.2 kg/min, RUN 2)

h (W/m^2K)	8.08E+03	8.95E+03	9.78E+03	1.03E+04
q" (W/m^2)	2.98E+01	2.50E+01	2.00E+01	1.50E+01
q (Watts)	1.50E+03	1.26E+03	1.00E+03	7.51E+02
LMTD (°C)	6.21E+00	5.25E+00	4.39E+00	3.69E+00
Δ T (°C)	3.13E+00	2.66E+00	2.23E+00	1.89E+00
h_i (W/m^2K)	1.52E+04	1.30E+04	1.08E+04	8.47E+03
Re_i	1.08E+04	8.74E+03	6.85E+03	5.01E+03
U_o (W/m^2K)	4.88E+03	4.84E+03	4.62E+03	4.12E+03
UN (± %)	7.96E+00	9.82E+00	1.28E+01	1.72E+01

TABLE D.27 SPRAY EVAPORATION OF HFC-236ea ON THE 1575-fpm TUBE AT A SATURATION TEMPERATURE OF 2°C (FLOW RATE = 2.6 kg/min, RUN 1)

h (W/m^2K)	5.81E+03	5.25E+03	4.43E+03	3.81E+03
q" (W/m^2)	1.48E+04	1.98E+04	2.50E+04	2.97E+04
q (Watts)	7.44E+02	9.95E+02	1.25E+03	1.49E+03
LMTD (°C)	7.17E+00	8.59E+00	1.06E+01	1.28E+01
Δ T (°C)	3.61E+00	4.32E+00	5.34E+00	6.42E+00
h_i (W/m^2K)	3.98E+03	5.12E+03	6.26E+03	7.43E+03
Re_i	5.52E+03	7.70E+03	1.01E+04	1.29E+04
U_o (W/m^2K)	2.09E+03	2.33E+03	2.37E+03	2.34E+03
UN (± %)	1.24E+01	9.28E+00	7.05E+00	5.87E+00

TABLE D.28 SPRAY EVAPORATION OF HFC-236ea ON THE 1575-fpm TUBE AT A SATURATION TEMPERATURE OF 2°C (FLOW RATE = 2.6 kg/min, RUN 2)

h (W/m^2K)	3.80E+03	4.57E+03	5.29E+03	5.74E+03	5.32E+03
q" (W/m^2)	2.98E+04	2.51E+04	1.96E+04	1.48E+04	9.66E+03
q (Watts)	1.49E+03	1.26E+03	9.85E+02	7.43E+02	4.85E+02
LMTD (°C)	1.29E+01	1.05E+01	8.49E+00	7.19E+00	6.03E+00
Δ T (°C)	6.46E+00	5.28E+00	4.27E+00	3.62E+00	3.04E+00
h_i (W/m^2K)	7.44E+03	6.25E+03	5.11E+03	3.99E+03	2.84E+03
Re_i	1.29E+04	1.01E+04	7.66E+03	5.54E+03	3.57E+03
U_o (W/m^2K)	2.33E+03	2.41E+03	2.33E+03	2.08E+03	1.62E+03
UN (± %)	5.85E+00	7.16E+00	9.43E+00	1.23E+01	1.63E+01

TABLE D.29 SPRAY EVAPORATION OF HFC-236ea ON THE 1575-fpm TUBE AT A SATURATION TEMPERATURE OF 2°C (FLOW RATE = 2.8 kg/min, RUN 1)

h (W/m^2K)	6.18E+03	5.52E+03	4.75E+03	4.08E+03
q" (W/m^2)	1.48E+04	1.98E+04	2.49E+04	2.98E+04
q (Watts)	7.42E+02	9.92E+02	1.25E+03	1.49E+03
LMTD (°C)	7.00E+00	8.41E+00	1.02E+01	1.24E+01
Δ T (°C)	3.52E+00	4.22E+00	5.14E+00	6.19E+00
h_i (W/m^2K)	3.97E+03	5.10E+03	6.23E+03	7.41E+03
Re_i	5.49E+03	7.64E+03	1.00E+04	1.27E+04
U_o (W/m^2K)	2.13E+03	2.37E+03	2.45E+03	2.43E+03
UN (± %)	1.31E+01	9.66E+00	7.41E+00	6.10E+00

TABLE D.30 SPRAY EVAPORATION OF HFC-236ea ON THE 1575-fpm TUBE AT A SATURATION TEMPERATURE OF 2°C (FLOW RATE = 2.8 kg/min, RUN 2)

h (W/m^2K)	4.09E+03	4.89E+03	5.50E+03	6.20E+03	5.39E+03
q" (W/m^2)	3.00E+04	2.50E+04	1.99E+04	1.48E+04	9.64E+03
q (Watts)	1.50E+03	1.25E+03	9.97E+02	7.44E+02	4.84E+02
LMTD (°C)	1.24E+01	1.01E+01	8.46E+00	7.01E+00	5.99E+00
Δ T (°C)	6.22E+00	5.08E+00	4.25E+00	3.53E+00	3.02E+00
h_i (W/m^2K)	7.41E+03	6.23E+03	5.11E+03	3.98E+03	2.84E+03
Re_i	1.27E+04	1.00E+04	7.65E+03	5.50E+03	3.57E+03
U_o (W/m^2K)	2.44E+03	2.49E+03	2.37E+03	2.14E+03	1.62E+03
UN (± %)	6.07E+00	7.55E+00	9.59E+00	1.32E+01	1.65E+01

TABLE D.31 SPRAY EVAPORATION OF HFC-236ea ON THE 1575-fpm TUBE AT A SATURATION TEMPERATURE OF 2°C (FLOW RATE = 3.0 kg/min, RUN 1)

h (W/m^2K)	6.63E+03	6.44E+03	5.97E+03	5.20E+03
q" (W/m^2)	1.50E+04	1.99E+04	2.48E+04	2.99E+04
q (Watts)	7.55E+02	1.00E+03	1.24E+03	1.50E+03
LMTD (°C)	6.95E+00	7.97E+00	9.18E+00	1.09E+01
Δ T (°C)	3.50E+00	4.01E+00	4.61E+00	5.47E+00
h_i (W/m^2K)	3.98E+03	5.08E+03	6.15E+03	7.28E+03
Re_i	5.50E+03	7.56E+03	9.74E+03	1.23E+04
U_o (W/m^2K)	2.18E+03	2.52E+03	2.73E+03	2.77E+03
UN (± %)	1.37E+01	1.08E+01	8.76E+00	7.05E+00

TABLE D.32 SPRAY EVAPORATION OF HFC-236ea ON THE 1575-fpm TUBE AT A SATURATION TEMPERATURE OF 2°C (FLOW RATE = 3.0 kg/min, REPEAT RUN FOR RUN 1)

h (W/m^2K)	6.64E+00	6.46E+00	5.93E+00	5.15E+00
q" (W/m^2)	1.49E+01	2.00E+01	2.50E+01	2.97E+01
q (Watts)	7.46E+02	1.00E+03	1.25E+03	1.49E+03
LMTD (°C)	6.88E+00	7.98E+00	9.27E+00	1.09E+01
Δ T (°C)	3.46E+00	4.01E+00	4.66E+00	5.46E+00
h_i (W/m^2K)	3.97E+03	5.08E+03	6.16E+03	7.27E+03
Re_i	5.48E+03	7.55E+03	9.77E+03	1.22E+04
U_o (W/m^2K)	2.18E+03	2.53E+03	2.72E+03	2.75E+03
UN (± %)	1.39E+01	1.08E+01	8.64E+00	7.06E+00

TABLE D.33 SPRAY EVAPORATION OF HFC-236ea ON THE 1575-fpm TUBE AT A SATURATION TEMPERATURE OF 2°C (FLOW RATE = 3.0 kg/min, RUN 2)

h (W/m^2K)	5.19E+03	5.93E+03	6.38E+03	6.63E+03	5.50E+03
q" (W/m^2)	3.00E+04	2.49E+04	2.01E+04	1.50E+04	9.57E+03
q (Watts)	1.51E+03	1.25E+03	1.01E+03	7.51E+02	4.80E+02
LMTD (°C)	1.10E+01	9.24E+00	8.06E+00	6.93E+00	5.91E+00
Δ T (°C)	5.49E+00	4.64E+00	4.05E+00	3.49E+00	2.98E+00
h_i (W/m^2K)	7.28E+03	6.15E+03	5.09E+03	3.97E+03	2.84E+03
Re_i	1.23E+04	9.75E+03	7.58E+03	5.49E+03	3.56E+03
U_o (W/m^2K)	2.77E+03	2.72E+03	2.52E+03	2.18E+03	1.64E+03
UN (± %)	7.02E+00	8.68E+00	1.06E+01	1.38E+01	1.70E+01

TABLE D.34 SPRAY EVAPORATION OF HFC-236ea ON THE 1575-fpm TUBE AT A SATURATION TEMPERATURE OF 2°C (FLOW RATE = 3.2 kg/min, RUN 1)

h (W/m^2K)	6.63E+03	6.45E+03	5.97E+03	5.26E+03
q" (W/m^2)	1.48E+04	1.97E+04	2.48E+04	3.01E+04
q (Watts)	7.42E+02	9.87E+02	1.24E+03	1.51E+03
LMTD (°C)	6.86E+00	7.87E+00	9.17E+00	1.09E+01
Δ T (°C)	3.45E+00	3.96E+00	4.60E+00	5.48E+00
h_i (W/m^2K)	3.96E+03	5.07E+03	6.16E+03	7.26E+03
Re_i	5.47E+03	7.53E+03	9.75E+03	1.22E+04
U_o (W/m^2K)	2.18E+03	2.52E+03	2.73E+03	2.78E+03
UN (± %)	1.39E+01	1.10E+01	8.76E+00	7.05E+00

TABLE D.35 SPRAY EVAPORATION OF HFC-236ea ON THE 1575-fpm TUBE AT A SATURATION TEMPERATURE OF 2°C (FLOW RATE = 3.2 kg/min, RUN 2)

h (W/m^2K)	5.33E+03	6.02E+03	6.48E+03	6.79E+03	5.69E+03
q" (W/m^2)	2.97E+04	2.47E+04	1.98E+04	1.47E+04	9.64E+03
q (Watts)	1.49E+03	1.24E+03	9.95E+02	7.39E+02	4.83E+02
LMTD (°C)	1.07E+01	9.11E+00	7.93E+00	6.77E+00	5.91E+00
Δ T (°C)	5.36E+00	4.57E+00	3.99E+00	3.41E+00	2.98E+00
h_i (W/m^2K)	7.25E+03	6.15E+03	5.06E+03	3.96E+03	2.82E+03
Re_i	1.22E+04	9.72E+03	7.52E+03	5.46E+03	3.54E+03
U_o (W/m^2K)	2.80E+03	2.74E+03	2.53E+03	2.19E+03	1.65E+03
UN (± %)	7.22E+00	8.85E+00	1.09E+01	1.43E+01	1.74E+01

APPENDIX E

DERIVATION OF UNCERTAINTY ANALYSIS EQUATIONS

This appendix presents the derivation of the uncertainty analysis equations for the shell-side heat transfer coefficients calculated in this study.

Substituting q and LMTD in Equation 4.4 by those given in Equations 4.2 and 4.3 and replacing U_o and R_w in Equation 4.5 by those given in the Equation 4.4 and Equation 4.6 results in the following equation for the shell-side heat transfer coefficient (h),

$$h = \left[\frac{A_o}{\dot{m}_i \cdot Cp_i \cdot \ln\left(\frac{T_{sat} - T_{i,in}}{T_{sat} - T_{i,out}}\right)} - \frac{A_o}{A_i}\frac{1}{h_i} - \frac{A_o \ln(D_o/D_i)}{2\pi k_w L} \right]^{-1} \tag{E.1}$$

Equation E.1 shows that for a given heat exchanger (tube) the uncertainty of h depends on the seven variables: $\dot{m}_i$, Cp_i, h_i, k_w, T_{sat}, $T_{i,out}$, and $T_{i,in}$. The other terms in Equation E.1 are constants for a given tube since D_o and D_i (and thus A_o and A_i) are constants. Therefore, the uncertainty in the calculated shell-side heat transfer coefficients according to the propagation of error approach described in the Phase I report [2] is defined as

$$\delta h = \left[\left(\frac{\partial h}{\partial \dot{m}_i}(\delta \dot{m}_i)\right)^2 + \left(\frac{\partial h}{\partial Cp_i}(\delta Cp_i)\right)^2 + \left(\frac{\partial h}{\partial h_i}(\delta h_i)\right)^2 + \left(\frac{\partial h}{\partial k_w}(\delta k_w)\right)^2 + \left(\frac{\partial h}{\partial T_{sat}}(\delta T_{sat})\right)^2 + \left(\frac{\partial h}{\partial T_{i,out}}(\delta T_{i,out})\right)^2 + \left(\frac{\partial h}{\partial T_{i,in}}(\delta T_{i,in})\right)^2 \right]^{1/2} \tag{E.2}$$

where $\delta\dot{m}_i$ is the uncertainty of the water mass flow rate, δCp_i is the uncertainty of the water's specific heat, δh_i is the uncertainty of the in-tube heat transfer coefficient, and δk_w is the uncertainty of the thermal conductivity of tube wall (k_w, W/m·K). δk_w was calculated using the tube wall temperature ($T_w = (T_{sat}+T_{i,bulk})/2$, °C) while δCp_i was calculated based on the bulk water temperature ($T_{i,bulk} = (T_{i,in}+ T_{i,out})/2$). The remaining three terms (δT_{sat},

$\delta T_{i,out}$, and $\delta T_{i,in}$) are referred to as the uncertainty due to the temperature measurements of the refrigerant saturation temperature, water outlet, and water inlet temperatures, respectively. The uncertainty in the shell-side heat transfer coefficient was caused by the existing uncertainty in the measurements. The instrumentation accuracy of the test facility is summarized in Chapter 4.

The following equations which are the partial derivatives of Equation E.1 with respect to the six independent variables are required in the determination of the uncertainty in the calculated shell-side heat transfer coefficients (i.e., Equation E.2).

$$\frac{\partial h}{\partial \dot{m}_i} = -h^2 \cdot \frac{-A_o}{\dot{m}_i^{\,2} \cdot Cp_i \cdot \ln\left(\frac{T_{sat} - T_{i,in}}{T_{sat} - T_{i,out}}\right)} \tag{E.3}$$

$$\frac{\partial h}{\partial Cp_i} = -h^2 \cdot \frac{-A_o}{\dot{m}_i \cdot Cp_i^{\,2} \cdot \ln\left(\frac{T_{sat} - T_{i,in}}{T_{sat} - T_{i,out}}\right)} \tag{E.4}$$

$$\frac{\partial h}{\partial h_i} = h^2 \cdot \left(\frac{A_o}{A_i} \frac{1}{h_i^{\,2}}\right) \tag{E.5}$$

$$\frac{\partial h}{\partial k_w} = -h^2 \cdot \frac{A_o \ln(D_o / D_i)}{2\pi k_w^{\,2} L} \tag{E.6}$$

$$\frac{\partial h}{\partial T_{sat}} = -h^2 \cdot \frac{A_o}{\dot{m}_i \cdot Cp_i} \cdot \frac{-1}{\left[\ln\left(\frac{T_{sat} - T_{i,in}}{T_{sat} - T_{i,out}}\right)\right]^2} \cdot \left(\frac{1}{T_{sat} - T_{i,in}} - \frac{1}{T_{sat} - T_{i,out}}\right) \tag{E.7}$$

For the calculation of the uncertainty in condensation,

$$\frac{\partial h}{\partial T_{i,out}} = -h^2 \cdot \frac{A_o}{\dot{m}_i \cdot Cp_i} \cdot \frac{-1}{\left[\ln\left(\frac{T_{sat} - T_{i,in}}{T_{sat} - T_{i,out}}\right)\right]^2} \cdot \left(\frac{1}{T_{sat} - T_{i,out}}\right) \tag{E.8}$$

$$\frac{\partial h}{\partial T_{i,in}} = -h^2 \cdot \frac{A_o}{\dot{m}_i \cdot Cp_i} \cdot \frac{-1}{\left[\ln\left(\frac{T_{sat} - T_{i,in}}{T_{sat} - T_{i,out}}\right)\right]^2} \cdot \left(\frac{-1}{T_{sat} - T_{i,in}}\right) \tag{E.9}$$

While for the calculation of the uncertainty in evaporation, Equation E.1 becomes

$$h = \left[\frac{A_o}{\dot{m}_i \cdot Cp_i \cdot \ln\left(\frac{T_{i,in} - T_{sat}}{T_{i,out} - T_{sat}}\right)} - \frac{A_o}{A_i}\frac{1}{h_i} - \frac{A_o \ln(D_o/D_i)}{2\pi k_w L}\right]^{-1} \tag{E.10}$$

The partial derivatives of Equation E.10 with respect to the six independent variables are the same as those of Equation E.1; i.e., Equations E.3 to E.9 can also be used to determine the uncertainty in evaporation.

The estimate of uncertainty is listed in Tables 4.1 to 4.3 and Appendix D and is presented as a percentage of the calculated heat transfer coefficient; i.e., $(\delta h/h)\times 100$.

TECHNICAL REPORT DATA
(Please read Instructions on the reverse before completing)

1. REPORT NO.	2.	3. RECIPIENT'S ACCESSION NO.
EPA-600/R-98-033		

4. TITLE AND SUBTITLE	5. REPORT DATE
Heat Transfer Evaluation of HFC-236ea with High Performance Enhanced Tubes in Condensation and Evaporation	April 1998
	6. PERFORMING ORGANIZATION CODE
7. AUTHOR(S)	8. PERFORMING ORGANIZATION REPORT NO.
S.-M. Tzuoo and M. B. Pate	
9. PERFORMING ORGANIZATION NAME AND ADDRESS	10. PROGRAM ELEMENT NO.
Iowa State University Department of Mechanical Engineering Ames, Iowa 50011	11. CONTRACT/GRANT NO. CR820755-01-4
12. SPONSORING AGENCY NAME AND ADDRESS	13. TYPE OF REPORT AND PERIOD COVERED
EPA, Office of Research and Development **Air Pollution Prevention and Control Division** **Research Triangle Park, NC 27711**	Task Final; 10/92-3/95 14. SPONSORING AGENCY CODE EPA/600/13

15. SUPPLEMENTARY NOTES APPCD project officer is Theodore G. Brna, Mail Drop 4, 919/541-2683.

16. ABSTRACT The report gives results of an evaluation of the heat transfer performance of pure hydrofluorocarbon (HFC)-236ea for high performance enhanced tubes which had not been previously used in Navy shipboard chillers. Shell-side heat transfer coefficient data are presented for condensation on a Turbo-CII tube, pool boiling on Turbo-B and -BII tubes, and spray evaporation on Turbo-B and -CII tubes and a 1575-fpm (fin-per-meter) tube. These tubes have nominal outside diameters of 19.1 mm (3/4-in.), and they were evaluated at a saturation temperature of 2 C (35.6 F) in evaporation and 40 C (104 F) in condensation. The condensation and pool boiling results for the high performance enhanced tubes were compared with those for a plain tube and two integral finned (1024- and 1575-fpm) tubes, which were evaluated earlier. The comparison shows that the high performance enhanced tubes are able to promote heat transfer processes better than the plain tube, and especially better than the integral finned tubes that are currently being used with chlorofluorocarbon (CFC)-114 in the Navy shipboard chillers. The Turbo-CII, -BII, and -B tubes performed best in condensation, pool boiling, and spray evaporation, respectively. The comparative heat transfer performance of spray evaporation with pool boiling was made by using Turbo-B and 1575-fpm tubes.

17. KEY WORDS AND DOCUMENT ANALYSIS

a. DESCRIPTORS	b. IDENTIFIERS/OPEN ENDED TERMS	c. COSATI Field/Group
Pollution Coolers Heat Transfer Refrigerants	Pollution Prevention Stationary Sources Chillers Shipboard Equipment	13B 13A 20M

18. DISTRIBUTION STATEMENT	19. SECURITY CLASS *(This Report)*	21. NO. OF PAGES
Release to Public	Unclassified	99
	20. SECURITY CLASS *(This page)*	22. PRICE
	Unclassified	

EPA Form 2220-1 (9-73)